Christian Frigerio

Aqueous synthesis and application of nanocrystals as luminescent molecular probes in continuous flow analytical methodologies

Tese do 3º Ciclo de Estudos Conducentes ao Grau de Doutor em Ciências Farmacêuticas com especialização em Química Analítica

Trabalho realizado sob a orientação do Professor Doutor João Luís Machado dos Santos e co-orientação do Professor Doutor José Luís Fontes da Costa Lima

Porto

Fevereiro de 2013

Acknowledgments

First and foremost, I would like to express my deepest thanks to my thesis advisor, Prof. Dr. João Luís Machado dos Santos, for his guidance and continuous encouragement throughout my PhD research period, and to Prof. Dr. José Luís Fontes da Costa Lima to allow me work in the Departement of Physical Chemistry. My sincere gratitude goes to Prof. Dr. Jorge M.A. Oliveira of Faculty of Pharmacy (FFUP), Rute A.S. Ferreira of CICECO/University of Aveiro and Dr. Peter Eaton of REQUIMTE/ Chemistry Department of the University of Porto for their time, help, and valuable advice.

I also wish to take this opportunity to thank all my collegues and good friend that I've done in the last four years working in this departement.

Last and most importantly I thank my extended family: my parents, my sister, all my friends from Coimbra and to all the peoples that are important for me. They already know it.

A very special thank to Nausica. I thank her for her patience, great enthusiasm, and her love that made everything easier.

Finally I want to thanks to my problem children, quantum dots, to annoy me during all this time.

FCT Fundação para a Ciência e a Tecnologia
MINISTÉRIO DA CIÊNCIA, TECNOLOGIA E ENSINO SUPERIOR

POPH PROGRAMA OPERACIONAL POTENCIAL HUMANO

QREN QUADRO DE REFERÊNCIA ESTRATÉGICO NACIONAL PORTUGAL 2007.2013

UNIÃO EUROPEIA
Fundo Social Europeu

Abstract

Quantum dots (QDs) are semiconductor nanocrystals (NC) exhibiting a size in the nanometer scale that, in recent years, have been subject to a growing interest due to their peculiar and valuable optoelectronic and physical-chemical properties. The research on these nanocrystals has been mostly focused on the synthesis of new materials and on the modification of those already available aiming at wide spreading the range of analytical techniques capable of using them. Nowadays, the vast number and diversity of prepared QDs enables to cover almost the complete Ultraviolet /Visible/Infrared (UV/Vis/IR) wavelength range and the variety of cappings that are used enables the utilization of these nanomaterials both in aqueous and organic solution. In this regard, one of the most important breakthroughs was the development of direct water-based synthesis approaches which fostered their scope of application both in terms of a chemical and a technological perspective, allowing, for instance, their utilization not only in batch but also in continuous flow methodologies. Considering the aim of this dissertation, automatic flow methodologies were successfully applied to the QDs synthesis and in analytical chemistry techniques. The high versatility of flow systems was exploited to carry out and to monitor the aqueous synthesis of CdTe-MPA QDs. The obtained results have demonstrated that a more efficient management of the precursor concentration, especially of NaHTe, was possible. This fact lead to an enhanced reproducibility of all synthesis process and, consequently, ensure that the prepared materials exhibited unvarying characteristics, essential item for future applications. The superior performance of the implemented system was exploited for the production of NC destined to a more exhaustive study about the influence of the growth rate on the crystal structure, population and optical properties. The population dispersion was found to be dependent on the growth rate, but a similar pattern of focussing and defocusing regimes was established for all the rates. Differently from what reported in literature it was verified that the quantum efficiency reaches a maximum for a certain size and did not decrease for faster growing regimes. Moreover automatically synthesized QDs were used in the development of a robust experimental model for the determination of the molar mass end molar extinction coefficient, two parameters of extremely importance especially for analytical applications of QDs.

The feasibility and robustness of implementing analytical methodologies resorting to CdTe QDs in an automated multipumping flow system (MPFS) was also demonstrated. Due to the extended range of variables to be optimized for QDs analytical applications, the multipumping flow methodology allowed a simplification of the entire process and the gathering of the ideal conditions in a simpler and faster way. The pulsed flowing stream generated by micro-pump actuation not only permitted the attainment of very stable flow

rates but also imparted a fast homogeneous mixing which contributed to improve the interactions development. Furthermore, the use of the merging zones strategy was of great benefit as it enabled the reduction of the time required for the analysis as well as of reagent consumption.

Chlorhexidine and acetil-cysteine fluorimetric determination by the concept of photoluminescence enhancing were performed. In these works was described for the first time the possibility of measuring an enhancement of the emission after interaction of the sample with the QDs surface.

CdTe QD were also successfully applied as chemiluminescence sensitizers enabling the chemiluminometric determination of glipizide and gliclazide. These molecules interact with the nanoparticles affecting their photochemical properties and/or reactivity. Once again the mixing capacity and high automation level of MPFS provided an expeditious way of implementing reaction schemes involving nanoparticles and the generation of short-lived species that are difficult to monitor in discrete methodologies.

Despite the great potentiality already showe, QDs have high heavy metals content, fact that makes them quite “unfriendly” for the environment. Independently from the reduced impact deriving by using multipumping systems, we felt the necessity of immobilize them onto solid support materials, allowing the fabrication of “continuous multiuse reactors”. A novel and efficient procedure for the covalent immobilization of QDs capped with compounds exhibiting an amino group has been developed. The method ensured a superior stability in aqueous conditions when compared to alternative methods based on electrostatic interactions, without compromise QDs optical properties.

Keywords: quantum dots, aqueous synthesis, multipumping flow system, fluorescence, surface chemistry

Resumo

Os pontos quânticos (QDs) são nanocristais de semicondutores (NC) que apresentam um tamanho na ordem dos nanómetros e que, nos últimos anos, têm sido objecto de um interesse crescente devido as suas peculiares e valiosas propriedades físico-químicas e optoelectrónicas. A pesquisa sobre esses cristais tem-se focado principalmente na síntese de novos materiais e na modificação dos já disponíveis visando a alargar a gama de técnicas analíticas capazes de utilizá-los. Hoje em dia, o grande número e variedade de QDs preparados permite cobrir quase completamente o intervalo de cumprimentos de onda entre ultravioleta /visível / infravermelho (UV / Vis / IR) e a variedade de *cappings* usados permite a aplicação destes nanomateriais, tanto em solução aquosa quanto em solventes orgânicos. A este respeito, um dos avanços mais importantes foi o desenvolvimento de métodos de síntese aquosa, que promoveram o âmbito de aplicação dos QDs, tanto do ponto de vista químico como tecnológico, permitindo, por exemplo, a utilização não só em *batch*, mas também em metodologias de fluxo contínuo. Considerando o objectivo desta dissertação, metodologias de fluxo automáticas foram aplicadas com sucesso para a síntese QDs e para desenvolver novos métodos analíticos. A versatilidade dos sistemas de fluxo foi disfrutada para executar e monitorizar a síntese aquosa de QDs de CdTe-MPA. Os resultados obtidos demonstraram a possibilidade de gerir mais eficientemente a movimentação e a concentração dos precursores, especialmente para o NaHTe. Como consequência deste facto foi possível atingir uma maior reprodutibilidade no processo de síntese e, consequentemente, assegurar que os materiais preparados apresentam características invariáveis, questão essencial para aplicações futuras. O sistema implementado foi utilizado para a produção de NC destinados a um estudo mais exaustivo da influência da velocidade de crescimento na estrutura do cristal, na população e nas propriedades ópticas. A dispersão da população mostrou-se dependente da velocidade de crescimento, mas foi possível individuar um padrão constante de focagem e desfocagem para todas as velocidades. Diferentemente de quanto descrito na literatura, verificou-se que a eficiência quântica atinge um máximo para um determinado tamanho e não tem tendência em diminuir para velocidades de crescimento maiores. Para além disso os QDs sintetizados através deste método foram utilizados para o desenvolvimento de um modelo experimental para a determinação da massa molar e do coeficiente de extinção molar, dois parâmetros de extrema importância, especialmente para QDs em química analítica.

A viabilidade e robustez da implementação de metodologias de análise que impliquem a utilização de QDs de CdTe em sistemas de fluxo baseados no conceito de multi-impulsão (MPFS) foram também demonstradas. Devido à ampla gama de variáveis que devem ser

optimizados para aplicar os QDs em métodos analíticos, a multi-impulsão permitiu uma simplificação de todo o processo e permitiu reunir as condições ideais duma forma mais simples e rápida. O fluxo pulsado gerado através da actuação de micro-bombas não só permitiu a realização de caudais muito estáveis, mas também proporcionou uma rápida e homogénea mistura dos reagentes, facilitando assim o ocorrer das interacções. Além disso, a utilização da estratégia de mistura por zonas de confluência trousse grandes benefícios, reduzindo o tempo necessário para a análise, e o consumo de reagentes.

Utilizando o conceito de *enhancing* da fotoluminescência foram desenvolvidos métodos para a determinação fluorométrica de clorexidina e acetil-cisteína. Nestes trabalhos foi pela primeira vez descrita a possibilidade de medir o aumento das fotoluminescência emitida pelo QDs após a interacção da amostra com a sua superfície.

Os QD de CdTe foram também aplicados com sucesso como sensibilizadores de quimiluminescência, e o método desenvolvido foi aplicado na determinação de glipizida e gliclazida. Estas moléculas interagem com as nanopartículas afectando as suas propriedades fotoquímicas e / ou reactividade. Mais uma vez, a elevada eficiência de mistura e o elevado nível de automação do MPFS forneceu uma forma fácil para a implementação de esquemas reaccionais que envolvem nanopartículas e que prevêem à geração de espécies com reduzido tempo de vida, que são difíceis de monitorizar em metodologias discretas.

Apesar das grandes potencialidades amplamente demonstradas, os QDs possuem um elevado teor de metais pesados, facto que os torna bastante hostis para o meio ambiente. Independentemente da grande redução do impacto ambiental obtenível utilizando os MPFS, sentiu-se a necessidade de imobilizar os NC em suportes sólidos, permitindo assim a fabricação de "reactores contínuos multiusos". Foi então desenvolvida uma nova e eficiente metodologia para imobilizar covalentemente QDs funcionalizados com compostos que apresentem um grupo amino. O método, comparado com técnicas baseadas em interacções electroestáticas, garantiu uma estabilidade superior em soluções aquosas, sem comprometer as propriedades ópticas dos QDs.

Palavras-chave: pontos quânticos, síntese aquosa, sistemas de fluxo por multi-impulsão, fluorescência, química de superfície.

Objective of this thesis

The preparation of stable water-soluble quantum dots (QDs) is a recent achievement and represented a significant breakthrough in terms of their availability and scope of application. Since this noteworthy breakthrough the number of works exploiting the potentiality of QDs increased exponentially in the most variables fields. Surface modification revealed to be an essential step in designing and implementing a suitable QD-based analytical strategy, because distinct ligands could be selected in order to assure recognition groups targeting a specific analyte.

The main objective of this work was not simply the synthesis and characterization of water-soluble QDs but focused as well on the modification of their surface enabling and increment of their photoluminescent properties (for application in fluorescence and chemiluminescence detection techniques) as well as to make them sensitive to selected target species. As the photoluminescence (PL) property of QDs is markedly affected by the surface nature, the interactions that are established between a given chemical specie and the QD surface would modify (either enhance or quench) the photoluminescence response. The magnitude of the PL change could be related with the specie concentration and is going to be exploited in the implementation of selective and sensitive analytical methodologies aiming at its quantification. In the same way quantum dots could be valuable tools in chemiluminescence applications, where they can act as sensitizers, final emitters or catalysers, providing the means for the implementation of fast and versatile monitoring procedures.

Another chief goal of this work was the combined utilisation of quantum dots potentiality and the analytical versatility provided by automated multi-pumping continuous flow methodologies in order to guarantee that all valuable features assured by an higher automation level of operation as well as a means to implement more compact miniaturised analytical systems that consumed less reagents and generate a lesser amount of liquid wastes. Of absolute importance was also the development of new conjugated materials maintaining the properties of QDs with the purpose of reducing even more the environmental impact of these nanoparticles.

Table of Contents

Index of figures

CHAPTER 1. Introduction

CHAPTER 2. Materials and Methods

CHAPTER 3. Automated Aqueous Synthesis of CdTe_MPA Capped Quantum Dots

CHAPTER 4. Cadmium telluride nanocrystals as luminescent sensitizers in flow analysis

CHAPTER 5. Evaluation of acetylcysteine promoting effect on CdTe nanocrystals photoluminescence by using a multipumping flow system

CHAPTER 6. Determination of chlorhexidine by induced fluorescence enhancement of MPA-capped CdTe quantum dots

Index of tables

CHAPTER 1. Introduction

CHAPTER 4. Cadmium telluride nanocrystals as luminescent sensitizers in flow analysis

CHAPTER 5. Evaluation of acetylcysteine promoting effect on CdTe nanocrystals photoluminescence by using a multipumping flow system

CHAPTER 6. Determination of chlorhexidine by induced fluorescence enhancement of MPA-capped CdTe quantum dots

List of acronyms and respective names

Acronym	Name
Ab	Antibody
ACZP	7-aminoclonazepam
AFM	Atomic force microscopy
AGB	Aminated glass beads
β-CD	β-cyclodextrin
BGE	Background electrolyte
BSA	Bovine serum albumin
dBSA	Denatured bovine serum albumin
CdTe	Cadmium telluride
CE	Capillary electrophoresis
CGE	Capillary gel electrophoresis
CL	Chemiluminescence
CRET	Chemiluminescence resonance energy transfer
CYS	Cysteine
Cy5	Cyanine dye
CZE	Capillary zone electrophoresis
DHLA	Dihydrolipoic acid
ε	Molar extinction coefficient
ECL	Electrochemiluminescence
E_g	Energy band gap
EPR	Electron paramagnetic resonance
FIA	Flow Injection Analysis
FRET	Förster resonance energy transfer

Acronym	Name
FTIR	Fourier transformed infrared spectroscopy
FWHM	Full width at half maximum
GSH	Glutathione
HOMO	Highest occupied molecular orbitals
HPSEC	High Performance size exclusion chromatography
IR	Infrared
ITO	Indium Tin Oxide
IUPAC	International Union of Pure and Applied Chemistry
LbL	Layer-by-layer
LC	Liquid chromatography
LIF	Laser induced fluorescence
LOD	Detection limit
LOQ	Quantification limit
LUMO	Lowest unoccupied molecular orbitals
MAA	Thioglycolic acid
MCFIA	Multicommutation
MBs	Molecular beacons
MCE	Microchip electrophoresis
MEKC	Micellar electrokinetic chromatography
MIPs	Molecular imprinted polymers
MPA	Mercaptopropionic acid
MPFS	Multipumping flow system
MSA	Mercaptosuccinic acid
MSFIA	Multisyringe
NAC	*N*-acetyl-l-cysteine
NC	Nanocrystals

Acronym	Name
OVA	Ovalbumin
PAA	Polyacrylamide
PEG	Polyethylene glycol
PEO	Polyethylene glycol
PL	Photoluminescence
PMMA	Poly(methyl methacrylate)
PTFE	Polytetrafluoroethylene
QDs	Quantum dots
QY	Quantum yield
RD	Relative standard deviation
SDS	Sodium dodecyl sulphate
SEC	Size exclusion chromatography
SIA	Sequential Injection Analysis
SIFA	Single Interface Flow Analysis
TEM	Transmission electron microscopy
TGA	Thioglycolic acid
UV	Ultraviolet
Vis	Visible
XRD	X-ray powder diffraction

CHAPTER 1

Introduction

1. Introduction

Quantum dots (QDs) are semiconductor nanocrystals (NC) exhibiting a size in the nanometer scale that, in recent years, have been subject to a growing interest due to their peculiar and valuable optoelectronic and physical-chemical properties [1]. These properties are markedly different from those exhibited by bulk semiconductor materials, which, despite revealing the same basic composition, are not susceptible to quantum confinement effects. These size-dependent phenomena only occur when the materials size is reduced to a few nanometers, which therefore enables the size-tuning of the QDs optical properties. One of the main reasons for the huge application potential anticipated for QDs in biological, analytical and optoelectronic fields results from both the capacity of these nanoparticles to emit light upon excitation and from the fact that this emission is susceptible to fluctuations due to interactions of the QDs with other molecules also present in the reaction medium.

The research on these nanocrystals has been mostly focused on the synthesis of new materials and on the modification of those already available aiming at wide spreading the range of analytical techniques capable of using them. Nowadays, the vast number and diversity of prepared core QDs enables to cover almost the complete Ultraviolet /Visible/Infrared (UV/Vis/IR) wavelength range and the variety of cappings that are used enables the utilization of these nanomaterials both in aqueous and organic solution. In this regard, one of the most important breakthroughs was the development of direct water-based synthesis approaches which fostered their scope of application both in terms of a chemical and a technological perspective, allowing, for instance, their utilization not only in batch but also in continuous flow methodologies. Since this advance, innumerous papers have been published dealing with different analytical applications of QDs and exploiting new detection strategies and reaction schemes. An important area, which should be without doubt continuously under scrutiny, concerns the surface chemistry of QDs, which markedly affects some of their most relevant properties. Effectively, the number of manuscripts available on this subject does not reflect its significance, eventually because it is extremely difficult to find analytical techniques capable of efficiently describe or “visualize” surface phenomena occurring at such a small area.

The objective of this first chapter is to introduce important theoretical concepts that are crucial to understand and perceive QDs properties and characteristics. Different synthesis strategies will be also analyzed with a particular emphasis on those involving the preparation of cadmium telluride (CdTe) QDs that were studied in this work. Flow analysis principles, especially those related with multi-pumping flow analysis, will be also

discussed alongside the application of QDs in these systems. Some essential surface chemistry concepts will be as well briefly examined.

2. Physical properties of Quantum Dots

Semiconductor quantum dots (QDs) are nanoscale materials that exist between a bulk and a molecular form [2-4]. Quantum dots can be composed by only one element, as in the case of Ge and Si, or be a combination of two or more elements (CdTe, CdSe, CdS, ZnO, InAs, InSb, GaAs). Due to their reduced size, lower than the Bohr radius of the material (from few hundred to several thousand atoms), they show peculiar characteristics depending on quantum confinement effects that make them quite different from bulk. Among these, the most important one is that for bulk materials the existing energy levels are continuous while for QDs they become discrete.
Being semiconductors QDs are characterized by an energy band gap (E_g) between the valence and the conduction band that is intimately associated to their highest occupied (HOMO) and lowest unoccupied (LUMO) molecular orbitals. When a quantum dot is excited with an energy superior to its band gap an electron is delocalized from the valence band to the conduction band. As a consequence, a quasi-particle called exciton is formed. The electron and the hole can subsequently recombine with each other and this process can give rise to the emission of a photon with energy close to the E_g. Because of the confinement effect the absolute energy level positions of both valence and conduction bands vary as a function of the size. The possibility of tuning the emission wavelength simply by varying the size is one of the main reasons for the broad acceptance of QDs and their extensive research. The radiative recombination is only possible if electron and hole recombine directly with each other. The occurrence of defects or trap states (mid-gap energy levels) on the crystal structure can attract and trap both electron and hole resulting in a quenching or shifting of the emission. The efficiency of the recombination process and, consequently, the perfection of the crystal structure can be estimated by measuring its quantum yield (QY) that is the ratio between the number of emitted and absorbed photons.

2.1. Exciton

Excitons [5] are uncharged quasi-particles formed by electron-hole pairs coulombically bounded. Semiconductors are materials capable of absorbing photons with energy equal

or superior to their band gap. The absorption of a photon normally fosters the delocalization of an electron from the valence band to the conduction band, leaving behind a vacant position called hole. In this excited state electrons and holes can move within the crystal lattice. In general, the exciton is treated as a single particle moving around a centre mass motion, ignoring the fact that in reality it is a composite particle. The existence of this centre mass motion permits assigning a reduced mass to the exciton $\mu = [(m_e^*)^{-1} + (m_h^*)^{-1}]^{-1}$, where m_e^* and m_h^* are, respectively, the reduced masses of the electro and the hole in the semiconductor. This treatment is called *effective mass approximation*.

Two general types of excitons exist: Mott-Wannier excitons, resulting from weak electron-hole interactions caused by a relative small Coulomb attraction, and Frenkel excitons, with higher Coulomb interactions. Because the dielectric constant in semiconductors is usually high, one deals mostly with Mott-Wannier excitons.

Upon formation the kinetic energy is released into the crystal lattice as the exciton settles into a lower energy state. This energy loss is called the *exciton binding energy* to signify that if a similar amount of energy is added to the exciton, the electron and hole will have enough energy to escape the Coulombic force. Consequently, the net energy of the exciton itself is the difference between the electronic band gap, *i.e.* the energy range corresponding to the region where no electrons or holes are allowed, and the exciton binding energy.

$$E_x = E_g - E_{bind} \qquad \text{Equation 1}$$

It should be emphasised that, because of this, the exciton is the lowest energy excited state and is very likely to form within the crystal. As a general rule, all excited states relax rapidly towards the exciton state.

2.2. Bohr radius

The Bohr radius a_o is considered the stable closest orbit to the nucleus in Bohr's planetary model of the atom [5]. A representative equation is obtained by considering the centripetal force of an electron circling an infinite heavy positively charged nucleus, with their mutual Columb attractive force:

$$\frac{mv^2}{r} = \frac{q^2}{4\pi\varepsilon_0 r^2} \qquad \text{Equation 2}$$

Since the electron has a wavelength, one can introduce a relationship between the wavelength of the particle and its associated Bohr radius:

$$n\lambda = 2\pi r \qquad \text{Equation 3}$$

By relating λ with the particles momentum (λ=h/ρ) and solving the equation 2 for υ and then for r, one obtain a generic Bohr radius;

$$r = \frac{4\pi\varepsilon_0 n^2 \hbar^2}{mq^2} \qquad \text{Equation 4}$$

The De Broglie radius can be then calculated for an electron or a hole in a material. For n = 1, one can assume that $m = m_e$ (electron mass) or m_h (hole mass). It must be also considered that the particles are not in the vacuum so one must change ε_o to $\varepsilon\,\varepsilon_o$, where ε is the relative dielectric constant of the material. This is called the effective mass approximation. Thus:

$$a_e = \frac{4\pi\varepsilon\varepsilon_0 \hbar^2}{m_e q^2} \qquad \text{Equation 5}$$

$$a_h = \frac{4\pi\varepsilon\varepsilon_0 \hbar^2}{m_h q^2} \qquad \text{Equation 6}$$

This concept can be easily extended to an exciton, by replacing the mass of the electron or hole with the reduced mass of the electron-hole pair, μ, where:

$$\frac{1}{\mu} = \frac{1}{m_e} + \frac{1}{m_h} \qquad \text{Equation 7}$$

Therefore:

$$a_B = \frac{4\pi\varepsilon\varepsilon_0 \hbar^2}{\mu q^2} \qquad \text{Equation 8}$$

When talking about semiconductor nanoparticles one is always referring the Bohr radius of the bulk material. From the equation above it is simple to understand how the Bohr radius is only related to the lattice nature, because it is a function of two parameters: the dielectric constant of the material (ε) and the relative mass of the exciton μ.

2.3. Quantum Confinement Regimes

The Bohr exciton concept is fundamental to understand the quantum confinement regimes. When working with nanoscaled semiconductor materials two regimes are possible, which depended from the nanoparticle size: weak confinement regimes, when the dimension of the nanostructure is larger than the exciton Bohr radius and strong confinement regime when the dimension is smaller than the Bohr radius. In the first case the material assumes the optical and electrical characteristic of the bulk material, because the exciton binding energy is weak. In a strong confinement regime the exciton wave function is forced into a lower space defined by the crystal size and its *confinement energy* increases. When this happens the band structure changes and two *quantum size effects* could be noticed. The first effect is made possible because of the relatively small number of atoms in a nanocrystal. As a result, only a finite number of molecular orbitals can contribute to the formation of the band structure. Therefore the continuity of the bands will be lost for energy values related with low density of states. Considering equation 9,

$$n(E) \propto \sqrt{E - E_c} \text{ (if } \mathrm{E} \geq \mathrm{Ec}) \qquad \text{Equation 9}$$

it is perceivable that the density of states is lower towards the edge of the band, so when the crystal size is reduced discrete energy levels will appear. Because of the quantization of the energy levels near the top of the valence band and at the bottom of the conduction band, sharp transitions at discrete energy values will emerge.

The second quantum size effect was previously mentioned and is a consequence of the confinement energy alteration. Because of the increasing confinement energy for decreasing crystal size, the valence and the conduction bands will move away from each other, increasing the band gap.

2.4. Strong Confinement: Particle-in-a-Box

There are few existing methods that could be used to understand the quantum confinement and to predict the energy levels based on size. The particle-in-a-box method is one of them.

This model can be applied to quantum dots, by considering the exciton as the particle and the quantum dot as the box, with the exciton effective mass substituting the particle mass and the boundaries of the box defined as the boundaries of the small crystallite. Not

pretending a profound analysis of the general theory of this model, which would impose a comprehensive examination of the Schrodinger equation, one intends to limit the discussion of this method to the approach proposed by L.E. Brus [6]. In the following equation;

$$E \approx E_g + \frac{\hbar^2 \pi^2}{2R^2}\left[\frac{1}{m_e} + \frac{1}{m_h}\right] - \frac{1.8e^2}{\varepsilon R} \qquad \text{Equation 10}$$

the term $1/m_e + 1/m_h$ is the effective exciton mass, R is the quantum dots radii, E_g is the bulk bandgap and ε is the semiconductor material dielectric constant. The presence of ε and μ show that the Bohr radius was took in account in this equation. The confinement term $1/R^2$ is identical to the particle-in-a-box relationship and it is evident that a decrease in this term results in an increase of E. The equation also takes into account the mutual attraction of the electron and hole with the term $-1/R$. This means that E shifts to lower values by increasing R but, because the exciton in the quantum dots is of the Mott-Wannier type, the Coulomb interaction becomes weaker and the main effect is that the electron and hole confinement energy increases.

It is important to remember that few approximations have been proposed to derive the Brus equation, so it is expectable that this model can fail in some cases. The most important approximations are:

- *Effective mass approximation*, this approximation breaks down when a significant number of the electronic wave functions inside the nanocrystal have a wave function overlapping the edge of the crystal. This happen for very small crystals.
- *Spherical nanocrystals*, the Brus equation works only for spherical or quasi-spherical crystals.
- *Infinite potential barrier*, in effect the potential step at the QDs surface is not infinite. This means that a little fraction of the electron and hole wave function can pass this barrier, a phenomenon called tunnelling. Theoretically the barrier must be also insensitive to the surrounding ambient and to externally applied potentials. If for the ambient is expectable a very small effect, the approximation would fail in the presence of large external potentials.

2.5. Quantum effect in quantum dots

In quantum dots the confinement exists in all 3 dimensions because for all of them the length of the exciton is inferior to the Bohr radius. For this reason carriers have zero

degrees of freedom, differently from quantum wells and quantum wires which have 2 and 1 degree of freedom, respectively (Figure 1). This way a quantum dot exhibits only phenomena related to quantum confinement in a lattice that is smaller than the volume required (number of repeating atoms) to describe the periodic properties of the system.

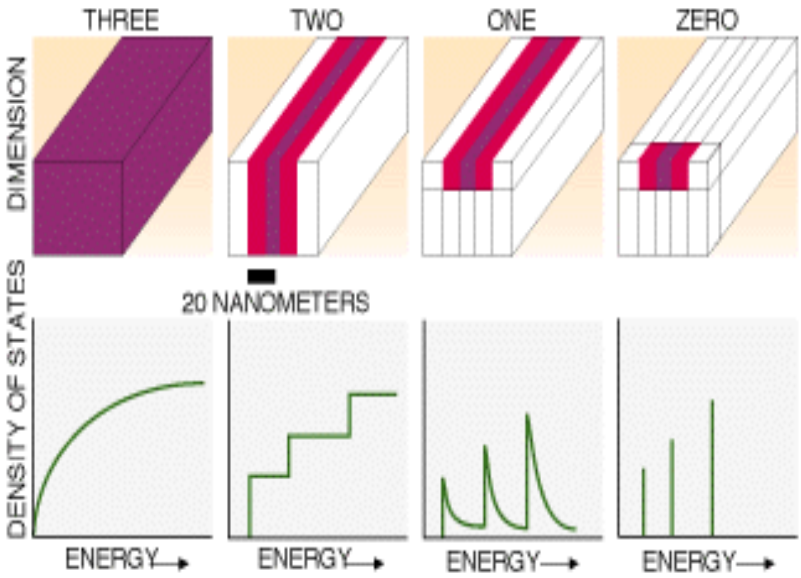

Figure 1 - Schematic representation of 0D, 1D, 2D and 3D systems. Quantum dots are considered a 0D system.

2.6. Surface to volume ratio

A very important characteristic of a nanoscale material is their large surface-to-volume ratio *R*. This fact is very advantageous when these materials are used as catalysts because they could be more efficient than ordinary materials. In the same way, for analytical purposes the extended surface could permit more straightforward interactions with the target molecule under analysis. The mathematical demonstration of the surface-to-volume ratio increase for decreasing sizes is very simple. Assuming the particle as a sphere,

$$A_{sphere} = 4\pi a^2 \qquad \text{Equation 11}$$

$$V_{sphere} = \frac{4}{3}\pi a^3 \qquad \text{Equation 12}$$

So:

$$R_{sphere} = \frac{4\pi a^2}{\frac{4}{3}} \pi a^2 = \frac{3}{a} \qquad \text{Equation 13}$$

3. Optical properties of quantum dots

3.1. Absorption

As it was already mentioned, semiconductor nanocrystals are nanostructures capable of absorbing a photon with energy higher than the band gap. Analyzing typical absorption spectra (Figure 2) it is possible to notice a relatively sharp maximum at the end of the absorption onset.

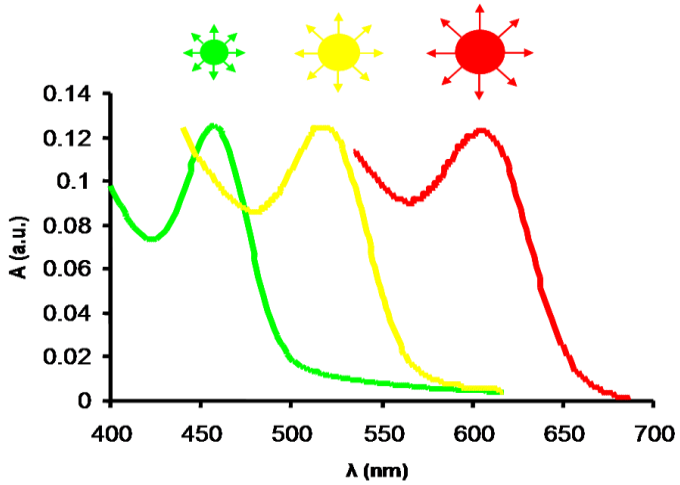

Figure 2 - Absorption spectra of different size QDs. It is evident the excitonic peak at the end of the absorption spectra.

This maximum corresponds to the excitonic peak, the first possible electronic transition. Its position on the spectrum depends on the band gap energy and thus, because of the quantum confinement effect, on the NC size. The definition of the excitonic peak, in terms of form and width, is strongly affected by the size distribution and by the shape of the NC. In particular in the presence of dispersed populations the maximum is reduced to a shoulder and the identification of the excitonic transition position could be a difficult task. Establishing a function of the QDs size regarding the energy of the 1s-1s transition,

estimated from the position of the first absorption peak, it is possible to determine the QDs size [6, 7] from this maximum. Using the Beer's law, the absorption (A) of a semiconductor with thickness l and absorption coefficient ε is a function of the radiation wavelength,

$$A = \varepsilon l \qquad \text{Equation 14}$$

Selecting rules are governing all the electronic transitions. In the case of semiconductors the wave vector k, must be conserved. k_{photon} is small when compared with the wave vectors of the electron before (k_e) and after excitation (k'_e).

$$k_e + k_{photon} = k'_e \qquad \text{Equation 15}$$

$$k_e = k'_e \qquad \text{Equation 16}$$

The absorption coefficient for a photon of a given energy is proportional to the probability of transition (P_{if}) between the two states, the density of states in the initial state (n_i) and in the final state (n_f). This process must be extended to all the transitions existing between states separated by an energy difference equal to the energy of the photon,

$$\varepsilon(h\nu) \propto (Eg - h\nu)^{\frac{1}{2}} \qquad \text{Equation 17}$$

when the wave vector is preserved, the semiconductor is defined as a direct band gap semiconductor and exhibits a large absorption coefficient [8].

3.2. Photoluminescence

One of the most important characteristics of QDs is their photoluminescence. This designation identifies all processes where the luminescence is generated through photon excitation (absorption of a given radiation). Fluorescence, in particular, is a short time emission process that involves the absorption of a photon with an energy superior to the band gap, a charge carrier non-radiative relaxation to the lowest excited state and finally the emission of a less energetic photon after a certain amount of time (fluorescence lifetime).

In semiconductor nanocrystals (Figure 3) the absorption of a photon promotes the excitation of an electron from the valence band to (or above) the conduction band. The

readily formed electron and hole migrate to the edge of their respective bands and then the electron returns to the valence band recombining with the hole and emitting a photon with energy matching the band gap.

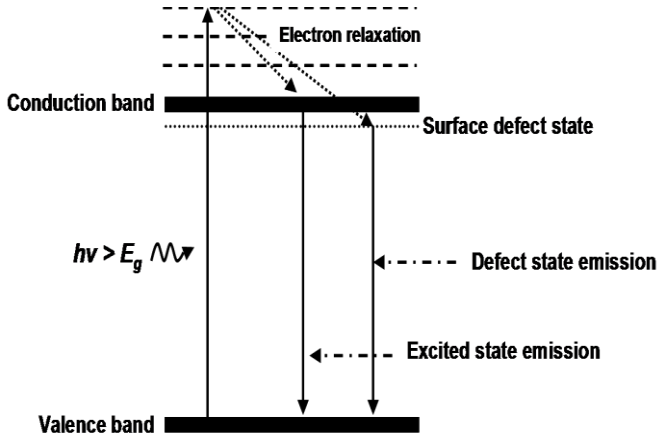

Figure 3 - Energy levels scheme of fluorescence mechanism in CdTe quantum dots.

Because of the presence of some imperfections on the crystal the radiative recombination does not always occur. These *"traps"* are Cd or Te atoms with dandling bonds, which can attract electron and holes, respectively, acting as mid gap states. In the case of an electron, when declining from the conduction band it can be captured by a trap and then relax to the valence band without emitting light or emitting a strongly red shifted radiation.
Independently from the trapping, the maximum of the emission peak is red-shifted with respect to the excitonic peak in the absorption spectra (Figure 4). This phenomenon is usually referred to as Stokes-shift and has its origin in the particular structure of the exciton energy levels of the NC. There are various explanations for the Stokes shift and the most common one refers to non-resonant absorption in wide size-dispersed samples. Resonant Stoke shift is usually due to a dark exciton ground state, but the nature of this can vary. A common dark ground state is caused by the exchange interaction between the electron and the hole producing a spin triplet ground state which is spin-forbidden for optical transition [9-11]. Another possibility consists on the electron and hole having different spatial envelope function symmetries.

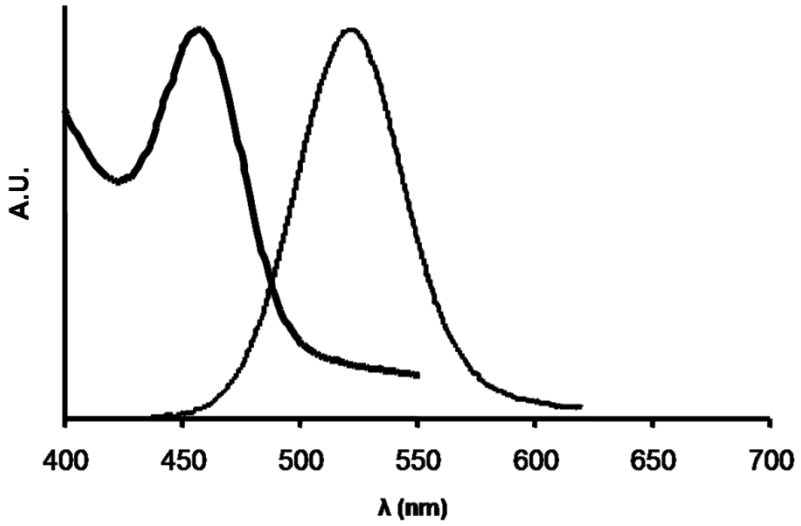

Figure 4 - Absorption and emission spectra of quantum dots.

3.3. Fluorescence quantum yield

The fluorescence quantum yield (QY) of quantum dots is the ratio between the number of emitted photons and the number of absorbed photons.

$$\phi_f = \frac{N_{em}(\lambda_{ex})}{N_{abs}(\lambda_{ex})} \qquad \text{Equation 18}$$

The maximum theoretical value is 1, but for QDs this situation is improbable due to two main reasons: first of all, because of the blinking phenomenon some dots are in the off state. The second reason is the presence of surface traps on the NC that act as fluorescence quenchers. Both of these limitations can be overcome by improving the surface passivation or the crystalline structure perfection. Using water synthesized CdTe QDs as an example one can see how the chemical nature of the thiol-capping can influence the QY [12, 13]. The reaction conditions can also compromise the QY, especially when the QDs are obtained by fast synthesis processes. In all instances, the best method to fix the imperfections and to diminish the possibility of a photo-oxidation of the NC is by growing an inorganic shell on the surface of the QD, creating a core/shell system.

4. Synthesis

Quantum dots can be synthesized by employing different techniques. The main difference relies on the surrounding media, and based on its nature one may have: *aqueous synthesis*, when the reaction medium is water, and *organic synthesis*, when the reaction medium is an organic compound. Considering that the work developed under the scope of this thesis focus the application of CdTe QDs synthesized in aqueous media this will be the approach highlighted. Before starting a succinct review of the available aqueous techniques it is important to refer some of the basic general principles concerning the crystal growth mechanism [14]. The crystal growth process can be divided in two main steps: *nucleation* and *growth*. Nucleation is the first stage in the synthesis of any kind of nanocrystal and can be defined as the first irreversible formation of a nucleus of the new phase. During QDs synthesis one will always speak in terms of homogeneous nucleation, because there is always a homogeneous stable phase that subsequently become metastable resulting, at the end of the synthesis, on a new phase different from the initial one. To get the formation of stable clusters it is necessary to overcome a certain barrier of energy in order to reach the system equilibrium between the crystalline phase and the solution phase. In the simplest case it could be considered that the two forces involved in this process, the gain of the *chemical potential* and the *total surface energy*, are competing between themselves. With the formation of a spherical nucleus with *n* atoms, the energy of the system will change as

$$\Delta G = n(\mu_c - \mu_s) + 4\pi r^2 \sigma \qquad \text{Equation 19}$$

were μ_c and μ_s are the chemical potential of the crystalline phase and of the solution phase respectively, r the nucleus radii and σ the surface tension. The last term involves the surface energy and is not negligible for nanocrystals because, owing to their low dimension, the most part of the atoms are on the surface. Consequently, a low number of interactions between surface and core atoms can therefore take place and the surface tension will be greater. Besides the particle size, the surface energy is also dependent from the shape of the nanoparticle. The presence of facets and their geometry results on different arrangement of the atoms and also influences the probability of occurrence of dangling bonds. Lower tensions are naturally found in crystals with closer packing of atoms and less vacant bonds. Assuming that the NC have a spherical shape and excluding any kind of variation of σ, Eq. 19 could be written as,

$$\Delta G = \frac{4\pi d_m}{3} r^3 (\mu_c - \mu_s) + 4\pi r^2 \sigma \qquad \text{Equation 20}$$

where d_m is the density of atoms in the crystal. At this point one can understand that: if the chemical potential of an atom in solution is lower that the chemical potential of an atom on the crystal the minimum of free energy of the system is achieved when all the atoms are in solution, so no crystals are formed. In the opposite case, the first term of the equation turns negative and the free energy will reach a maximum for a certain radii r_c (figure 5), named *critical size*, when nucleation happens. Plotting the system free energy in function of r a graphical representation of the nucleation is obtained.

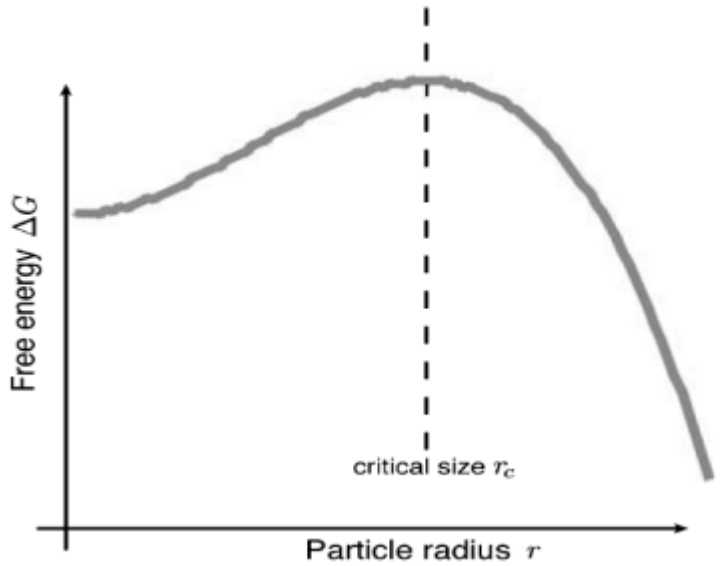

Figure 5 - Schematic representation of the nucleation barrier. Adapted from [14].

It is perceptible that the addition of monomers to this cluster will require energy until the radius r_c is reached. The value of the critical size can be calculated by:

$$r_c = \frac{-2\sigma}{\Delta G v} \qquad \text{Equation 21}$$

After this point any further addition of monomers will no longer require energy but will, in opposition, release energy. The critical size is characterized by a zero growth rate because the crystal is in equilibrium with the solution. For crystals smaller than r_c the dissociation of monomers is greater than the incorporation of fresh ones and the crystals melt down.

After nucleation, crystals will grow by deposition of monomers on the surface. Two steps are important during the growth stage: first the monomers need to reach the crystal surface and then they have to react with it. Monomers migration is dictated by diffusion, being the rate dependent of the diffusion constant *D*, while the speed of deposition depends only on reactivity between monomers and crystal surface. Accordingly, the growth rate $\dot{r} = \mathrm{d}r/\mathrm{d}t$ of a crystal with a radius *r* depends only on the rate at which the monomers are deposited on the crystal surface (following the two above mentioned processes), and is measured as the time derivative of the number of monomers *n* in the crystal.

$$\dot{r} = \frac{dr}{dt} = \frac{\dot{n}}{4\pi r^2 d_m} \qquad \text{Equation 22}$$

In a practical synthesis, a strong excess of monomers is added to initiate the growth process. Under these conditions the effect of the diffusion can be neglected and the growth rate will depend only on the monomer-crystal reaction rate. This growth regime is called *reaction controlled growth* and it is important only if a great excess of monomers is present. With this regime no defocusing of the NC population size is observed. After a while the concentration of free monomers decreases and the growth rate becomes dictated by the rate at which the monomers reach the surface. The flux *J* of monomers in the direction of the growing crystal is driven by a gradient of concentration *C*. Since the monomers are incorporated onto the crystal the concentration on its surface reaches the minimum. However, away from the surface and in the bulk of the solution this concentration is maximal. For that reason, the direction of the monomers flux will be towards the crystal surface. With some mathematical derivations one can write the growth rate as:

$$\frac{dr}{dt} = \frac{D}{r d_m}(C_b - C_i) \qquad \text{Equation 23}$$

where *D* is the diffusion constant, and C_b and C_i are the monomer bulk and surface concentrations, respectively. Because the crystal is not infinitely stable, the Gibbs-Thompson competing effect on the growth must be taken into account. This is based on the fact that smaller crystals have higher vapour pressure so their monomers are easily lost to solution, as previously referred. By applying the Gibbs-Thompson equation to

calculate the concentration of monomers found in the vicinity and away from the NC surface it is possible to calculate the growth rate as

$$\frac{dr}{dt} = \frac{2\sigma D C_{\infty}}{d^2{}_m k_B T} \frac{1}{r}\left(\frac{1}{r^*} - \frac{1}{r}\right) \qquad \text{Equation 24}$$

The critical size r^* is similar to r_c in the nucleation equation. As it can be perceived in Figure 6, the grow rate become negative for a crystal with a size inferior to r^*. This value depends primarily on the monomer concentration and also on the surface tension and temperature. It is also interesting to notice that the maximum of the growth rate is attained at $2r^*$. The synthesis is a dynamic process where the monomers are consumed and this fact promotes a shift of r^* and $2r^*$ to higher values. If all the crystals in the population are bigger than $2r^*$ then a *size focusing regime* is achieved, in which the smaller crystals grow faster than the bigger ones reducing size dispersion.

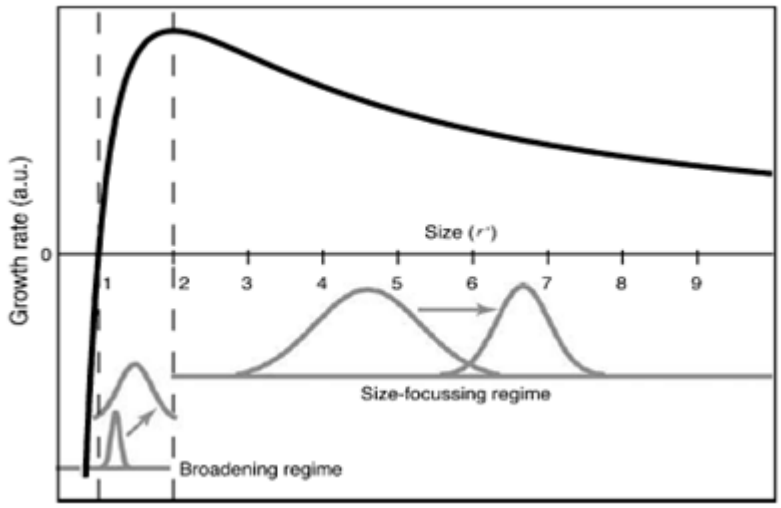

Figure 6 - Graphical representation of the growth rate in function of the size. Examples of broadening regime and size focussing regime are depicted. Adapted from [14]

When $2r^*$ reaches the lower tail of size distribution then a *broadening regime* is attained because the smaller crystal are growing slower than the bigger one. In the worst scenario, when r^* is larger than the radius of the smallest NC, the *Ostwald ripening regime* takes place wherein the smaller crystals melt down to free monomers that are subsequently incorporated into the bigger crystals. This situation is especially undesirable because size dispersion increases dramatically and the total NC concentration decreases.

4.1. Aqueous synthesis of quantum dots

The first work on the chemical synthesis of colloidal semiconductors nanocrystals was carried out in aqueous media in 1982 [15]. A colloidal silica solution was both used as carrier and stabilizer of CdS [15] and ZnS [16] colloidal solutions. By using styrene/maleic acid co-polymers or phosphates and polyphosphates as stabilizers, stable colloidal solutions of a wide range of semiconductor NC were synthesized [16-24], and all of the theoretical background about quantum confinement effects was introduced [25, 26]. Further development of the stabilizing techniques led, finally, to the use of thiol molecules [27, 28] in 1993. In the meantime, the hot-injection synthesis in high-temperature boiling organic solvents was developed in 1993 [29], representing a remarkable progress in QDs synthesis that focused the attention in this technique for the coming years, while the research on the aqueous synthesis was somehow left aside. During this time few groups continued working in an alternative approach to the organometallic synthesis and the work of Rogach in 1996 [30] could be considered a milestone for the successful aqueous colloidal synthesis of CdTe QDs, setting the foundations for all the future studies and developments in this field.

The aqueous synthesis process and conditions are extensively explained in many manuscripts [31]. Briefly, it consists in dissolving the right amount of Cd^{2+} (in the form of a salt) and thiol stabilizer (R-SH) in water followed by the subsequent adjustment of pH to the desired value. Then Te^{2-} is added to the solution, forming CdTe precursors. Finally, under reflux at 100ºC, in open air conditions, the formation and growth of the QDs occur. The numbers of variables affecting the synthesis process is very limited and are thoroughly discussed in literature. The first critical aspect is Te^{2-} generation. In earlier works [30, 31, 33, 37, 41, 45, 46] Al_2Te_3 was used to generate gaseous H_2Te, by reaction with H_2SO_4, and this gas was then transferred into the synthesis flask by using a N_2 flow (Figure 7). However, the limited availability of Al_2Te_3 and its increasing cost forced the search for an alternative source of Te. An electrochemical method [32] was one of these alternatives and was used for the synthesis of CdTe [33, 47] and HgTe [34] QDs. The most studied and applied approach consisted on the production of NaHTe by reduction of Te powder with $NaBH_4$ in water, firstly described by Zhang *et al.* [35]. Some variations to this method make either use of KBH_4 to form KHTe [36], or of the reaction of Te with $NaBH_4$ without heating with formation of sodium tetraborate precipitate and NaHTe supernatant [38-40, 42-44, 48, 49, 50, 51], or of the reaction of Te and $NaBH_4$ under heating [52-56].

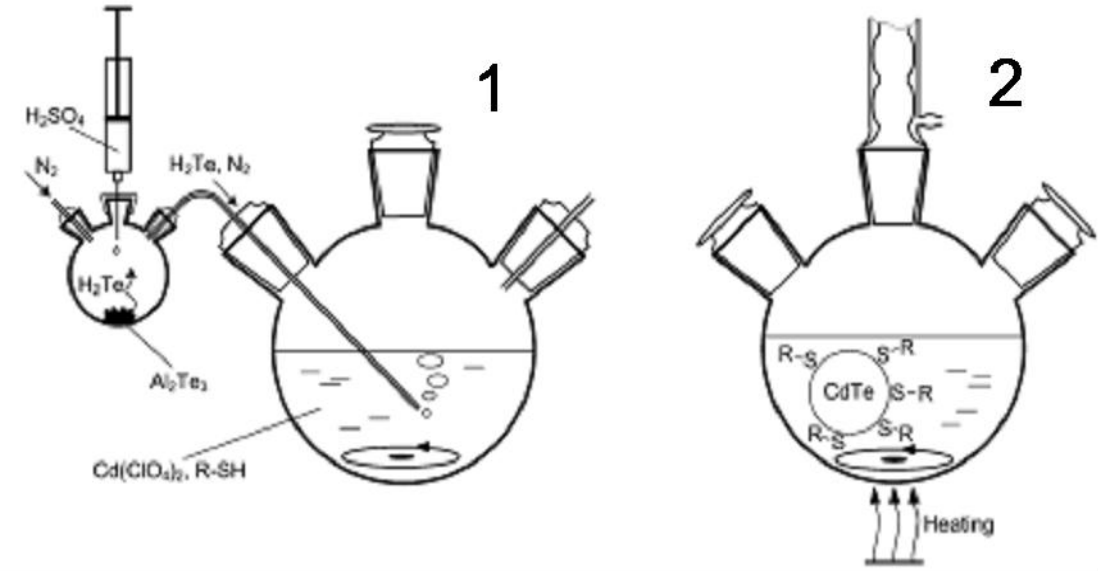

Figure 7 - Schematic representation of the aqueous synthesis of thiol-capped CdTe QDs. First phase: formation of CdTe precursors. Second phase: nucleation and growth of CdTe nanocrystals. Adapted from [31].

The main goal in QDs synthesis is to produce nanocrystals with a QY as higher as possible and with narrow size-distribution. For this reason an impressive number of studies examined the influence of pH and of the molar rate of R-SH:Cd and Cd:Te, showing that these variables are crucial in a synthetic process. On the other hand, the optimum values for these parameters depend on the nature of the capping ligand. The first capping agents used [30] were 2-mercapto-ethanol [57-58] and 1-thio-glycerol [59-61]. The former was seldom employed while the later was used in several studies, allowing the obtaining of QDs with QY up to 24.8%, at pH 11.5 with a molar ratio Cd:Te:TG of 1.0/0.5/2.4.

Hitherto, the most used and studied capping agents for CdTe QDs are mercaptopropionic acid (MPA) and thioglycolic acid (TGA). The main reason for their successful application is that they allow the most stable CdTe nanocrystals in aqueous solution. TGA was initially used as capping agent by Gao *et al* [62] but the proposed synthesis produced poorly luminescent QDs (QY 3%). Later studies demonstrated that by using a different Cd:TGA ratio (1:3) the QY showed an increase of up to 40-60% [41, 63-65]. The recommended pH value for TGA QDs synthesis is between 11.2 and 11.8 and the increase of the pH was found to accelerate the NC growth, permitting a "focusing" of the population's size [64].

Zhang *et al* [66] proposed the first application of MPA to passivate CdTe QDs surface. Subsequent studies [40, 43, 61, 65, 67-72] showed that, by changing the pH and the molar ratio, it was possible to obtain a lesser size-dispersed population and more perfect QDs. Guo *et al* [56] demonstrated that at extremely high pH values (pH=11.9) with Cd:Te

molar ratio between 10:1 and 30:1 it was possible to achieve an ultrafast synthesis of QDs, covering all the emission spectra (≈530 to ≈800nm) in 2 hours, and not in several days as it happened with the normal route, whilst maintaining the full width at half maximum (FWHM) between 50 and 90 nm and QY between 15 and 40%. Another thiol-acid used to synthesize negatively charged QDs was mercaptosuccinic acid. The first developed process was a one-pot synthesis at pH 5 with a Cd:Te:MSA ratio of 1:0.33:3, that produced QDs with a remarkable QY (83%) [73]. By further optimization of pH (11.2) and of precursor molar ratio, CdTe-MSA QDs with red emission (650nm) were synthesized in 2h in normal open air conditions maintaining high QY [74]. More recently, other acidic capping agents have been applied: dihydrolipoic acid (DHLA) [75] passivated QDs reached a QY of about 40% by hydrothermal synthesis, using a reaction temperature of 160 ºC, Cd:DHLA:Te ratio of 1:1.6:0.2 and pH in the range 10.8-11.2. 3-Mercaptobutyric Acid [76] was also employed in a hydrothermal synthesis with good results in terms of QY% (59%).

Especially interesting in terms of their increased biocompatibility and because of the presence of both carboxylic and amine groups are CdTe QDs capped with glutathione (GSH). Synthesis of these NC is performed normally in a one-pot approach [59, 77-79], in which there isn't a temporal separation between the generation of Te^{2-} and the crystal growth, being all the reagents added at the same stage. The first report on CdTe-GSH synthesis [77] showed that it was possible to grow crystals with high QY (60%) at pH 9, and that the growth rate influenced crystal quality. The one-pot synthesis was also possible without heating, using N_2H_4 as reagent [79]. Similar good results were also achieved by Zheng *et al* [80] with a classical synthetic 2-steps approach, by using a pH of 11.5 and Cd:Te:GSH ratio of 1:0.2:1.2. This synthesis was also used in a later work [44]. Cysteine (CYS), like GSH, is a molecule that exhibits –COOH and -NH_2 groups and has been already applied in QDs synthesis, especially for bio-labelling purposes. Mamedova *et al* used a typical two-steps synthesis [81], which was also used in later studies [44, 48, 61, 82, 83]. A one-pot synthesis employing N_2H_4 was also developed [59]. Positively charged CdTe QDs can be synthesized by using cysteamine as capping agent. The resulting NCs are stable in aqueous solutions at slightly acidic and neutral pH values (5.5±7.0) [84]. More recent studies successfully synthesized cysteamine-capped QDs by a classical 2-steps method [31, 87], a hydrothermal method [85], by ultrasonic irradiation [86] and with a one-pot procedure [88, 89].

As extensions or complementary alternatives for the conventional aqueous synthetic routes, hydrothermal [35, 36, 54, 85], microwave-assisted [39, 67, 70, 71, 90, 91] and photochemical synthesis [53, 54] processes of CdTe nanocrystals in aqueous solution have been implemented. Although all of these methods can effectively accelerate the growth of the CdTe QDs, the microwave-assisted synthesis revealed to be more feasible for

controlling the optical properties of the resultant nanocrystals [92]. As an example, TGA-capped CdTe QDs with fluorescence efficiency of 82% can be obtained within 15 min under microwave irradiation [72] while MPA-capped CdTe nanocrystals emitting in the near-infrared region (733 nm) can be obtained within 45 min [70].

5. Surface chemistry

Quantum dots size (usually in the range 1-10 nm), and the resultant quantum confinement effects, determine most of their optical, electronic and mechanical properties, rendering them quite different from bulk materials [8]. As it was previously referred, in bulk semiconductors the large number of atoms leads to the formation of almost a continuum of energy levels. The valence band, comprising the lower energy levels, is filled with electrons and separated from the unoccupied conductance band, corresponding to the higher energy levels, by a fixed energy gap. In quantum dots, due to their small size, the energy levels are discrete and the energy gap between the valence and conductance band depends on the nanocrystal size. The absorption of a photon, leading to the excitation of an electron from the valence band to the conductance band, is related with the band gap energy. Since QDs emission is size-dependent they can be tailored in a controlled way by adjusting the synthesis conditions to assure a fluorescence emission matching virtually any wavelength of the visible region. Apart from the band-gap tunability, QDs exhibit other relevant photoluminescent properties, namely an intense and highly stable against photobleaching fluorescence, potentially high quantum yield, broad absorption and narrow, symmetric emission spectra and long excited-state decay lifetimes. Moreover, the broad absorption bandwidth, due to the presence of multiple electronic states at higher energy levels, allows simultaneous excitation of multicolour QDs by using a single light source.

In terms of analytical applicability it should be emphasized that since adequate QDs fluorescence is only verified when the nanocrystals exhibited a proper surface passivation, the occurrence of surface imperfections that act as charge carriers traps could prevent electron-hole recombination favouring deactivation by non-radiative processes, thus reducing the QDs quantum yield, which could limit their analytical usefulness in situations involving, for instance, a fluorescence quenching. On the other hand, it is important to take into account that most of the analytical, catalytic or bio-targeting applications demand aqueous environments as reaction media and thus either the QDs are capped with hydrophilic ligands or suitable surface modifications strategies are used to

replace the non-polar encapsulating layer by more polar species, while preserving the stability and the luminescence properties.

In the application of quantum dots, controlling the nanocrystal size, morphology and surface-ligands is of primordial importance to control the optical properties, and therefore the photoluminescence response [93]. Depending on the analyte-targeting strategy other specific characteristics should be also taken into account. These include, but are not necessarily limited to: the occurrence of surface imperfections (traps), capping reactivity, capping thickness, surface charges, and solution stability. The influence on the QDs photoluminescence of ligands, ions, small molecules, adsorbates or other surface interactions that could affect the efficiency of electron-hole recombination could be used as a detection strategy. In effect, QDs quantum yield is a direct consequence of the occurrence of radiative (higher QY) or non-radiative (lower QY) recombination mechanisms. An analyte inducing a concentration related luminescence enhancement or quenching upon charge transfer, mechanical adsorption, ion chelating or ligand exchange could be most likely determined by using QDs. In this regard, an analyte promoting a luminescence enhancement could be more adequately determined by using QDs with lower QY, while when a luminescence quenching is intended QDs with initially high QY are likely to provide improved results.

Aside from their well known photoluminescent properties QDs show catalytic properties for redox reactions, size dependent catalytic action and controllable charge and electron transfer events. These properties could be exploited to maximise the response signals of instrumental methods of analysis, enhancing detection and improving sensitivity, to increase the selectivity or the kinetics of a given chemical reaction or even to implement new reactional schemes. Chemiluminescence (CL) and electrochemiluminescence (ECL) measurements are based in redox reactions involving suitable luminogenic compounds or precursors and/or adequate electrochemical conditions. The reactional process usually entails the formation of short-lived intermediate radicals that result in unstable products that decompose to form electronically-excited molecules that relax upon light emission [94]

Quantum dots can be applied as luminescent probes for many species either biological or chemical. The sensitivity of the involved photophysical processes related to the formation of the fluorophore-target analyte pair depends markedly on the outer stabilizing capping layer surrounding the nanocrystals. Therefore, an important balance between the solution stability of the QDs associated with the capping and the target recognition event affecting the photoluminescent properties of the nanoparticle should be maintained during measurements. This is a noteworthy dilemma when batch-procedures are involved. The need for stable readouts associated with chemical equilibrium could be a hindrance

because surface interactions not only change the photoluminescence response but also the quantum dots solution stability. Consequently, more pronounced signal intensity could be achieved only at the expenses of a poorer stability, which could ultimately result in no reading at all. Automation of all reactional processes, including sample and reagents (QDs) mixing, reaction development and analytical signal measurement and/or acquisition could allow overcoming this hindrance by means of reproducible solutions insertion and timed reaction development without the need for attaining equilibrium conditions.

6. Automatic methods of analysis

In the last decades has increased the need for the development and implementation of automatic methods of analysis in order to facilitate the carrying out of analytical procedures and to allow performing a large number of determinations in a reduced time. Automation of analytical procedures in chemical analyses enables to respond quickly and effectively to the demands of analysis involving a large number of samples or complex sample manipulations with diminished human intervention and the reduction or elimination of several factors that could impair the performance of the analytical procedures. The development of automated methods and its implementation in analytical laboratories has been justified by several reasons, among which the most important are: the reduction or replacement of human participation in routine or hazardous tasks resulting in increased safety and in the prevention of subjective errors; improved analytical performance especially regarding results precision and accuracy; more rational use of the potential of the analytical instrumentation and better management of chemical reagents, resulting in more cost-effective procedures. In effect, reagents and sample consumption could be significantly reduced providing an optimization/rationalization of the analytical costs. Moreover, a judicious management of reagent consumption assured improved environmental safety, because of the decreased production of wastes and the minor laboratory staff exposure to toxic chemicals. The minimization of the costs is in harmony with rising social demands for improved living standards that expect continuous controls of the environmental pollution, of water resources, enhanced food and drink quality control and management, etc, wherein it is usually necessary to resort to laborious and time-consuming analytical routines of a large number of samples [95]. Automatic methods of analysis have been also applied in different fields including clinical and toxicological analysis, industrial process control, routine analysis of air, water and soil and quality control of food, pharmaceutical and agricultural products [95]. The increasing

interest and implementation of such methodologies has led to apply new concepts and expressions, requiring a standardization effort by the IUPAC (International Union of Pure and Applied Chemistry) in order to standardize definitions. The IUPAC Commission for Analytical Nomenclature established a series of definitions which distinguish and specify the essential characteristics of automatic methods of analysis. One of the most important IUPAC recommendations concerns the clear distinction between automatic and automated devices [96]. *Automatic devices* are defined as those that execute certain required actions to be performed at given points in an operation, without human intervention. These systems have no autonomous decision capacity, because there isn't a feedback system, so they carry out the same operations sequence always in the same way. On the contrary, *automated devices* possess a feedback system which allows them to make decisions without human intervention, and differently to automatic systems they are self-monitoring and self-adjusting, possessing a higher independence of actuation. In this field, other terms are frequently used and it is important to clarify the concepts associated with them in order to avoid ambiguousness. For this reason, IUPAC clearly made a distinction between mechanization, instrumentation and automation [96]:

(i) Mechanization is the use of mechanical devices to replace, refine, extend or supplement human effort.

(ii) An instrument is a device used to observe, measure or communicate a parameter, which replaces, refines or supplements human action.

(iii) Automation can be defined as the combined use of mechanical and instrumental devices to replace, improve, extend or supplement human effort and faculties in the performance of a process, in which at least one operation is controlled, without human intervention, through a feedback system.

Feedback systems are instrumental devices that combine sensing and commanding elements which can alter the performance of the process at different moments. Automatic methods of analysis can be divided into different categories, depending on the sample processing strategy [95]:

(i) Discrete or batch methods: in this group are included all those techniques based on static analysis criteria. The samples preserve their physical integrity and are stored in separated vessels. Detection can be done directly on the vessel or the sample can be transferred to the detector.

(ii) Robotic methods: involve the use of a robot controlled by a computer. The robot performance mimics the actions of a human operator. A laboratory robot consists usually on a moving arm fitted with a 'hand' that affords the movements required to transfer objects between places. Its work is limited to its close environment; this entails setting up a workstation where the robot and all the instruments on hand are interfaced to a

computer. Theoretically, there are no analytical constraints to the robot's performance, so every kind of task can be exploited by this method. Robot can be distinguished from other automatic systems because of their ability to perform different tasks different from those programmed in advance, a characteristic due to the programming, reprogramming or even self-programming routines that could be included in the software that manages the device.

(iii) Flow methods: the sample solutions are successively introduced at the same point into a channel carrying a liquid or gas, commonly known as carrier stream, being the samples propelled towards the detection. During the propulsion of samples from the insertion point to the detector, they can be subjected to one or more chemical reactions (or any other type of analytical operation) in order to properly condition the samples for the determination. Thus, the channels carrying the samples can merge or not with other channels carrying reagents, buffers, masking agents, etc. Upon reaching the detector, the analytical signal is continuously monitored over time and each sample or reaction product yields a transient signal whose height or area could be related with the parameter under evaluation.

According to the type of used flow these flow methods can be classified as segmented flow methods and non-segmented flow methods:

(i) Segmented flow methods, were firstly introduced by Skeggs [97]. The flowing stream is segmented by air bubbles that are primarily intended to prevent sample dispersion and the maintenance of the identity and integrity of each sample. The bubbles inserted are removed prior to the detection, in order to avoid interferences in the analytical signal.

(ii) Non-segmented flow methods, were developed by Ruzicka and Hansen in 1975 [98]. In this technique small volumes of sample are inserted directly into the carrier system and the flow is not segmented by air bubbles. The injected sample forms a zone, which is then transported toward a detector that continuously records a certain physical parameter (absorbance, fluorescence, electrode potential etc.). The enormous analytical value of these methods arise from the lower installation and operation costs, higher flexibility based on a modular structure that allows its simplified reconfiguration to new analytical situations and also the higher facility of operation and control. Additionally, these methods enable the minimisation of consumption of sample and reagents and a reduction in the analysis time.

6.1. Multipumping flow system

Despite the potential already demonstrated by flow techniques such as Flow Injection Analysis (FIA) [98], Sequential Injection Analysis (SIA) [99], Multicommutation (MCFIA)

[100], Multisyringe (MSFIA) [101] and Single Interface Flow Analysis (SIFA) [102] in this work, and due to their analytical potential, versatility and ease of implementation and control, all analytical flow systems were based in the multipumping flow concept [103].
Multipumping flow system (MPFS) is a strategy for fluid management allowing the implementation of continuous flow-based analytical procedures that was developed in 2002 [103]. This technique differs from other flow approaches in several aspects, including manifold components and configuration, operational mode and flow hydrodynamics characteristics.

6.1.1. Manifold components and configuration

The MPFS manifold (Figure 8) is based on the utilization of solenoid micro-pumps that are operated individually or in combination for the propulsion (or impulsion) of liquids, which can act, at the same time, as sample/reagent insertion devices and commutation units. All the fundamental operations in an automatic flow system, like sample insertion, reagent addition, solutions mixing and the transport of the reaction zone toward the detector are performed by the same manifold component (solenoid micro-pumps) that are the only active devices. Reductions of the number of manifold active components permits a very simple configuration and control of the flow system minimizing the probability of occurrence of equipment malfunctions or errors. Micro-pumps are solenoid operated devices designed to provide a precise, repeatable and discrete dispense of solution volumes. These solenoid micro-pumps are provided with a non-metallic and chemically inert path, and they also offer a high grade of accuracy, precision, robustness and miniaturization.

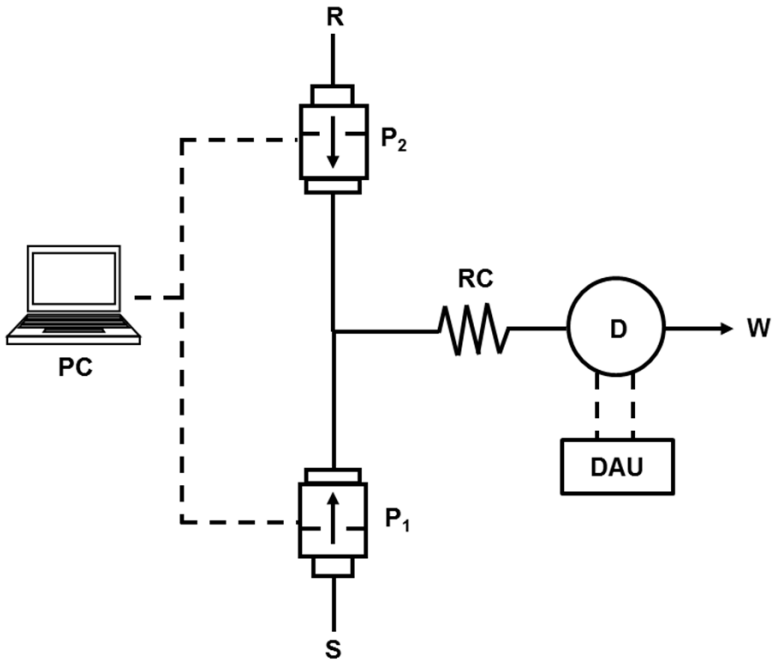

Figure 8 - Diagram of a typical MPFS manifold. PC, computer; S, sample; R, reagent; P1 and P2, solenoid micro-pumps; RC, reactor; D, detector; DAU, data acquisition unit; W, waste

6.1.2. Operational mode

In a multipumping flow system a high flexibility, in terms of solution insertion, flow rate management and sampling strategy, is guaranteed by the individual control of the micro-pumps. The sample and reagent solutions insertion into the system is controlled by means of a time-based or a pulse-counting routine. This provides a great versatility and precision in the selection of a given sample/reagent volume. Considering the fixed stroke volume characteristic of the micro-pumps, the sample and reagent volume can be easily calculated by the number of pulses inserted into the flow system through the repeated actuation of the respective micro-pump. Also, the flow rate can be easily determined by the stroke volume and the frequency of the micro-pump actuation (pulse frequency). An advantage of the operational mode of MPFS is that the position of the sampling zone in the flow system can be monitored by means of pulse-counting or volume-measuring routines, which enables a more efficient control of the sample transport throughout the flow manifold. This characteristic is extremely useful for the synchronization of the reagents addition and of the establishment of the reaction zone. Simultaneously, the efficient control of the position of sample zone allows an efficient control of the sample zone movement, facilitating for instance the halt of the flowing stream at a given location,

which can be fundamental in the implementation of kinetic methods and stopped-flow strategies [104].

Because of the micro-pumps characteristics and their individual controlled actuation different sampling strategies can be exploited in MPFS: (i) single sample volumes that consist in the insertion of a unique volume of sample solution comprised between two identical plugs of reagent or directly into the flowing carrier stream, providing only two reaction interfaces. (ii) binary sampling strategy, easily performed in a MPFS by the alternated actuation of sample and reagent micro-pumps. Using this strategy intercalation of plugs of sample and reagent solutions is obtained, establishing multiple reaction interfaces, with the advantage of a better reaction zone homogenization when compared with the single volumes approach. (iii) merging zones approach is carried out by simultaneous actuation of sample and reagent micro-pumps permitting an instantaneous homogenization of the sample/reagent system. These different strategies enable a versatile manipulation of the sample/reagent mixing and sample dispersion, therefore of reaction development.

6.1.3. Flow hydrodynamic characteristics

A fundamental difference between multipumping flow systems and more conventional flow-based methods resides in the hydrodynamic properties of the flowing stream. If in almost all continuous flow systems the flow is laminar, in MPFS is characterized by chaotic pulses that are generated by the actuation of the solenoid pump, which, upon the displacement of the pump diaphragm produces a burst of solution. The pulsed flow can be imagined as a chaotic movement of the solution in all directions that, consequently, promotes a faster and more efficient mixture of samples and reagents solutions regarding the methodologies based on a laminar flow regime, wherein the interpenetration between solutions only depends on the phenomena of diffusion and convection [104]. This characteristic can be advantageous for slow chemical reactions or when high viscous solutions are employed, a situation at which this system can provide an enhancement of the sensitivity.

Due to the hydrodynamic characteristics of MPFS, a higher degree of sample/reagent mixture can be achieved, as it was already corroborated by some scientific works [103, 105, 106] in which the performance of a MPFS and a conventional continuous flow-based system with laminar flow regime were evaluated under the same circumstances by using similar manifold configurations.

Lapa *et al* [103] exploiting a reaction with diphenylcarbazide for the determination of Cr(VI) concluded that the analytical signals provided by the multipumping system (pulsed flow) were three times higher than those obtained with the FIA system (laminar flow). When comparing the flow pattern inherent to multipumping and multicommutation concept, by using a dye solution and by implementing a slow chemical reaction, Dias *et al* [105] verified that the utilization of pulsed flows allowed enhanced mixing conditions, lower reagent/sample consumption, improved analytical sensitivity and reduced sample broadening when compared with laminar flow. More recently, Fortes *et al* [106] confirmed that by using MPFS the height and width of the recorded peak as well as the washing time were significantly improved, permitting better sensitivity and higher sampling rate relatively to flow systems relying on laminar flow.

Despite the superior characteristics of pulsed flows, which are the hallmark of the flow systems based on the multipumping concept, they have, as all other flow techniques, a boundary or a limit in terms of the full exploitation of this potential. In effect, being the pulse volume an important parameter regarding the efficiency of the reaction zone homogenization, since it determines the volume of segments that are mixed and/or intercalated, it is clear that the utilization of very high stroke volumes leads to more difficulties of sample/reagent mixing, which could result in irregular and poorly reproducible analytical signals [107]. This problem is easily overcome by resorting to micro-pumps with lower stroke volumes that ensure a more reproducible pulsed flowing stream allowing the enhancement of the mixing efficiency and enabling the attainment of improved analytical signals. The pulse volume also affects the analytical signal profile, can be seen in figure 8.

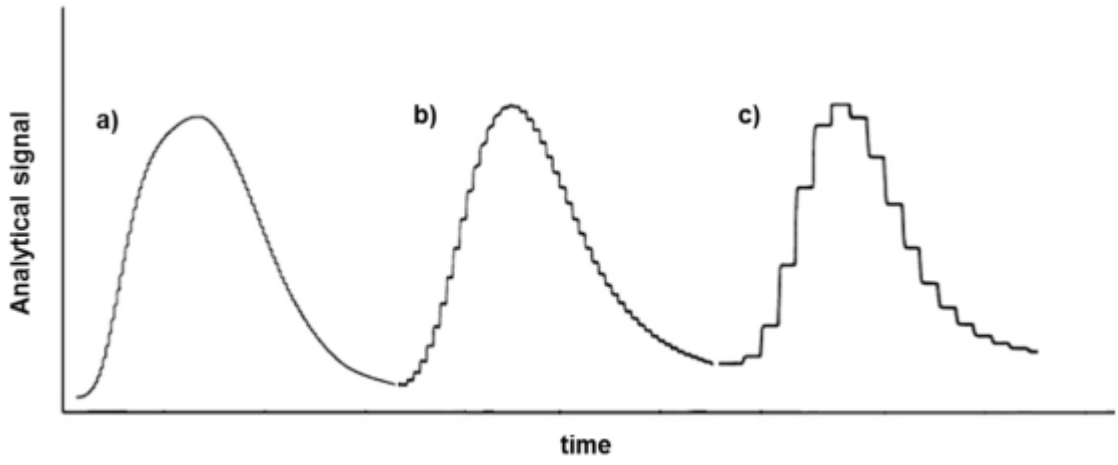

Figure 9 - Analytical signal profiles obtained by inserting into a MPFS, a Brilliant Green solution (95.0 mg L-1) by means of a 3 μL (a), 8μL (b) and 25 μL (c) per stroke solenoid micro-pumps. Peaks recorded at 12 cm min-1. Adapted from [103]

The nature of the pulsed flow can be perceptible when analyzing the stair-like profile of the recorded analytical signals. This profile is mainly dependent on the volume of the stroke, pulse frequency, length of the reactor and internal volume of the detector's flow cell.

7. Analytical applications of quantum dots

Due to vast number of analytical applications employing quantum dots available in literature, that make impossible the carrying out of a comprehensive review, this section aims exclusively at discussing some of the analytical applications of quantum dots that resort to automated method of analysis, therefore profiting from their advantageous features, which allow overcoming most of the limitations associated with discrete or batch approaches. As it was previously referred, it was decided to include in this automation topic flow-based techniques, which are valuable tools that could assure all the requisites for a more expeditious and efficient utilisation of QDs as chemosensors in combination with distinct detection modes, as well as flow-related techniques such as liquid chromatography and capillary electrophoresis. In terms of detection techniques, the QDs-related photoluminescent properties (fluorescence and chemiluminescence), are obviously put in evidence [12].

7.1. Fluorescence

As it was previously referred, in recent years QDs have emerged as remarkable fluorescent materials in numerous biological applications with noteworthy advantages regarding comparable organic molecular probes. The photoluminescence properties of QDs are indeed their most relevant feature in a chemical analysis perspective. The ability to absorb light at a broad bandwidth and to emit at a narrow spectrum, being the emission intensity dependent on the quantum yield, which in turn is conditioned by the type of surface interactions that the QDs established with the target analyte, has been exploited to implement assorted fluorescent analytical methodologies.

7.1.1. Direct fluorescence measurements

Pioneering studies focusing the interactions between quantum dots and metal ions showed that the luminescence response was markedly affected by the nanocrystals surface capping ligands [108, 109]. As a result, by suitable selection within a variety of QDs surface ligands it would be possible to establish specific chemosensors. Amid the multiple organic capping agents that have been subsequently exploited for QDs surface modification and to implement selective analytical applications, mercapto-acids [110, 111], and mercaptoamines [31] were those providing the best results. The type of modification on the QDs luminescence response depends on the capping and also on the chemical nature of the target analyte being its magnitude ideally concentration related. Distinct QDs fluorescence modification strategies have been exploited such as intensity enhancing and quenching and emission wavelength shifting. The most exploited mechanism was, with no doubt, the quenching effect (Figure 9), where a given analytes reduces the QDs PL emission by interacting with his surface or capping. Depending on the interaction between quencher and QDs, quenching could be either static or dynamic, and these could be distinguished by their differing dependence on temperature. For static quenching the rate constants decreased with increasing temperature while for dynamic quenching the opposite phenomenon occurred [112].

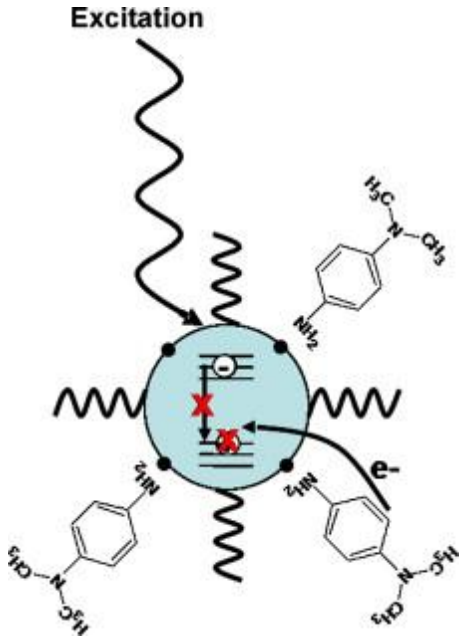

Figure 10 - Schematic quenching process for QDs particle [12].

A literature survey reveals that a great number of analytical methods have been already developed with analytical purposes, especially for metals [113-122] and organic molecules

monitoring [87, 123-131]. All of these methods, except one, relied on batch approaches involving the manual handling of sample and reagents solutions for reaction implementation and signal measurement. The only exception resorted to an automated continuous flow system. In this work, Butwong et al. [132] developed a methodology for the determination of arsenic in water based on the fluorescence quenching of CdS-MAA quantum dots using a sequential injection analysis (SIA) system coupled to an online gas-diffusion unit for arsine (AsH_3) generation. The generated arsine diffused through the polytetrafluoroethylene (PTFE) membrane and interacted with CdS-MAA QDs promoting the fluorescence quenching. The main parameters that influenced the fluorescence intensity such as CdS-MAA QDs concentration, pH, the nature and the concentration of the buffer were evaluated. pH strongly affected the quenching ability of CdS-MAA QDs fluorescence intensity by AsH_3. The highest relative fluorescence intensity (I_o/I) was observed when using a pH of 4.6, indicating a maximum quenching. The use of acetate buffer (10 mmol L^{-1}) provided higher fluorescence intensity when compared with the phosphate buffer. The proposed interaction mechanism was based both on the fact that there was no significant shift of the FWHM of the absorption and fluorescence spectra when increasing the concentration of arsenic and also in the appearance, in the IR spectra, of new peaks at 1160, 1050 and 1020 cm^{-1}. These evidences, in combination with the ability of AsH_3 to reduce covalent bonds, supported the authors' assumption that the quenching of CdS–MAA QDs fluorescence intensity occurred as a consequence of the formation of new bonds As–S on MAA functional group on CdS–MAA QDs surface. The developed analytical system combining the sensitivity and selectivity provided by the QDs fluorescence quenching with the simplicity, ease of operation and automation level of the automated flow system revealed to be a successful and expeditious strategy for the determination of arsenic in spiked ground water samples, showing that this synergy has a huge potential that could be advantageously applied in countless analytical circumstances.

7.1.2. FRET

In the last decades Förster resonance energy transfer, also known as fluorescence energy transfer (FRET), has gained a noteworthy relevance as a powerful tool in physical chemistry and biophysics. Perrin and Förster first theoretically described the process of non-radiative transfer of energy from a donor (or sensitizer) chromophore, in an excited electron state, to an acceptor chromophore over distances of up to 10 nm. Along with the orientation factor, the spectral donor emission/acceptor absorption overlap and the distance (r) between the donor and the acceptor are parameters that affect the FRET

effectiveness. In this regard, the distinctive QDs size-dependent photoluminescent properties make them superlative donors (10). In effect, the tunable size achieved during the QDs synthesis makes it possible to vary this parameter (r) as well as it enables matching the QDs emission wavelength with the acceptor absorption maximum, creating and adjusting sensing systems with enhanced sensitivity.

In literature, many assays using QDs and FRET have been reported in which QD-based nanosensors with QDs as FRET donors and organic dyes as acceptors have been used [133]. However, the opposite situation, in which the organic dyes acted as donors and the QDs as acceptors, has been seldom exploited. On the other hand, the combined utilization of automated methods of analysis, such as continuous flow analysis systems, and quantum dots for the implementation of FRET based assays has been only vaguely examined in chemical and biological studies. Indeed, only a few examples in which QDs-based FRET is combined with microfluidic devices are found in literature.

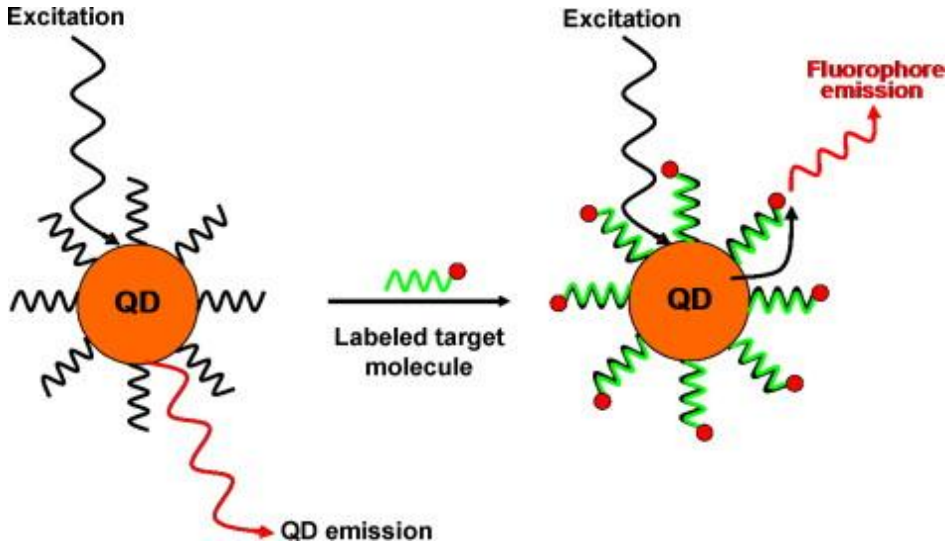

Figure 11 - FRET process for QDs [12].

In 2006, Zhang and Johnson [134] described a novel approach to improve the detection sensitivity of QD-based nanosensors using single molecule detection in a capillary flow. By using commercially available streptavidin-coated QDs as FRET donors and cyanine dye (Cy5) as acceptor, QD-based biosensors were developed for the rapid and sensitive detection of DNA. To this end, single-stranded Cy5-labeled 25-mer DNA (ssDNA) and double-stranded Cy5-labeled 25-mer DNA (dsDNA) were assembled onto the 605QD surface by specific streptavidin-biotin binding. The binding of dsDNA/ssDNA to 605QD resulted in the formation of 605QD/DNA/Cy5 complexes. Upon excitation with a wavelength of 488 nm, FRET occurred between 605QD and Cy5s in the complexes. The authors verified that the FRET efficiency improved with the increasing DNA-to-605QD

ratio in both 605QD/dsDNA/Cy5 and 605QD/ssDNA/Cy5 complexes since a single 605QD had multiple Cy5-labeled dsDNA/ssDNA assembled on its surface. When comparing the two complexes, the FRET efficiency was higher in 605QD/ssDNA/Cy5 complexes because of the higher flexibility of ssDNA in solution, which could form a random coiled conformation that consequently brought the Cy5 acceptor spatially closer to the 605QD. The deformation of DNA in the capillary stream increased the FRET efficiency of 605QD/DNA/Cy5 complexes comparatively with the one that was achieved in bulk measurements.

The same conjugates QDs (605QD) were used to develop an expeditious convergence of microfluidics and QD-FRET technique for monitoring the self-assembly of chitosan/DNA polyplexes under laminar flow in real time [135]. The 605QD, used as FRET donor (excited at 488 nm), and Cy5, used as acceptor, were labeled to plasmid DNA (pDNA) and chitosan, respectively, and subsequently the pDNA/chitosan interactions were monitored via FRET signals. According to the authors, the convergence of QD-FRET and microfluidics enables an innovative platform to monitor fundamental reactions with high sensitivity and milliseconds resolution.

More recently a solid-phase nucleic acid assay within an electrokinetically driven microfluidic system using immobilized QDs biosensors was presented [136]. A green-emitting CdSe/ZnS QDs was conjugated with two different oligonucleotide sequences, one of the oligonucleotide sequences being available as a linker for immobilization via hybridization with complementary oligonucleotides located on a microfluidic channel while the second one served as a probe to transduce hybridization with the target nucleic acid in the sample solution. This way, CdSe/ZnS QDs was used as FRET donor and a Cy3 label, on the target oligonucleotide sequences, was used as acceptor providing an analytical signal to monitor the hybridization detection.

7.2. Chemiluminescence

Chemiluminescence (CL) is typically defined as the emission of light by a molecule as consequence of a chemical reaction. In recent years, however, research has been focused not only in molecules but also in the CL of nanomaterials systems, to expand the field of applications of this mode of detection and to attain improved sensitivity and stability, mainly resulting from the high surface area and special structure of nanoparticles. Effectively, most CL reactions show low quantum efficiencies and therefore weak luminescence. This hindrance can be overcome by resorting to fluorescent compounds with high quantum efficiencies acting as sensitizers. In this particular QDs, due to their

reactivity, brightness and continuous band gap tunability, have attracted great attention. Indeed, the use of QDs for instance as chemiluminescence emitters in combination with CL equipment capable of wavelength discrimination can profit from multicolour labelling at a wide range of wavelengths without excitation light source [137]. Moreover, the combined utilisation of differently sized nanocrystals targeting distinct molecules could enable multi-parametric monitoring.

There are three possible mechanisms that could be used to explain the participation of QDs in a CL reaction: i) as emitter species, after direct oxidation; ii) as catalysts of a reaction involving others luminophores; iii) or as emitter species, after chemiluminescence resonance energy transfer (CRET).

The identification of the QDs role in a CL emission could be a challenging task. In fact, when for instance the QDs are the final emitters, it is particularly difficult to find out if the CL generation mechanism is associated with a direct QDs oxidation or a CRET phenomenon has occurred. Sometimes, it is also possible that the two mechanisms take place simultaneously. Nevertheless, in a broad perspective, when in a CL system the QDs are the only luminescent compounds one can definitely presume that a direct oxidation took place. However, if an additional luminophore is also included in the reactional scheme, the mechanism can be either CRET, if the final emitters are the QDs, or CL catalysis by the QDs, when the final emitter is the luminophore.

7.2.1. Direct chemiluminescence

Direct QDs chemiluminescence (Figure 11) QDs happens when an electron is injected in the conduction band (eq. 25) and a hole is injected in the valence band (eq. 26). The chemically generated exciton then relaxed and upon electron-hole recombination (eq. 27) radiant energy is emitted as showed in eq. 28;

$$O_2^- + CdTe \rightarrow CdTe(e^-_{1Se}) + O_2 \qquad \text{Equation 25}$$

$$OH^\bullet + CdTe \rightarrow CdTe(h^+_{1Sh}) + OH^- \qquad \text{Equation 26}$$

$$CdTe(e^-_{1Se}) + CdTe(h^+_{1Sh}) \rightarrow (CdTeNCs)^* \qquad \text{Equation 27}$$

$$(CdTeNCs)^* \rightarrow (CdTeNCs) + hv \qquad \text{Equation 28}$$

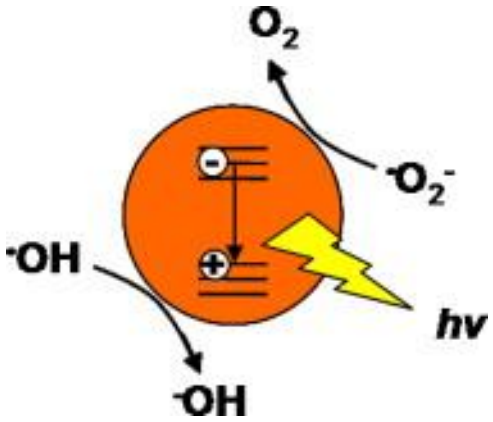

Figure 12 - Chemiluminescence emission process for QDs [12].

Wang et al [137] were the first to directly oxidize CdTe TGA capped nanocrystals in solution with a corresponding CL emission. In this work, the evaluation of the influence of the oxidants used in the reaction showed that the intensity of the CL generated was dependent on the oxidant nature, as H_2O_2 > $KMnO_4$ > KIO_4 > Ce^{4+} > $K_3Fe(CN)_6$ > $(NH_4)_2S_2O_8$, even considering that H_2O_2 was 1 mol L^{-1} and $KMnO_4$ was 1x10^{-4} mol L^{-1} and that the CL reaction was faster in the case of $KMnO_4$. Following these results, the authors have used a flow-injection chemiluminometric system and the CdTe-TGA/ H_2O_2 system to study other fundamental parameters affecting light emission such as pH, QDs size and concentration and the presence of different kinds of surfactants. The obtained results demonstrated that the CL intensity increased linearly with the H_2O_2 concentration (until 1 mol L^{-1}) and the QDs concentration (until 1 mmol L^{-1}). In alkaline medium the reaction was strongly enhanced and the optimal value for the NaOH concentration was 0.2 mol L^{-1}. An important finding was that QDs CL emission was dependent of the QDs size, according to the CL energy matching theory [138]. Surfactants also promoted light emission, especially cetyltrimethylammonium bromide (CTAB) and β-cyclodextrin (β-CD). CTAB, due to his cationic nature, interacted with TGA in the QDs surface and promoted the formation of nanocrystals aggregates, reducing the distance between nanocrystals and minimizing the energy loss by non-radiative processes, two aspects that favoured the formation of excited states. β-CD did not promote aggregation but formed a micellar nanoenvironment that reduced non-radiative processes. The reaction mechanism proposed for the CdTe-TGA/ H_2O_2 system is presented in Table 1.

By employing the same CL reaction system Li et al [139] studied the influence of metal ions on the generated CL using a steady-injection system. The effect of the main variables, including pH, H_2O_2 concentration and size and concentration of QDs, were confirmed. Of the metal ions studied Ba^{2+}, Ca^{2+}, Cu^{2+}, Fe^{2+} and Pb^{2+} promoted a CL enhancing. Under the optimal reaction conditions for Fe^{2+} a linear relationship between CL intensity and Fe^{2+} concentration in the range from 0.1 to 10mmol L^{-1} was verified, while for Pb^{2+} CL a ternary

function response to the logarithm of Pb^{2+} concentration in a range from 0.01 to 10 mmol L^{-1} was observed under the same circumstances. Cr^{3+}, Ni^{2+}, Zn^{2+} and Ag^{+}, on the other hand, were responsible for a decrease in the CL intensity proportional to the logarithm of metal concentration. The authors proposed the application of the developed system for the detection of these metal ions.

In another work, Li et al [140] used a similar flow-injection analysis (FIA) system to investigate the CdS-MA/H_2O_2 and apply it to assess the effects of selected biological molecules as model compounds for future applications. The general principles regarding the influence of pH and NaOH and H_2O_2 concentrations were once again confirmed, as it was the enhancing of CL response for increasing QDs size and concentration. The influence of cationic surfactant CTAB was similar to the previously referred, but differently from CdTe-TGA/H_2O_2 system. β-CD did not promote a signal enhancing, maybe because of the different capping used. The most important difference resided in the reaction mechanism that was proposed (Table 1). They authors sustained that peroxide and superoxide radicals were formed by the reaction of a base (OH^-) with H_2O_2, and that O_2^- can form $OH^{\cdot}$ by Haber-Weiss reaction. Nonetheless, the core reaction that led to the formation of the exciton was identical. The developed CL system was tested with some reducer molecules and ions that reveal to inhibit, with no exception, the CL signals. This happened because compounds with reducing activity can compete with QDs for the reactive oxygen species, while the metal ions can interact with the QDs surface changing the CL properties. The obtained results showed that the CL system exhibited a very good sensitivity for some compounds allowing the determination at concentration levels between 10^{-6} and 10^{-9} mol L^{-1} and wide dynamic concentration ranges of 2-3 orders of magnitude.

The HCO_3^- – H_2O_2 – CdSe/CdS-MAA CL system was implemented in FIA by Chen et al [141] and applied in the determination of ascorbic acid in human serum. An improved analytical system performance was verified in alkaline pH (11.16), $NaHCO_3$ 0.5 mol L^{-1} and H_2O_2 0.5 mol L^{-1}. It was also detected the CL dependence of QDs size with an enhancement of the analytical signal up to 2.14 nm. For bigger nanoparticles a CL decrease was observed. The CL intensity also increased until a QDs concentration of $6x10^{-6}$ mol L^{-1} decreasing for higher values probably because the chemical energy of the system was not enough to excite all QDs. The proposed reaction mechanism (Table 1) suggested the presence in the system of 3 emitters; $^1O_2$ that recombines into $^3O_2$ and emits light, $(CO_2)_2$* converted into CO_2 emitting light and the already mentioned excited form of the QDs (CdSe/CdS*) formed by $OH^{\cdot}$ direct hole injection into the 1Sh quantum confined orbital and by $^{\cdot}O_2^-$ electron injection into the 1Se orbital. The determination of ascorbic acid showed a linear range between $1x10^{-4}$ and $1x10^{-7}$ mol L^{-1}, and a detection limit of $6.7x10^{-9}$

mol L^{-1}. The developed method was applied to the analysis of human serum with low interference and acceptable performance.

Table 1 - Reactions for direct chemiluminescence [12].

Wang et al. [137]	$RSH + O_2 + OH^- \rightarrow O_2^- + RS + H_2O$ $O_2^- + CdTe \rightarrow CdTe(e^-_{1Se}) + O_2$ $O_2^- + H_2O_2 \rightarrow {}^{\bullet}OH + {}^1O_2$ ${}^{\bullet}OH + CdTe \rightarrow CdTe(h^+_{1Sh})$ $CdTe(e^-_{1Se}) + CdTe(h^+_{1Sh}) \rightarrow (CdTeNCs)^*$ $(CdTeNCs)^* \rightarrow (CdTeNCs) + h\nu$
Li et al. [140]	$H_2O_2 + OH^- \rightarrow HO_2^- + H_2O$ $H_2O_2 + HO_2^- \rightarrow O_2^- + OH^- + H_2O$ $O_2^- + H_2O_2 \rightarrow {}^{\bullet}OH + OH^- + {}^1O_2$ ${}^{\bullet}OH + CdS \rightarrow CdS(h^+_{1sh})$ ${}^{\bullet}OH + H_2O_2 \rightarrow H_2O + HO_2{}^{\bullet}$ $HO_2{}^{\bullet} + OH^- \rightarrow O_2^- + H_2O$ $O_2^- + CdS \rightarrow CdS(e^-_{1Se}) + O_2$ $CdS(h^+_{1Sh}) + CdS(e^-_{1Se}) \rightarrow (CdSNCs)^* \rightarrow h\nu$ $(CdS\ NCs)^* \rightarrow CdS\ NCs + h\nu$
Chen et al. [141]	$HCO_3^- + H_2O_2 \leftrightarrow HCO_4^- + H_2O$ $HCO_4^- \rightarrow {}^{\bullet}CO_3^- + {}^{\bullet}OH$ $H_2O_2 + {}^{\bullet}CO_3^- \rightarrow HCO_3^- + HO_2{}^{\bullet}$ $HO_2{}^{\bullet} \rightarrow H^+ + {}^{\bullet}O_2^-$ ${}^{\bullet}O_2^- + {}^{\bullet}OH \rightarrow {}^1O_2 + OH^-$ ${}^1O_2 \rightarrow {}^3O_2 + h\nu$ ${}^{\bullet}OH + HCO_3^- \rightarrow OH^- + {}^{\bullet}HCO_3$ $2{}^{\bullet}HCO_3 \rightarrow (CO_2)_2^* + H_2O_2$ $(CO_2)_2^* \rightarrow CO_2 + h\nu$ $CdSe/CdS + {}^{\bullet}O_2^- \rightarrow CdSe/CdS(e^-_{1Se}) + O_2$ $CdSe/CdS + {}^{\bullet}OH \rightarrow CdSe/CdS(h^+_{1Sh}) + {}^-OH$ $CdSe/CdS(e^-_{1Se}) + CdSe/CdS(h^+_{1Sh}) \rightarrow CdSe/CdS^*$ $CdSe/CdS^* \rightarrow CdSe/CdS + h\nu$

A similar HCO_3^- – H_2O_2 – CdTe system was tested [142] with the purpose of attaining a better comprehension of the CL reaction. The conclusion reached upon the utilisation of different selective scavengers for $^1O_2$, $OH^\cdot$ and $^\cdot O_2^-$ was in agreement with the general mechanism proposed in the previous work, putting an emphasis on the role of the excited form of CdTe as the emitter.

Recently, carbon dots were successfully applied to promote an enhancement of the CL signal obtained with $NaNO_2$ – H_2O_2 system [143]. This reaction was applied in a FIA system for the determination of nitrite in milk, river water and pond water samples. The CL enhancement was found sensitive to carbon dots, H_2SO_4, nitrite and H_2O_2 concentrations. CL intensity linearly increased for nitrite concentrations between $1x10^{-7}$ and $1x10^{-5}$ mol L^{-1} with a detection limit of $5.3x10^{-8}$ mol L^{-1}. As in previous examples, the CL emission for carbon dots was also due to the recombination of the already injected hole and electron (Table 1).

7.2.2. Chemiluminescence catalysts

QDs can be used in CL systems also as catalyst, due to the redox properties of both the conduction and valence bands. A strong oxidizer can inject a hole in the valence band of the nanocrystal or a reducer can inject an electron in the conduction band (Figure 12). In this manner QDs can either promote the formation of short-lived radical species (for instance hydroxyl and superoxide radicals) able to oxidize CL organic dyes, such as luminol, leading to a CL emission, or act themselves individually as radicals. Besides, in the generation of oxidizing species by photoirradiation of solutions of QDs [144], these can be considered as catalysts because the formed exciton acts itself as a redox system, producing radical species.

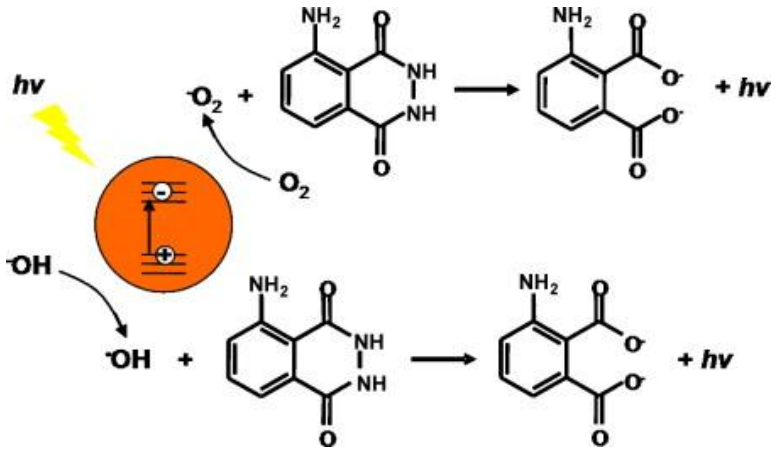

Figure 13 - Chemiluminescence emission with QDs as catalysts [12].

Wang et al [145] verified that the combined utilisation of TAG-capped CdTe QDs and luminol in the presence of $KMnO_4$ brought about a great sensitizing effect on the CL emission, the enhanced signals being a consequence of the accelerated luminol CL induced by the oxidized species of CdTe. Two interesting applications were therefore implemented by using both a 3-channel FIA CL sandwich-type immunoassay to detect human IgG and a 4-channel FIA CL system to detect catecholamines and other phenols compounds as well as ascorbic acid. For the detection of immunoglobulin a reactor with anti-IgG conjugate with Au nanoparticles was used. In a first step an IgG solution was passed trough the system, permitting the binding with the anti-IgG/Au conjugate reactor. Subsequently a QDs/anti-IgG solution was inserted forming the "sandwich" Au/anti-IgG-IgG-QDs/anti-IgG. Finally the reactor was placed near the CL detector and a luminol - $KMnO_4$ solution was inserted and subsequently sensitized by CdTe QDs containing probe to generate enhanced CL in alkaline medium, at a relative intensity directly related to the bound QDs/anti-IgG. The phenol compounds determination was carried out simply by measuring the CL quenching produced when these compounds were mixed in-line with the reagent solutions used to establish the luminol- $KMnO_4$-QDs CL system. The CL radiation spectra showed that the emitter specie was luminol, and that QDs played a promoting role, according to the mechanism displayed on Table 2.

Enhancement by ZnS-MPA QDs of the CL intensity of the luminol – KIO_4 system was demonstrated by Li et al [146] by means of a 3-channel FIA system. The CL enhancement was attributed to the catalytic effect of ZnS QDs, which presumably fostered the electron transfer process facilitating radical generation. Using a $2x10^{-5}$ mol L^{-1} KIO_4 solution in alkaline medium, the system was applied in the determination of lemofloxacine, a fluoroquinolone, which further enhanced the CL signal. It was proposed that upon KIO_4 oxidation and catalysis by ZnS, lemofloxacine was oxidized and promoted to an excited electronic state, which when relaxing favoured the formation of more excited 3-aminophthalate, the CL emitting specie (Table 2). The method was applied in the determination of lemofloxacin in capsules.

Table 2 - Chemiluminescence reactions for QDs as catalyst [12].

Wang et al. [145]	$Lum^- + {}^-OH + KMnO_4 \rightarrow Lum.^-$ $Lum.^- + KMnO_4 + (CdTe).^+ \rightarrow Lum^*$ $Lum^* \rightarrow Lum + h\nu$
Li et al. [146]	$IO_4^- + O_2 + 3OH^- + ZnS \rightarrow 2.O_2^- + .OH + IO_3^- + H_2O$ $Lum + {}^-OH \rightarrow Lum^- + H_2O$ $ZnS + FQs \rightarrow ZnS–FQs$ $ZnS–FQs + IO_4^- \rightarrow (ZnS–FQs(.OH)_2)$ $(ZnS–FQs(.OH)_2) + Lum^- \rightarrow Lum.^-$ $Lum.^- + .O_2 + (ZnS - FQs)_{ox} \rightarrow Lum^*$ $Lum^* \rightarrow Lum + h\nu$
Silvestre et al. [148]	$CdTe + h\nu \rightarrow CdTe(e^-_{Cb} + h^+_{Vb})$ $e^-_{Cb} + h^+_{Vb} \rightarrow h\nu_{PL}$ $^-OH + h^+_{Vb} \rightarrow .OH$ $O_2 + e^-_{Cb} \rightarrow .O_2^-$ $.OH/O_2.^- + lum \rightarrow lum^*$ $Lum^* \rightarrow lum + h\nu$

Another widely used CL system, pyrogallol- H_2O_2, was studied by Kanwal et al [147] and coupled with MSA-capped CdTe to accomplish enhanced CL generation. The QDs effect was size and concentration dependent. The proposed mechanism was quite unclear, mainly for what concerned the QDs role, although it was manifest that the final emitter was pyrogallol. The system was applied to Cr^{3+} determination with good results in terms of sensitivity (6 pmol L^{-1}) and selectivity.

An approach that put in evidence the role of QDs as catalysts was proposed by Silvestre et al [148]. In this work the capacity of QDs to generate oxidizing species in alkaline medium by photoirradiation (Table 2) was used to degrade organic matter and to develop an indirect chemiluminometric approach for the determination of chemical oxygen demand in wastewaters. By implementing an automated single interface reaction flow system the authors irradiated MPA-capped CdTe quantum dots generating radical species that degrade distinct organic compounds used as model compounds. The radicals also oxidised luminol used as luminogenic probe. The developed approach was applied to the analysis of certified materials (wastewaters) with good results.

7.2.3. CRET

CRET is the acronym of chemiluminescence resonance energy transfer (CRET) and could be defined as the non-radiative energy transfer between a chemiluminescent donor and a fluorescent acceptor that, like in FRET, are in close proximity (< 10 nm). In a very simplified mechanism description a luminogenic compound is oxidized and then excites the fluorescent acceptor. A CL system - such as, for instance, luminol/H_2O_2, which is one of the most sensitive CL reactions - is generally used, satisfying an essential condition that is the CL emission spectrum should have a maximum at a wavelength that overlaps the absorption spectrum of the fluorescent acceptor. QDs, exhibiting broad excitation spectra, are therefore well suited fluorescent acceptors to be used in CRET processes (Figure 13).
In CRET, and differently from what was referred in the previous section, QDs are the finals emitters and not the sensitizers, being this evidence clearly perceptible when monitoring the emission spectra. Also, with CRET it is difficult to understand if the QDs excited species are formed by a resonance energy transmission process or by a redox process, because in all reactions various reducing and oxidizing species are present. Another important issue is that in various situations QDs play a double role in the reaction: acting initially as sensitizers and after that as final emitters, sometimes even co-emitting with a CL organic dye.

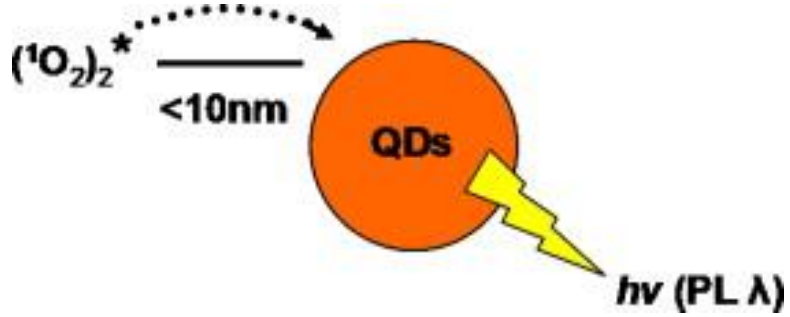

Figure 14 - Chemiluminescence emission in a CRET system [12].

TGA-capped CdTe QDs were applied in a Ce(IV) – SO_3^- CL FIA system by Sun et al [149] for the determination of various reducing organic compounds. The best CL signal was obtained using $5x10^{-4}$ mol L^{-1} Ce(IV) in 0.02 mol L^{-1} H_2SO_4 solution. The size and concentration dependent CL emission increase was already described. For the reaction mechanism (Table 3), it was assumed that a resonance energy transfer occurred between SO_2* and CdTe QDs that were the final emitters as confirmed by the CL spectra. All of the tested compounds produced a decrease on the CL emission.
Fortes et al [150] implemented an automated multi-pumping flow system combining Ce(IV) – SO_3^- – QDs CL system, using MPA-capped CdTe QDs for the determination of

two anti-diabetic drugs in pharmaceutical formulations. Both glipizide and gliclazide quenched the CL emission, probably due to radical scavenging activity. The results obtained in the analysis of 7 commercial samples were satisfactory and in agreement with those obtained with the reference method.

Effect of the capping-ligand in a $K_3Fe(CN)_6$ – CdTe system was studied by Zhang et al [151] using a FIA system. The reaction was found to be favoured in alkaline solution, like in all other circumstances in which a direct QDs oxidation took place. Amid the three studied capping-ligands MAA, GSH and CYS, GSH provided the highest CL emission. This work demonstrated that the CL reaction could be strongly affected by the capping nature. Another important finding of this study was that the capacity of CdTe QDs to generate CL emission was inversely proportional to the QDs fluorescence. This fact was probably due to the low capping efficiency that allowed easier oxidation or electron injection (also explaining the low quantum yield). Again in this case, a direct proportionality between CL, QDs size and concentration, was observed. The proposed reaction mechanism is showed in Table 3. $K_3Fe(CN)_6$ – CdTe-GSH system was successfully apply to detect 9 different ions (Ca^{2+}, Co^{2+}, Mn^{2+}, Hg^{2+}, Mg^{2+}, Cu^{2+}, Ni^{2+}, Cr^{3+} and Fe^{3+}).

An interesting example of CRET is the system studied by Kanwal et al [152]. MSA-capped CdTe QDs conjugated with IgG were used to successfully enhance the CL emission of luminol - H_2O_2 and to determine some reducing compound and metal ions. The reaction showed a higher CL intensity in alkaline pH with a H_2O_2 concentration of 0.1mol L^{-1}. The mechanism proposed for the CL is a resonance energy transfer between CdTe QDs and luminol that, in this specific case, is the main emitter. A particularly interesting observation of this work is that if CRET occurs and the QDs are not the final emitters, the CL intensity enhancement is inversely proportional to the QDs size, which is exactly the opposite of what happens in direct QDs chemiluminescence.

The fist application of molecular imprinted polymers (MIPs) capped QDs in a CL-FIA system was carried out by Liu et al [153] aiming at determining 4-nitrophenol in water. In this work the enhancing effect of MIP-capped Mn-doped ZnS QDs in a H_2O_2 – $NaIO_4$ system was assayed revealing an enhancement of the CL emission. The proposed mechanism is described in Table 3 and the emitters were the QDs. Determination of 4-nitrophenol was accomplished in a first stage by fluorimetry and subsequently, and more extensively, by chemiluminescence assay. The utilisation of MIPs as capping agents allowed overcoming the hindrance of lack of selectivity inherent to QDs, and the method showed a good sensitivity and broad working analytical range.

A comprehensive study on the enhancing effect on NaClO - H_2O_2 CL system promoted by L-cysteine capped Mn-doped ZnS QDs was carried out by Zhou et al [154]. The enhancing effect was studied in a batch assay and by using a FIA system. The CL increment was

found dependent on the QDs concentration and more effective for Mn-doped QDs, probably because the incorporated metal acted as catalyst in the CL reaction. Of great significance was also the dependence of CL on the capping "density". In fact, up to 4% (by mass) of L-cysteine capping the CL intensity showed an increase. However, for higher values it decreased probably because a high capping density can turn difficult the interaction of active species with the QDs core. The reaction (Table 3) was studied in detail by electron paramagnetic resonance (EPR) using NaN_3 as quencher. The obtained results revealed that QDs participated in the reaction in two distinct ways: initially they acted as catalysts in the formation of $^{\cdot}OH$ and $^{\cdot}O_2^-$ and in a second stage they accepted energy from $(^1O_2^-)_2^*$ and acted as final emitters.

Table 3 - Chemiluminescence reactions for CRET [12].

Sun et al. [149]	$Ce(IV) + HSO_3^- \rightarrow HSO_3^{\cdot} + Ce(III)$ $2HSO_3^{\cdot} \rightarrow S_2O_6^{2-} + 2H^+$ $S_2O_6^{2-} \rightarrow SO_4^{2-} + SO_2^*$ $SO_2^* + CdTe\ QDs \rightarrow SO_2 + (CdTe\ QDs)^*$ $(CdTe\ QDs)^* \rightarrow CdTe\ QDs + h\nu$
Zhang et al. [151]	$K_3Fe(CN)_6 + ligand \rightarrow K_4Fe(CN)_6 + M^*$ $M^* + CdTe\ QDs \rightarrow M + (CdTe\ QDs)^*$ $(CdTe\ QDs)^* \rightarrow CdTe\ QDs + h\nu$
Liu et al. [153]	$IO_4^- + H_2O_2 \rightarrow {}^{\cdot}O_2^- + H_2O$ ${}^{\cdot}O_2^- \rightarrow (O_2)_2^*$ $(O_2)_2^* + QD \rightarrow O_2 + (QD)^*$ $(QD)^* \rightarrow QD + h\nu$
Zhou et al. [154]	$ClO^- + H_2O_2 \rightarrow ClO^{\cdot} + {}^{\cdot}OH + {}^-OH$ $^-OH + H_2O_2 \rightarrow HO_2^- + H_2O$ $H_2O_2 + QDs_{(catalyst)} \rightarrow 2{}^{\cdot}OH$ $2{}^{\cdot}OH + HO_2^- \rightarrow {}^{\cdot}O_2^-$ ${}^{\cdot}O_2^- + {}^{\cdot}OH \rightarrow {}^-OH + {}^1O_2$ $ClO^{\cdot} + {}^{\cdot}OH \rightarrow HO\text{—}ClO + {}^-OH$ $HO–ClO + {}^-OH \rightarrow Cl^- + H_2O + {}^1O_2$ $^1O_2 + {}^1O_2 \rightarrow (^1O_2)_2^* \rightarrow 2O_2 + h\nu$ $(^1O_2)_2^* + QDs \rightarrow QDs^* + 2O_2$ $QDs^* \rightarrow QDs + h\nu$

QDs have a great potential of application in CRET. One of the non-explored possibilities will, for instance, take advantage of the combined utilisation of multiple differently-sized QDs, emitting at different wavelengths and labelling different analytes, which upon receiving energy from the same donor could be detected simultaneously.

7.2.4. Electrogenerated chemiluminescence (ECL)

Electrochemiluminescence or electrogenerated chemiluminescence (ECL) is a form of chemiluminescence in which the light emitting reaction is preceded by an electrochemical reaction. This involves the generation of reactive species, at an electrode surface, that undergo electron-transfer (redox) reactions to form excited states which emit light upon an energy-relaxation process (Figure 14). ECL does not only exhibit the advantages of chemiluminescence detection, like the high sensitivity and wide concentrations working range, but it assures alongside specific advantages, such as an enhanced selectivity, due to the absence of a background signal arising from the emission of excited species not specifically involved in the detection process, extended analytical application by means of analyte electrochemical modification, and improved detection spatial resolution as the time and position of the light emitting reaction can be controlled.

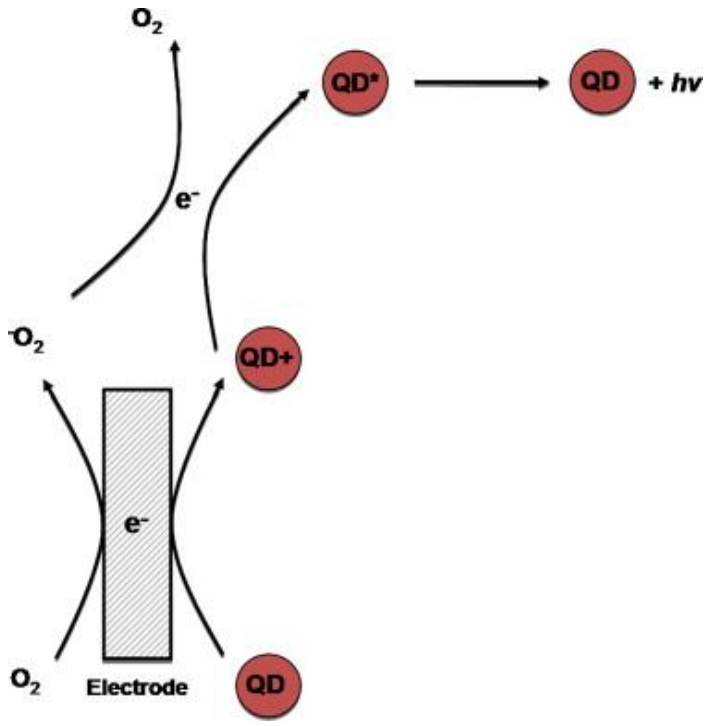

Figure 15 - Electrochemiluminescence of QDs [12].

Apart from their ability to participate in photoluminescent and chemiluminescent processes, QDs were found to generate light under an applied potential, initially in non-aqueous [155], and more recently in aqueous conditions [156]. In spite of the great success already achieved in QDs-based ECL systems, the fundamental understanding of these systems has not been, until now, entirely clarified. Generally, the ECL mechanisms of QDs are considered as one of three main types: annihilation, coreactant ECL and cathodic luminescence. Annihilation ECL does not need additional reagents for emission and involves the formation of cation and anion QDs radicals throughout electron transfer between oxidized and reduced species. The formed oppositely charged radicals should be chemically stable and maintain they charged states until they interact, annihilating each other, to generate the excited species that emit light. Cathodic luminescence is a cathodic light emission observed during electrolysis of aqueous electrolyte solutions that originates from hot electron injection. Coreactant ECL is the most common approach and relies on reaction between a luminophore and an additional reagent (coreactant), which usually enhances luminescence efficiency, under a unidirectional applied potential. Electron transfer occurs only between electrochemically-generated QDs species and the coreactant. Several compounds have been used as coreactants such as tri-n-propylamine, oxalate, peroxydisulfate, hydrogen peroxide, etc.

Despite the great number of ECL analytical applications resorting to QDs nanotechnology [157, 158], only a very restrict number or works, all published during 2011, are based on automated approaches. Wan et al [159] have proposed a flow injection electrochemiluminescence (FI-ECL) sensor, by using TGA-capped CdTe quantum dots, for the determination of durabolin in food samples. The QDs were layer-by-layer self-assembled on Indium Tin Oxide (ITO) glass and the slide was packed in a homemade flow cell for ECL measurements. The number of assembled layers affected system performance being the highest ECL intensity observed for 4 layers. Durabolin acted as coreactant increasing the ECL emission linearly for concentration values between $1.0x10^{-8}$ and $1.0x10^{-5}$ g mL^{-1}. The detection limit was $2.5x10^{-9}$ mL^{-1}. The developed FI-ECL was cost-effective, and provided high sensitivity and high sample throughput. Another flow injection analysis ECL approach was developed by Jinjin et al [160] for the high sensitive determination of dopamine in cerebro-spinal fluid. The authors constructed a nanoliter-sized (300 nL) flow-cell containing the ECL working electrode obtained by immobilization of a composite of TGA-capped CdTe QDs, carbon nanotubes and chitosan on ITO glass slides. Triethylamine was used as coreactant, increasing the ECL emission up to a concentration of 40 mM. During sample measurement an ECL quenching effect was verified due to the energy transfer from the excited CdTe QDs to the oxidized products of dopamine. The

working analytical concentrations ranged from 10 pM to 4 nM with a detection limit of 3.6 pM. The developed flow-cell is expected to be used as a component of microfluidic devices.

7.3. Liquid chromatography

The well known liquid chromatography (LC) is in essence a physical separation technique for mixtures resolution relying on the distribution of the analyte between a stationary phase, typically a solid, and a liquid mobile phase. The type of interactions between sample and stationary/mobile phases allows a deeper differentiation (ion-exchange, adsorption, partition, affinity, size exclusion, etc). Nowadays, high performance liquid chromatography is the premier technique for modern chemical analysis and related applications. In a single step process it can separate a mixture into its individual components and simultaneously provide a quantitative estimate of each constituent. The analytical efficiency of a liquid chromatography method depends not only on adequate separation but also on suitable inline detection and quantification. The most common LC detectors are based on UV/Vis or fluorescence spectroscopy, electrochemical measurements or mass spectrometry.

An ideal LC detector should provide high sensitivity, fast response, wide linear dynamic range and low noise level. In this regard, fluorescence has been shown to be extremely useful as a detection process offering not only selectivity but also some of the highest sensitivities available in LC along with low instrument instability due to the very low light background. The greatest weakness is that relatively few compounds fluoresce in a practical range of wavelengths. In this context, QDs can be a valuable tool in LC as they could act as labels enabling the signalling and identification of the analyte similarly to what happens in capillary electrophoresis [180-185]. Moreover, upon bioconjugation of QDs with a variety of biomolecules such as proteins and immunoglobulins it is possible to attain the specificity and high sensitivity needed for the targeted analyte detection being as well an expeditious strategy for multiparametric array analysis by means of multiplexed analyte detections.

Despite the great analytical potential, in the past no typical liquid chromatographic method has used QDs as labels for compound detection although a few size exclusion chromatography (SEC) approaches have been proposed to separate QDs and QDs-conjugates from precursors. In the first work published in this field [161] High Performance size exclusion chromatography (HPSEC) was used to separate the products of conjugation of cohesin/dockerin protein polymers with CdSe/ZnS. It was possible to separate two major fractions of bioconjugate species: a first eluting peak representing the

highest molecular mass cohesin/dockerin-QDs clusters and a later eluting peak containing single QDs containing protein conjugate. This work also confirmed the occurrence of strong interactions between self-assembled, recombinant protein polymers and CdSe/ZnS quantum dots.

Wang et al [162] proposed a SEC system for isolation of QDs from free polymers after conjugation reactions and to quantify the amount of polymer bound to the QDs surface. Separation of QDs conjugated from free conjugation polymer was easily achieved as the former were eluted much faster, while the number of the polymeric ligands bound to each QDs was quantified by determining the linked polymer using the nanocrystals as fluorescent tracers.

A SEC system for separation of different size QDs was also implemented by applying a QDs repelling surface of a concentrated poly(methyl methacrylate) (PMMA) brush onto a silica monolithic column [163]. In what could be considered the only effective analytical application, Chouhan et al [164], without resorting to conventional chromatographic equipment, implemented a fluoroimmunochromatographic technique for methylparathion determination at picogram level by using thiol-stabilized CdTe QDs as fluorescent probes in a flow-injection analysis system comprising an immunoreactor column packed with immobilized anti-MP IgY antibodies.

7.4. Capillary electrophoresis

Capillary electrophoresis (CE) is a separation technique based on the different analytes mobility under the influence of a spatially uniform electric field due to their different charge/size ratios. Briefly, in CE a narrow fused capillary filled with an electrolyte solution is used to separate the charged analytes. The ends of the capillary are immersed into vials containing the background electrolyte (BGE) and the electrodes. The sample solution is inserted in the capillary with different strategies: by pressure, gravity or an applied voltage. By means of the application of a high voltage the analyte forms zones due to the different electrophoretic mobility and migrate toward the outlet side. The use of an in-line detector, prior to the outlet, permitted the detection of the analyte.

Due to their electric surface charge QDs are well suited for application in CE explaining the motifs behind the emergence, in recent years, of CE as a powerful tool for characterizing [165-168] and separating QDs [169-174], and also to take advantage of the photoluminescent properties of QDs by using these nanoparticles as fluorescent labels in distinct analytical methodologies [180-184].

Among the different CE operation modes characterized by distinct separation mechanism that were used in combination with QDs nanotechnology, the most relevant are:

- capillary zone electrophoresis (CZE) [166-170, 172, 179, 182, 184, 186]
- micellar electrokinetic chromatography (MEKC) [171, 176, 177, 183, 185]
- capillary gel electrophoresis (CGE) [165]
- microchip electrophoresis (MCE) [180, 181]

Being one of the most powerful separation techniques with noteworthy advantages in terms of simplicity, low sample consumption, high separation efficiency and rapidity, in early works, CE techniques where mostly used for characterization, regarding composition and size distribution, and separation of QDs [165-172], as well as to typify their potential ecotoxicity as a consequence of an increased environmental prevalence of these nanomaterials due to a more widespread utilisation and, hence, waste disposal [173, 174].
The pioneering work on the separation of CdTe-MPA QDs by means of a CGE system was carried out by Song et al [165] by employing a laser induced fluorescence (LIF) detector. Using linear polyacrylamide (PAA) as sieving medium, a good resolution for different size QDs was achieved. Of great importance was the described effect of peak broadening, a consequence of the high polydispersity that acted as a noteworthy limitation when dealing with close size QDs separation, and the enhanced PL emission observed at higher pH. CZE technique was used for the first time by Pyell et al [168] to separate and determine the size of CdSe/ZnS/SiO_2 QDs with distinct electrophoretic mobilities depending not only on size but also on pH and ionic strength of the separation electrolyte [175]. The obtained results matched the size distribution determined by transmission electron microscopy (TEM) and showed that the electrophoretic mobility was independent on the applied electric field force. Similar evidence was found by Li et al [172] by using polyethylene glycol (PEG) (4%) as sieving medium. The separation of three different sized core/shell CdSe/ZnS QDs was achieved confirming that the electrophoretic mobility of the analysed nanocrystals was inversely proportional to their size. More recently micellar electrokinetic chromatography (MEKC) was used by Carrillo-Carrión et al. [176] achieving the highest resolution level for QDs (0.5 nm).
In the previous works the focus was mainly set on the separation of QDs with the same composition but with different size. Since the electrophoretic mobility can also change with the surface charge another important variable that should be taken into consideration, along with the size, is the nature of the capping/coating/bioconjugation of the QDs. Huang et al [166] applied a CE method to separate CdTe QDs capped with MPA from those conjugated with bovine serum albumin (BSA). The importance of the net

charge due to the presence of different capping agents in CZE was highlighted in the work of Pereira et al [167] and more extensively studied by Zhang et al [171] for equally sized CdTe QDs capped with MPA, MAA and GSH by MEKC. The micellar environment was created upon addiction of *sodium dodecyl sulfate* (SDS) and permitted an even higher selectivity due to the different interactions of the assayed organic cappings. This same principle is the basis of the work of Oszwałdowski et al [178], which have assessed a micellar plug containing QDs and TX-100 or DOSS by CZE. The developed methodology increased the separation ratio and permitted a preconcentration of the QDs. It also put in evidence that the distribution of the nanostructures between a micellar and micellar free zone is controlled by the QDs affinity and is the decisive factor in the separation process.

Vicente and Colón [169] successfully developed a method for separation of different CdSe/ZnS conjugates QDs using CE with PEO as sieving agent, confirming the results of the previous works. They studied the effect of the reaction of two bioconjugated QDs that resulted in the appearance of a third peak but of difficult resolution.

One of the biggest problems for CE resolution of bioconjugates is the heterogeneity of the final products. Pereira and Lai [170] were the first describing the peak broadening arising from QDs bioconjugation (selective or non-selective) with proteins and immunoglobulins. They explained the higher polydispersity observed as a likely consequence of the variable number of biomolecules that could conjugate a single QDs and the existence of multiple linkage sites on these molecules participating in the bioconjugation process. These results were confirmed by Lišková et al [179] in a systematic study of the products obtained by different bioconjugation methods using CZE and achieving a great resolution without sieving media.

In the last two years EC was coupled with QDs to develop news analytical methods combining the separation potentiality of EC with the optical properties and reactivity of QDs. Chen et al [180] proposed an ultrasensitive detection method for the determination of 7-aminoclonazepam (7-ACZP) in urine by using a microfluidic chip–based immunoassay with laser induced fluorescence (LIF) detection. Denatured bovine serum albumin (dBSA) coated CdTe-TGA QDs were conjugated with anti-7-ACZP antibody. 7-ACZP and 7-ACZP-OVA (ovalbumin) compete to form immunological complexes with the dBSA-coated CdTe QDs conjugated antibody (Ab). Separation was achieved based on the mobility difference between the antibody and antibody-antigen complex. The utilisation of QDs as biomarkers enabled the detection of drug residues at a pictogram level.

A CRET-based method coupled to microchip electrophoresis was the first work published with this purpose [181]. In a luminol-NaBrO-QDs chemiluminescence system the nanocrystals were pointed out as final acceptor and emitter specie. The developed

approach was successfully applied in the detection of various compounds and extensively studied for the simultaneous separation and detection of amino acids in a single cell.

An EC-CL system was also used for the separation and determination of dopamine and epinephrine (Zhao et al) [182]. A QDs-luminol-H_2O_2 system was added to the running buffer enabling the attainment of a very high CL intensity. The two catecholamines, which are recognized radical scavengers, promoted a pronounced quenching of the CL signal due to inhibition of the catalytic process. The method was applied in the determination of the neurotransmitters in human urine samples.

Chen and Fung [183] proposed a method for the determination of organophosphorus pesticides. By exploiting the capacity of these compounds to interact with QDs they optimize a MEKC-LIF system for their separation and determination in vegetables. The CdTe/CdS QDs were immobilized onto the inside capillary surface in the LIF window and showed good stability to borate buffer (pH 8-10), methanol 5% and ageing.

CdTe capped with L-cysteine or glutathione were linked to molecular beacons (MBs) to detect dual and single base mutation in DNA by EC [184]. The linkage with MBs yielded a quenching of the QDs emission due to a FRET mechanism between the nanocrystal and the quencher present on the MBs. When the target DNA linked the MBs a rise in the QDs fluorescence was observed due to interruption of the FRET mechanism. A decrease in the migration time was also recognized due to modification of the MBs conformation. Using two QDs-MBs conjugates it was possible to discriminate single base from dual base mutations because the former do not link to the MBs and thus do not alter the migration time.

CdTe-MPA QDs were applied as buffer additives for the determination of acrylamide by MECK with LIF detection [185]. In this case the interaction with QDs produced a quenching of the background PL proportional to acrylamide concentration.

The fluorescence and mobility effect resulting from the interaction of fluvic acids with QDCOOH and QDNH2 were studied by Celiz et al [186]. A decreasing trend in the electrophoretic mobility and a decrease in the PL emission were observed in presence of increasing concentrations of fluvic acids.

References

[1] Alivisatos AP. Semiconductor Clusters, Nanocrystals, and Quantum Dots. Science 1996 Feb; 271 (5251): 933-7.

[2] Brus L. Quantum Crystallites and Nonlinear Optics Appl Phys A 1991 Dec; 53 (6): 465-74.

[3] Alivisatos AP. Perspectives on the Physical Chemistry of Semiconductor Nanocrystals. Phys Chem 1996 Aug; 100 (31): 13226-39.

[4] Weller H. Quantized Semiconductor Particles: A novel state of matter for materials science. Adv Mater 1993 Feb; 5 (2): 88-95.

[5] Kuno M. Introductory nanoscience. New York: Garland Science, Taylor and Francis Group, LLC. 2012

[6] Brus L. Electronic wave functions in semiconductor clusters: experiment and theory. J Phys Chem 1986 Jun; 90 (12): 2555-60.

[7] Schooss D, Mews A, Eychmuller A, Weller H. Quantum-dot quantum well CdS/HgS/CdS: theory and experiment. Phys Rev B 1994 Jun; 49 (24): 17072-8.

[8] Trindade T, O'Brien P, Pickett NL. Nanocrystalline Semiconductors: Synthesis, Properties, and perspectives. Chem Mater 2001 Nov; 13 (11): 3843-58.

[9] Nirmal M, Norris DJ, Kuno K, Bawendi MG, Efros AL, Rosen M. Observation of the "Dark Exciton" in CdSe Quantum Dots. Phys Rev Lett 1995 Nov; 75 (20): 3728-31.

[10] Efros AL, Rosen M, Kuno M, Nirmal M, Norris DJ, Bawendi MG, Band-edge exciton in quantum dots of semiconductors with a degenerate valence band: Dark and bright exciton states. Phys Rev B 1996 Aug; 54 (7): 4843-56.

[11] Demchenko DO, Wang L. Optical transitions and nature of Stokes shift in spherical CdS quantum dots. Phys Rev B 2006 Apr; 73 (15): 155326.

[12] Frigerio C, Ribeiro DMS, Rodrigues SSM, Abreu LRG, Barbosa JAC, Prior JAV, Marques KL, Santos JLM. Application of quantum dots as analytical tools in automated chemical analysis: A review. Anal Chim Acta 2012 Jul; 735: 9-22.

[13] Rogach AL, Franzl T, Klar TA, Feldmann J, Gaponik N, Lesnyak V, Shavel A, Eychmuller A, Rakovich YP, Donegan JF. Aqueous synthesis of thiol-capped CdTe nanocrystals: state-ofthe- art. J Phys Chem C 2007 Sep; 111 (40): 14628-37.

[14] Rogach AL. Semiconductor Nanocrystals Quantum Dots Synthesis, Assembly, Spectroscopy and Applications. Vien: Springer-Verlag. 2008.

[15] Henglein A. Photodegradation and fluorescence of colloidal cadmium sulfide in aqueous solution. Ber Bunsen-Ges Phys Chem 1982 Apr; 86 (4): 301-5.

[16] Weller H, Koch U, Gutierrez M, Henglein A. Photochemistry of colloidal metal sulfides. 7. Absorption and fluorescence of extremely small zinc sulfide particles (the world of the neglected dimensions). Ber Bunsen-Ges Phys Chem 1984 Jul; 88 (7): 649-56.
[17] Alfassi Z, Bahnemann D, Henglein A. Photochemistry of colloidal metal sulfides. Photoelectron emission from cadmium sulfide and cadmium sulfide–zinc sulfide cocolloids. J Phys Chem 1982 Nov; 86 (24): 4656–57.
[18] Rossetti R, Nakahara S, Brus LE. Quantum size effects in the redox potentials, resonance Raman spectra, and electronic spectra of cadmium sulfide crystallites in aqueous solution. J Chem Phys 1983 Jul; 79 (2): 1086–8.
[19] Nozik AJ, Williams F, Nenadovic MT, Rajh T, Micic OI. Size quantization in small semiconductor particles. J Phys Chem 1985 Jan; 89 (3): 397–9.
[20] Ramsden JJ, Graetzel M. Photoluminescence of small cadmium sulfide particles. J Chem Soc, Faraday Trans 1 1984 Jan; 80 (4): 919–33.
[21] Rossetti R, Hull R, Gibson JM, Brus LE. Excited electronic states and optical spectra of zinc sulfide and cadmium sulfide crystallites in the 15 to 50A size range: evolution from molecular to bulk semiconducting properties. J Chem Phys 1985 Jan; 82 (1): 552–9.
[22] Weller H, Fojtik A, Henglein A. Photochemistry of semiconductor colloids: properties of extremely small particles of cadmium phosphide (Cd3P2) and zinc phosphide (Zn3P2). Chem Phys Lett 1985 Jun; 117 (5): 485–8.
[23] Fojtik A, Weller H, Henglein A. Photochemistry of semiconductor colloids. Size quantification effects in Q-cadmium arsenide. Chem Phys Lett 1985 Oct; 120 (6): 552–4.
[24] Resch U, Weller H, Henglein A. Photochemistry and radiation chemistry of colloidal semiconductors. 33. Chemical changes and fluorescence in CdTe and ZnTe. Langmuir 1989 Jul; 5 (4): 1015–20.
[25] Efros AL. Interband absorption of light in a semiconductor sphere. Sov Phys Semiconduct 1982 16: 772–5.
[26] Brus L. A simple model for the ionization potential, electron affinity, and aqueous redox potentials of small semiconductor crystallites. J Chem Phys 1983 Dec; 79 (11): 5566–71.
[27] Rajh T, Micic OI, Nozik AJ. Synthesis and characterization of surface-modified colloidal cadmium telluride quantum dots. J Phys Chem 1993 Nov; 97 (46): 11999–12003
[28] Vossmeyer T, Katsikas L, Giersig M, Popovic IG, Diesner K, Chemseddine A, Eychmuller A, Weller H. CdS nanoclusters: synthesis, characterization, size dependent oscillator strength, temperature shift of the excitonic transition energy, and reversible absorbance shift. J Phys Chem 1994 Aug; 98 (31): 7665–7673

[29] Murray CB, Norris DJ, Bawendi MG. Synthesis and characterization of nearly monodisperse CdE (E=sulfur, selenium, tellurium) semiconductor nanocrystallites. J Am Chem Soc 1993 Sep; 115 (19): 8706–87.
[30] Rogach AL, Katsikas L, Kornowski A, Su D, Eychmuller A, Weller H. Synthesis and characterization of thiol-stabilized CdTe nanocrystals. Ber Bunsen-Ges Phys Chem 1996 Nov; 100 (11): 1772–78.
[31] Gaponik N, Talapin DV, Rogach AL, Hoppe K, Shevchenko EV, Kornowski A, Eychmuller A, Weller H. Thiol-capping of CdTe nanocrystals: an alternative to organometallic synthetic routes. J Phys Chem B 2002 Jun; 106 (29): 7177-85.
[32] Engelhard T, Jones ED, Viney I, Mastai Y, Hodes G. Deposition of tellurium films by decomposition of electrochemically-generated H_2Te: application to radiative cooling devices. Thin Solid Films 2000 Jul; 370 (1-2): 101–5.
[33] Rogach AL, Franzl T, Klar TA, Feldmann J, Gaponik N, Lesnyak V, Shavel A, Eychmuller A, Rakovich YP, Donegan JF. Aqueous synthesis of thiol-capped CdTe nanocrystals: state-ofthe- art. J Phys Chem C 2007 Sep; 111 (40): 14628-37.
[34] Kovalenko MV, Kaufmann E, Pachinger D, Roither J, Huber M, Stangl J, Hesser G, Schaffler F, Heiss W. Colloidal HgTe nanocrystals with widely tunable narrowband gap energies: from telecommunications to molecular vibrations. J Am Chem Soc 2006 Mar; 128 (11): 3516–17.
[35] Zhang H, Wang L, Xiong H, Hu L, Yang B, Li W. Hydrothermal synthesis for high-quality CdTe nanocrystals. Adv Mater 2003 Oct; 15 (20): 1712–15.
[36] Yang R, Yan Y, Mu Y, Ji W, Li X, Zou M, Fei Q, Jin Q. A Rapid and Facile Method for Hydrothermal Synthesis of CdTe Nanocrystals Under Mild Conditions. J. Nanosci. Nanotechnol. 2006 Aug; 6 (1): 215–20.
[37] Byrne SJ, Corr SA, Rakovich TY, Gun'ko YK, Rakovich YP, Donegan JF, Mitchellc S, Volkov Y. Optimisation of the synthesis and modification of CdTe quantum dots for enhanced live cell imaging. J Mater Chem 2006 Jun; 16 (28): 2896–2902.
[38] Li L, Qian H, Fang N, Ren J. Significant enhancement of the quantum yield of CdTe nanocrystals synthesized in aqueous phase by controlling the pH and concentrations of precursor solutions. J Luminesc 2006 Apr; 116 (1-2): 59-66.
[39] He Y, Sai L, Lu H, Hu M, Lai W, Fan Q, Wang L, Huang W. Microwave-Assisted Synthesis of Water-Dispersed CdTe Nanocrystals with High Luminescent Efficiency and Narrow Size Distribution. Chem Mater 2007 Jan; 19 (3): 359-65.
[40] Li M, Ge Y, Chen Q, Xu S, Wang N, Zhang X. Hydrothermal synthesis of highly luminescent CdTe quantum dots by adjusting precursors' concentration and their conjunction with BSA as biological fluorescent probes. Talanta 2007 Apr; 72 (1): 89-94.

[41] Murase N, Gaponik N, Weller H. Effect of chemical composition on luminescence of thiol-stabilized CdTe nanocrystals. Nanoscale Res Lett 2007 Apr; 2 (5): 230-4.
[42] Liu Y, Shen Q, Yu D, Shi W, Li J, Zhou J, Liu X. A facile and green preparation of high-quality CdTe semiconductor nanocrystals at room temperature. Nanotechnology 2008 Jun; 19 (24): 245601.
[43] Aldeek F, Balan L, Lambert J, Schneider R. The influence of capping thioalkyl acid on the growth and photoluminescence efficiency of CdTe and CdSe quantum dots. Nanotechnology 2008 Nov; 19 (46): 475401.
[44] Zhang Y, Zhang H, Ma M, Guo X, Wang H. The influence of ligands on the preparation and optical properties of water-soluble CdTe quantum dots. Appl Surf Sci 2009 Feb; 255 (9): 4747–53.
[45] Liu Y, Yu J. Selective synthesis of CdTe and high luminescence CdTe/CdS quantum dots: The effect of ligands. J Coll Interf Sci 2009 May; 333 (2) 690–8.
[46] Yuwen L, Lu H, He Y, Chen L, Hu M, Bao B, Boey F, Zhang H, Wang L. A facile low temperature growth of CdTe nanocrystals using novel dithiocarbamate ligands in aqueous solution. J Mat Chem 2010 Feb; 20 (14): 2788–93.
[47] Khalavka Y, Mingler B, Friedbacher G, Okrepka G, Shcherbak L, Panchuk O. Influence of temperature on the synthesis of thiol-stabilized CdTe nanoparticles in aqueous solutions. Phys Status Solidi A 2010 Aug; 207 (2): 370-4.
[48] Li M, Zhou H, Zhang H, Sun P, Yi K, Wang M, Dong Z, Xu S. Preparation and purification of L-cysteine capped CdTe quantum dots and its self-recovery of degenerate fluorescence. J Luminesc 2010 Oct; 130 (10): 1935–40.
[49] Gao F, Han J, Zhang J, Li Q, Sun X, Zheng J, Bao L, Li X, Liu Z. The synthesis of newly modified CdTe quantum dots and their application for improvement of latent fingerprint detection. Nanotechnology 2011 Feb; 22 (7): 075705.
[50] Choi SY, Shim JP, Kim DS, Kim TY, Suh KS. Aqueous Synthesis of CdTe Quantum Dot Using Dithiol-Functionalized Ionic Liquid. J Nanomat 2012; Article ID 519458.
[51] Zhang C, Xu J, Zhang S, Ji X, He Z. One-Pot Synthesized DNA–CdTe Quantum Dots Applied in a Biosensor for the Detection of Sequence-Specific Oligonucleotides. Chem. Eur. J. 2012 Jul; 18 (27): 8296-8300.
[52] Fang Z, Liu L, Xu L, Yin X, Zhong X. Synthesis of highly stable dihydrolipoic acid capped water-soluble CdTe nanocrystals. Nanotechnology 2008 Jun; 19 (23): 235603.
[53] Gao X, Wu J, Wei X, He C, Wang X, Guob G, Pu Q. Facile one-step photochemical synthesis of water soluble CdTe(S) nanocrystals with high quantum yields. J Mater Chem 2012 Feb; 22 (13): 6367-73.

[54] Liu M, Zhao H, Chen S, Wang H, Quan X. Photochemical synthesis of highly fluorescent CdTe quantum dots for "on–off–on" detection of Cu(II) ions. Inorg Chim Acta 2012 Sep; 392: 236-40.
[55] Zou L, Wang J, Fang Z, Gu Z, Zhong X. Synthesis of Positively Charged Luminescent CdTe Nanocrystals in Aqueous Solution. J Disp Sci Tech 2009 Feb; 30 (3): 388-93.
[56] Zou L, Gu Z, Zhang N, Zhang Y, Fang Z, Zhu W, Zhong X. Ultrafast synthesis of highly luminescent green- to near infrared-emitting CdTe nanocrystals in aqueous phase J Mater Chem 2008 Apr; 18 (24): 2807–15.
[57] Stirner T, Kirkman NT, May L, Ellis C, Nicholls JE, Kelly SM, O'Neill M, Hogg JHC. CdTe Nanocrystals: Synthesis, Optical Characterization, and Pseudopotential Calculation of the Band Gap. J Nanosci Nanotech 2001 Dec; 1 (4): 451-5.
[58] El-sadeka MSA, Nooraldenb AY, Babuc SM, Palanisamy PK. Influence of different stabilizers on the optical and nonlinear optical properties of CdTe nanoparticles. Optics Comm 2011 Jun; 284 (12): 2900-04.
[59] Zhou D, Lin M, Chen Z, Sun H, Zhang H, Sun H, Yang B. Simple Synthesis of Highly Luminescent Water-Soluble CdTe Quantum Dots with Controllable Surface Functionality. Chem Mater 2011 Nov; 23 (21): 4857–62.
[60] Xu S, Wang C, Zhang H, Wang Z, Yang B, Cui Y. pH-sensitive photoluminescence for aqueous thiol-capped CdTe nanocrystals. Nanotechnology 2011 Aug; 22 (31): 315703.
[61] Silva FO, Carvalho MS, Mendonça R, Macedo WAA, Balzuweit K, Reiss P, Schiavon MA. Effect of surface ligands on the optical properties of aqueous soluble CdTe quantum dots. Nanosc Res Lett 2012 Sep; 7: 536.
[62] Gao MY, Kirstein S, Mohwald H, Rogach AL, Kornowski A, Eychmuller A, Weller H. Strongly Photoluminescent CdTe Nanocrystals by Proper Surface Modification. J Phys Chem B 1998 Oct; 102 (43): 8360-3.
[63] Li C, Murase N. Surfactant-dependent photoluminescence of CdTe nanocrystals in aqueous solution. Chem Lett 2005 Dec; 34 (1): 92-3.
[64] Shavel A, Gaponik N, Eychmuller A. Factors governing the quality of aqueous CdTe nanocrystals: calculations and experiment. J Phys Chem B 2006 Oct; 110 (39): 19280–84.
[65] Guo J, Yang W, Wang C Systematic study of the photoluminescence dependence of thiolcapped CdTe nanocrystals on the reaction conditions. J Phys Chem B 2005 Sep; 109 (37): 17467–73.
[66] Zhang H, Zhou Z, Yang B, Gao MJ. The Influence of Carboxyl Groups on the Photoluminescence of Mercaptocarboxylic Acid-Stabilized CdTe Nanoparticles Phys. Chem. B 2003 Jan; 107 (1): 8-13.

[67] Duan J, Song L, Zhan J. One-Pot Synthesis of Highly Luminescent CdTe Quantum Dots by Microwave Irradiation Reduction and Their Hg2+-Sensitive Properties. Nano Res 2009 Jan; 2 (1): 61-8.
[68] Yuan Z, Zhang A, Cao Y, Yang J, Zhu Y,Yang P. Effect of Mercaptocarboxylic Acids on Luminescent Properties of CdTe Quantum Dots. J Fluoresc 2012 Jan; 22 (1):121–7.
[69] Feteha M, Ebrahim S, Soliman M, Ramdan W, Raoof M. Effects of mercaptopropionic acid as a stabilizing agent and Cd:Te ion ratio on CdTe and CdHgTe quantum dots properties. J Mater Sci: Mater Electron 2012 Nov; 23 (11):1938–43.
[70] Li L, Qian H, Ren J. Rapid synthesis of highly luminescent CdTe nanocrystals in the aqueous phase by microwave irradiation with controllable temperature. Chem Commun 2005 Dec; 4: 528–30.
[71] He Y, Lu H, Sai L, Lai W, Fan Q, Wang L, Huang W. Synthesis of CdTe Nanocrystals through Program Process of Microwave Irradiation. J Phys Chem B 2006 Jul; 110 (27): 13352-6.
[72] Y He, L Sai, H Lu, M Hu, W Lai, Q Fan, L Wang, Huang W. Microwave-Assisted Synthesis of Water-Dispersed CdTe Nanocrystals with High Luminescent Efficiency and Narrow Size Distribution. Chem Mater 2007 Feb; 19 (3): 359-65.
[73] Ying E, Li D, Guo S, Dong S, Wang J. Synthesis and Bio-Imaging Application of Highly Luminescent Mercaptosuccinic Acid-Coated CdTe Nanocrystals. PLoS ONE 2008 May; 3: e2222.
[74] Chao W, Qiang M, Xingguang S. Synthesis of CdTe Nanocrystals with Mercaptosuccinic Acid as Stabilizer. J Nanosci Nanotech 2008 Sep; 8 (9): 4408-14.
[75] Fang Z, Liu L, Xu L, Yin X, Zhong X. Synthesis of highly stable dihydrolipoic acid capped water-soluble CdTe nanocrystals. Nanotechnology 2008 Jun; 19 (23): 235603.
[76] Fang T, Ma K, Ma L, Bai J, Li X, Song H, Guo H. 3-Mercaptobutyric Acid as an Effective Capping Agent for Highly Luminescent CdTe Quantum Dots: New Insight into the Selection of Mercapto Acids. J Phys Chem C 2012 May; 116 (22): 12346–52.
[77] Qian H, Dong C, Weng J, Ren J. Facile One-Pot Synthesis of Luminescent, Water-Soluble, and Biocompatible Glutathione-Coated CdTe Nanocrystals. Small 2006 Jun; 2 (6): 747-51.
[78] Yuana J, Guoa W, Yinb J, Wanga E. Glutathione-capped CdTe quantum dots for the sensitive detection of glucose. Talanta 2009 Mar; 77 (5): 1858–63.
[79] Pérez-Donoso JM, Monrás JP, Bravo D, Aguirre A, Quest AF, Osorio-Román IO, Aroca RF, Chasteen TG, Vásquez CC. Biomimetic, Mild Chemical Synthesis of CdTe-GSH Quantum Dots with Improved Biocompatibility. PLoS ONE 2012 Jan; 1 (7): e30741.

[80] Zheng Y, Gao S, Ying JY. Synthesis and Cell-Imaging Applications of Glutathione-Capped CdTe Quantum Dots. Adv Mater 2007 Feb; 19 (3): 376–80.
[81] Mamedova NM, Kotov NA, Rogach AL, Studer J. Albumin-CdTe Nanoparticle Bioconjugates: Preparation, Structure, and Interunit Energy Transfer with Antenna Effect. Nano Lett 2001 Jun; 1 (6), 281-6.
[82] Denga D, Qina Y, Yang X, Yua J, Yi Pana Y. The selective synthesis of water-soluble highly luminescent CdTe nanoparticles and nanorods: The influence of the precursor Cd/Te molar ratio. J Cryst Growth 2006Nov; 296 (2): 141–9.
[83] Mntungwa N, Pullabhotla VSR, Revaprasadu N. Facile synthesis of cysteine and triethanolamine capped CdTe nanoparticles. Coll Surf B 2013 Jan; 101: 450– 6.
[84] Radtchenko IL, Sukhorukov GB, Gaponik N, Kornowski A, Rogach AL, Möhwald H. Core/Shell Structures Formed by the Solvent-Controlled Precipitation of Luminescent CdTe Nanocrystals on Latex Spheres. Adv Mat 2001 Nov; 13 (22): 1684-7.
[85] Yang W, Li W, Dou H, Sun K. Hydrothermal synthesis for high-quality CdTe quantum dots capped by cysteamine. Mat Lett 2008 Jun; 62 (17-18): 2564–6.
[86] Kuang R, Kuang X, Pan S, Zheng X, Duan J, Duan Y. Synthesis of cysteamine-coated CdTe quantum dots for the detection of bisphenol A. Microchim Acta 2010 Apr; 169 (1-2): 109–15.
[87] Zhang T, Sun X, Liu B. Synthesis of positively charged CdTe quantum dots and detection for uric acid. Spectrochim Acta Part A 2011 Sep; 79 (5): 1566–72.
[88] Wang R, Wang Y, Feng Q, Zhou L, Gong F, Lan Y. Synthesis and characterization of cysteamine-CdTe quantum dots via one-step aqueous method. Mater Lett 2012 Jan; 66 (1): 261–3.
[89] Peia J, Zhu H, Wang X, Zhang H, Yang X. Synthesis of cysteamine-coated CdTe quantum dots and its application in mercury (II) detection. Anal Chim Acta 2012 Dec; 757 63–8.
[90] Song Q, Ai X, Topuria T, Rice PM, Alharbi FH, Bagabas A, Bahattab M, Bass JD, Kim H, Scott JC, Miller RD. Microwave-assisted synthesis of monodispersed CdTe nanocrystals. Chem Commun 2010 May; 46 (27): 4971–3.
[91] Dong C, Ren J. Water-soluble mercaptoundecanoic acid (MUA)-coated CdTe quantum dots: one-step microwave synthesis, characterization and cancer cell imaging. J Luminesc 2012 27: 199–203.
[92] Li Y, Jing L, Qiao R, Gao M. Aqueous synthesis of CdTe nanocrystals: progresses and perspectives. Chem Commun 2011 May; 47 (33): 9293–9311.
[93] Algar WR, Tavares AJ, Krull UJ. Beyond labels: A review of the application of quantum dots as integrated components of assays, bioprobes, and biosensors utilizing optical transduction. Anal Chim Acta 2010 Jul; 673 (1): 1-25.

[94] Giokas DL, Vlessidis AG, Tsogas GZ, Evmiridis NP. Nanoparticle-assisted chemiluminescence and its applications in analytical chemistry. TRAC-Trends Anal Chem 2010 Nov; 29 (10): 1113-26.
[95] Calatayud JM. Flow injection analysis of pharmaceuticals: automation in the laboratory. 1st ed. London: Taylor & Francis Series in Pharmaceutical Sciences. 1996.
[96] Valcárcel M, Luque de Castro MD. Automatic Methods of Analysis. New York: Elsevier Science Publishers Inc. 1988.
[97] Skeggs LT. An automatic method for colorimetric analysis. Am J Clin Pathol 1957 Sep; 28 (3): 311-22.
[98] Ruzicka J, Hansen H. Flow injection analysis: Part I. A new concept of fast continuous flow analysis. Anal Chim Acta 1975 Aug; 78 (1): 145-57.
[99] Ruzicka J, Marshall GD. Sequential injection: a new concept for chemical sensors, process analysis and laboratory assays. Anal Chim Acta 1990 Oct; 237 (2): 329-43.
[100] Reis BF, Giné MF, Zagatto EAG, Lima JLFC, Lapa RAS. Multicommutation in flow analysis. Part I. Binary sampling: concepts, instrumentation and spectrophotometric determination of iron in plant digest. Anal Chim Acta 1994 Jul; 293 (1-2): 129-38.
[101] Cerda V, Estela JM, Forteza R, Cladera A, Becerra E, Altimira P, Sitjar P. Flow techniques in water analysis. Talanta 1999 Nov; 50 (4): 695-705.
[102] Ribeiro MFT, Santos JLM, Lima JLFC, Dias ACB, Zagatto EAG. Single reaction interface in flow analysis. Talanta 2005 Dec; 68 (2): 351-8.
[103] Lapa RAS, Lima JLFC, Reis BF, Santos JLM, Zagatto EAG. Multi-pumping in flow analysis: concepts, instrumentation, potentialities. Anal Chim Acta 2002 Aug; 466 (1): 125-32.

[104] Lima JLFC, Santos JLM, Dias ACB, Ribeiro MFT, Zagatto EAG. Multi-pumping flow systems: an automation tool. Talanta 2004 Dec; 64 (5): 1091–8.
[105] Dias ACB, Santos JLM, Lima JLFC, Quintella CM, Lima AMV, Zagatto EAG. A critical comparison of analytical flow systems exploiting streamlined and pulsed flows. Anal Bioanal Chem 2007 Jul; 388 (5-6): 1303-10.
[106] Fortes PR, Feres MA, Sasaki MK, Alves ER, Zagatto EAG, Prior JAV, Santos JLM, Lima JLFC. Evidences of turbulent mixing in multi-pumping flow systems. Talanta 2009 Sep; 79 (4): 978-83.
[107] Weeks DA, Johnson KS, Solenoid pumps for flow injection analysis. Anal Chem 1996 Aug; 68 (15): 2717–9.
[108] Fernandez-Arguelles MT, Jin WJ, Costa-Fernandez JM, Pereiro R, Sanz-Medel A. Surface-modified CdSe quantum dots for the sensitive and selective determination of

Cu(II) in aqueous solutions by luminescent measurements. Anal Chim Acta 2005 Sep; 549 (1-2): 20-5.
[109] Wang JH, Wang HQ, Zhang HL, Li XQ, Hua XF, Cao YC, Huang ZL, Zhao YD. Purification of denatured bovine serum albumin coated CdTe quantum dots for sensitive detection of silver(I) ions. Anal Bioanal Chem 2007 Jun; 388 (4): 969-74.
[110] Gao M, Kirstein S, Möhwald H, Rogach AL, Kornowski A, Eychmüller A, Weller H. Strongly Photoluminescent CdTe Nanocrystals by Proper Surface Modification. J Phys Chem B 1998 Oct; 102 (43): 8360-3.
[111] Dong CQ, Weng JF, Ren JC. Facile One-Pot Synthesis of Luminescent, Water-Soluble, and Biocompatible Glutathione-Coated CdTe Nanocrystals. Small 2006 Jun; 2 (6): 747-51.
[112] Lakowicz JR, Principles of Fluorescence Spectroscopy, 4th ed. New York: Springer. 2006.
[113] Xia Y, Zhu C. Use of surface-modified CdTe quantum dots as fluorescent probes in sensing mercury (II). Talanta 2008 Mar; 75 (1): 215-21.
[114] Zhang L, Xu C, Li B. Simple and sensitive detection method for chromium(VI) in water using glutathione-capped CdTe quantum dots as fluorescent probes. Microchim Acta 2009 Jul; 166 (1-2): 61-68.
[115] Wang J, Liang J, Sheng Z, Han H. A novel strategy for selective detection of Ag+ based on the red-shift of emission wavelength of quantum dots. Microchim Acta 2009 Dec; 167 (2-3): 281-287.
[116] Wu P, Li Y, Yan X. CdTe Quantum Dots (QDs) Based Kinetic Discrimination of $Fe2^{+}$ and $Fe3^{+}$, and CdTe QDs-Fenton Hybrid System for Sensitive Photoluminescent Detection of $Fe2^{+}$. Anal Chem 2009 Aug; 81 (15): 6252-57.
[117] Hou M, Na J. Determination of vanadium(V) with CdTe quantum dots as fluorescent probes. Anal Bioanal Chem 2010 Aug; 397 (8): 3589-93.
[118] Wang J, Zhou X, Ma H, Tao G. Diethyldithiocarbamate functionalized CdSe/CdS quantum dots as a fluorescent probe for copper ion detection. Spectrochimica Acta Part A 2011 Oct; 81 (1): 178-83.
[119] Xu H, Miao R, Fang Z., Zhong X. Quantum dot-based “turn-on” fluorescent probe for detection of zinc and cadmium ions in aqueous media. Anal Chim Acta 2011 Feb; 687 (1) 82-8.
[120] Liang G, Liu H, Zhang J, Zhu J. Ultrasensitive Cu^{2+} sensing by near-infrared-emitting CdSeTe alloyed quantum dots. Talanta 2010 Mar; 80 (5): 2172-6.
[121] Koneswaran M, Narayanaswamy R. l-Cysteine-capped ZnS quantum dots based fluorescence sensor for $Cu^{:}$ ion. Sens Actuators B 2009 May; 139 (1): 104-9.

[122] Zhong W, Liang J, Yu J. Systematic study of the interaction of cobalt ions with different-sized CdTe quantum dots. Spectrochim Acta Part A 2009 Oct; 74 (3): 603-6.
[123] Fan X, Liu S, He Y. Study on the interaction of CdTe quantum dots with coumaric acid and caffeic acid based on fluorescence reversible tune. Coll. Surf. B 2011 Nov; 88 (1): 23-30.
[124] X. Fan, J. Peng, S. Yan, L. Wang, Y. He, Study on the interaction of CdTe quantum dots with ferulic acid and protocatechuic aldehyde by optical spectroscopy. J Luminesc 2011 Oct; 131 (10): 2230-36.
[125] He YQ, Yin PF, Gong HP, Peng JJ, Liu SP, Fan XQ, Yan SG. Characterization of the interaction between mercaptoethylamine capped CdTe quantum dots with human serum albumin and its analytical application. Sens Actuators B 2011 Sep; 157 (1): 8-13.
[126] Gore AH, Mote US, Tele SS, Anbhule PV, Rath MC, Patil SR, Kolekar GB. A novel method for ranitidine hydrochloride determination in aqueous solution based on fluorescence quenching of functionalised CdS QDs through photoinduced charge transfer process: Spectroscopic approach. Analyst 2011 Apr;136 (12): 2606-2612.
[127] Devi LM, Negi DPS. Sensitive and selective detection of adenine using fluorescent ZnS nanoparticles. Nanotechnol. 2011 Jun; 22: 245502.
[128] Zhang X, Liu Z, Ma L, Hossu M, Chen W. Interaction of porphyrins with CdTe quantum dots. Nanotechnol 2011 May; 22 (19): 195501.
[129] Peng JY, Hu XY. A simple fluorescence quenching method for roxithromycin determination using CdTe quantum dots as probes. J Luminesc 2011 May ; 131 (5): 952-5.
[130] Algarra M, Campos BB, Miranda MS, da Silva JCGE. CdSe quantum dots capped PAMAM dendrimer nanocomposites for sensing nitroaromatic compounds. Talanta 2011 Feb; 83 (5): 1335-40.
[131] Ma QA, Yu W, Huang H, Su XG. Determination of L-tyrosine Based on Luminescence Quenching of Mn-Doped ZnSe Quantum Dots in Enzyme Catalysis System. J Fluoresc 2011 Jan; 21 (1): 125-31.
[132] Butwong N, Noipa T, Burakham R, Srijaranai R, Ngeontae W. Determination of arsenic based on quenching of CdS quantum dots fluorescence using the gas-diffusion flow injection method. Talanta 2011 Aug; 85 (2): 1063-1069.
[133] Medintz LI, Mattoussi H. Quantum dot-based resonance energy transfer and its growing application in biology. Phys Chem Chem Phys 2009 Jan; 11 (1): 17–45.
[134] Zhang C, Johnson LW. Quantum Dot-Based Fluorescence Resonance Energy Transfer with Improved FRET Efficiency in Capillary Flows. Anal Chem 2006 Aug; 78 (15): 5532-7.

[135] Ho YP, Chen HH, Leong KW, Wang TH. The convergence of quantum-dot-mediated fluorescence resonance energy transfer and microfluidics for monitoring DNA polyplex self-assembly in real time. Nanotechnol 2009 Mar; 20: 095103.
[136] Chen L, Algar WR, Tavares AJ, Krull UJ. Toward a solid-phase nucleic acid hybridization assay within microfluidic channels using immobilized quantum dots as donors in fluorescence resonance energy transfer. Anal Bioanal Chem 2011 Jan; 399 (1): 133-41.
[137] Wang Z, Li J, Liu B, Hu J , Yao X, Li J, Chemiluminescence of CdTe Nanocrystals Induced by Direct Chemical Oxidation and Its Size-Dependent and Surfactant-Sensitized Effect. J Phys Chem B 2005 Dec;109 (49): 23304-11.
[138] Garc-Campa AM, Baeyens WRG, Chemiluminescence in analytical chemistry. New York: Marcel Dekker. 2001.
[139] Li X, Li J, Tang J, Kang J, Zhang Y. Study of influence of metal ions on CdTe/H_2O_2 chemiluminescence. J Luminesc 2008 Jul; 128 (7): 1229-34.
[140] Li Y, Yang P, Wang P, Huang X, Wang L. CdS nanocrystal induced chemiluminescence: reaction mechanism and applications. Nanotechnol 2007 Jun; 18 (22): 225602.
[141] Chen H, Li R, Lin L, Guo G, Lin J-M. Determination of l-ascorbic acid in human serum by chemiluminescence based on hydrogen peroxide–sodium hydrogen carbonate–CdSe/CdS quantum dots system. Talanta 2010 Jun; 81 (4-5): 1688-96.
[142] Chen H, Lin L, Lin Z, Guo G, Lin J-M. Chemiluminescence Arising from the Decomposition of Peroxymonocarbonate and Enhanced by CdTe Quantum Dots. J Phys Chem A 2010 Sep; 114 (37): 10049-58.
[143] Lin Z, Xue W, Chen H, Lin J-M. Peroxynitrous-Acid-Induced Chemiluminescence of Fluorescent Carbon Dots for Nitrite Sensing. Anal Chem 2011 Nov; 83 (21): 8245-51.
[144] Micic OI, Curtis CJ, Jones KM, Sprague JR, Nozik AJ. Synthesis and Characterization of InP Quantum Dots. J Phys Chem 1994 May; 98 (19): 4966-69.
[145] Wang Z, Li J, Liu B, Li J. CdTe nanocrystals sensitized chemiluminescence and the analytical application. Talanta 2007 Jan; 77 (3): 1050-6.
[146] Li S, Li X, Zhang Y, Huang F, Wang F, Wei X. Enhanced chemiluminescence of the luminol–KIO4 system by ZnS nanoparticles. Microchim Acta 2009 Nov; 167 (1-2): 103-8.
[147] Kanwal S, Fu X, Su X. Size dependent active effect of CdTe quantum dots on pyrogallol-H_2O_2 chemiluminescence system for chromium(III) detection. Microchim Acta 2010 Apr; 169 (1-2): 167-72.
[148] Silvestre CIC, Frigerio C, Santos JLM, Lima JLFC. Quantum dots assisted photocatalysis for the chemiluminometric determination of chemical oxygen demand using a single interface flow system. Anal Chim Acta 2011 Aug; 699 (2): 193-7.

[149] Sun C, Liu B, Li J. Sensitized chemiluminescence of CdTe quantum-dots on Ce(IV)-sulfite and its analytical applications. Talanta 2008 Apr; 75 (2): 447-54.
[150] Fortes PR, Frigerio C, Silvestre CIC, Santos JLM, Lima JLFC, Zagatto EAG. Cadmium telluride nanocrystals as luminescent sensitizers in flow analysis. Talanta 2011 Jun; 84 (5): 1314-7.
[151] Zhang L, Xu C, Li B. Chemiluminescence of CdTe quantum dots using $K_3Fe(CN)_6$ as oxidant and its capping ligand-dependent effect. Microchem J 2010 Jul; 95 (2): 186-191.
[152] Kanwal S, Traore Z, Zhao C, Su X. Enhancement effect of CdTe quantum dots–IgG bioconjugates on chemiluminescence of luminol–H_2O_2 system. J Luminesc 2010 Oct; 130 (10): 1901-1906.
[153] Liu J, Chen H, Lin Z, Lin JM. Preparation of Surface Imprinting Polymer Capped Mn-Doped ZnS Quantum Dots and Their Application for Chemiluminescence Detection of 4-Nitrophenol in Tap Water. Anal Chem 2010 Sep; 82 (17): 7380-6.
[154] Zhou Y, Chen H, Ogawa N, Lin JM. Chemiluminescence from NaClO–H_2O_2 and enhanced by l-cysteine capped Mn-doped ZnS quantum-dots. J Luminesc 2011 Sep; 131 (10): 1991-7.
[155] Ding ZF, Quinn BM, Haram SK, Pell LE, Korgel BA, Bard AJ. Electrochemistry and Electrogenerated Chemiluminescence from Silicon Nanocrystal Quantum Dots. Science 2002 May; 296 (5571): 1293-7.
[156] Han H, Sheng ZH, Liang JG. Electrogenerated chemiluminescence from thiol-capped CdTe quantum dots and its sensing application in aqueous solution. Anal Chim Acta 2007 Jul; 596 (1): 73–8.
[157] Lei J, Ju H. Fundamentals and bioanalytical applications of functional quantum dots as electrogenerated emitters of chemiluminescence. TrAC-Trends Anal Chem 2011 Sep; 30 (8): 1351-9.
[158] Huang H, Li J, Zhu J. Electrochemiluminescence based on quantum dots and their analytical application. Anal Methods 2011 Oct; 3 (1): 33-42.
[159] Wan F, Yu J, Yang P, Ge S. An electrochemiluminescence sensor for determination of durabolin based on CdTe QD films by layer-by-layer self-assembly. Anal Bioanal Chem 2011 May; 400 (3): 807-14.
[160] Jinjin Z, Ming C, Caixia Y, Yifeng T. Development and application of an electrochemiluminescent flow-injection cell based on CdTe quantum dots modified electrode for high sensitive determination of dopamine. Analyst 2011 ; 136 (19) 4070-4.
[161] Ding S, Rumbles G, Jones M, Tucker MP, Nedeljkovic J, Simon MN, Wall JS, Himmel ME. Bioconjugation of (CdSe)ZnS Quantum Dots Using a Genetically Engineered Multiple Polyhistidine Tagged Cohesin/Dockerin Protein Polymer. Macromol Mater Eng 2004 Jul; 289 (7): 622-8.

[162] Wang M, Dykstra TE, Lou X, Salvador MR, Scholes GD, Winnik MA. Colloidal CdSe Nanocrystals Passivated by a Dye-Labeled Multidentate Polymer: Quantitative Analysis by Size-Exclusion Chromatography. Angew Chem 2006 Mar; 45 (14): 2221-4.
[163] Arita T, Yoshimura T, Adschiri T. Size exclusion chromatography of quantum dots by utilizing nanoparticle repelling surface of concentrated polymer brush. Nanoscale 2010 Jun; 2 (8): 1467-73.
[164] Chouhan RS, Vinayaka AC, Thakur MS. Thiol-stabilized luminescent CdTe quantum dot as biological fluorescent probe for sensitive detection of methyl parathion by a fluoroimmunochromatographic technique. Anal Bioanal Chem 2010 Jun; 397 (4): 1467–75.
[165] Song X, Li L, Quian H, Fang N, Ren J. Highly efficient size separation of CdTe quantum dots by capillary gel electrophoresis using polymer solution as sieving medium. Electrophor 2006 Apr; 27 (7): 1341-6.
[166] Huang X, Weng J, Sang F, Song X, Cao C, Ren J. Characterization of quantum dot bioconjugates by capillary electrophoresis with laser-induced fluorescent detection. J Chromat A 2006 Apr; 1113 (1-2): 251-254.
[167] Pereira M, Lai EPC, Hollebone B. Characterization of quantum dots using capillary zone electrophoresis. Electrophor 2007 Aug; 28 (16): 2874-81.
[168] Pyell U. CE characterization of semiconductor nanocrystals encapsulated with amorphous silicium dioxide. Electrophor 2008 Feb; 29 (3): 576-89.
[169] Vicente G, L.A. Colón LA. Separation of Bioconjugated Quantum Dots Using Capillary Electrophoresis. Anal Chem 2008 Mar; 80 (6): 1988-94.
[170] Pereira M, Lai EPC. Capillary electrophoresis for the characterization of quantum dots after non-selective or selective bioconjugation with antibodies for immunoassay. J Nanobiotechnol 2008 Oct; 6 (10): 1-15 .
[171] Zhang Y, Zhang H, Ma M, Guo X, Wang H. The influence of ligands on the preparation and optical properties of water-soluble CdTe quantum dots. Appl Surf Sci 2009 Feb; 255 (9): 4747-53.
[172] Li Y, Wang H, Wang J, Guan L, Liu B, Zhao Y, Chen H. A highly efficient capillary electrophoresis-based method for size determination of water-soluble CdSe/ZnS core–shell quantum dots. Anal Chim Acta 2009 Aug; 647 (2): 219-25.
[173] Stewart DTR, Celiz MD, Vicente G, Colón LA, Aga DS. Potential use of capillary zone electrophoresis in size characterization of quantum dots for environmental studies. Trac Trends Anal Chem 2011 Jan; 30 (1): 113-22.
[174] López-Lorente AI, Simonet BM, Valcárcel M. Electrophoretic methods for the analysis of nanoparticles. Trac Trends Anal Chem 2011 Jan; 30 (1): 58-71.

[175] Ohshima H, Approximate Analytic Expression for the Electrophoretic Mobility of a Spherical Colloidal Particle. J Colloid Interface Sci 2001 Jul; 239 (2): 587-90.
[176] Carrillo-Carillón C, Moliner-Martínez Y, Simonet BM, Valcárcel M. Capillary Electrophoresis Method for the Characterization and Separation of CdSe Quantum Dots. Anal Chem 2011 Apr; 83 (7): 2807-13.
[178] Oszwałdowski O, Zawistowska-Gibuła K, Roberts KP. Capillary electrophoretic separation of nanoparticles. Anal Bioanal Chem 2011 Mar; 399 (8): 2831-42.
[179] Liskova M, Voracova I, Kleparnik K, Hezinova V, Prikryl J, Foret F. Conjugation reactions in the preparations of quantum dot-based immunoluminescent probes for analysis of proteins by capillary electrophoresis. Anal Bioanal Chem 2011 Apr; 400 (2): 369-79.
[180] Chen W, Peng CF, Jin ZY, Qiao RR, Wang WY, Zhu SF, Wang LB, Jing QH, Xu CL. Ultrasensitive immunoassay of 7-aminoclonazepam in human urine based on CdTe nanoparticle bioconjugations by fabricated microfluidic chip. Biosens Bioelectron 2009 Mar; 24 (7): 2051-6.
[181] Zhao S, Huang Y, Shi M, Liu R, Liu Y. Chemiluminescence Resonance Energy Transfer-Based Detection for Microchip Electrophoresis. Anal Chem 2010 Mar; 82 (5): 2036-41.
[182] Zhao Y, Zhao S, Huang J, Ye F. Quantum dot-enhanced chemiluminescence detection for simultaneous determination of dopamine and epinephrine by capillary electrophoresis. Talanta 2011 Oct; 85 (5): 2650-4.
[183] Chen Q, Fung Y. Capillary electrophoresis with immobilized quantum dot fluorescence detection for rapid determination of organophosphorus pesticides in vegetables. Electrophor 2010 Sep; 31 (18): 3107-14.
[184] Li Y, Guan L, Wang J, Zhang H, Chen J, Lin S, Chen W, Zhao Y. Simultaneous detection of dual single-base mutations by capillary electrophoresis using quantum dot-molecular beacon probe. Biosens Bioelectron 2011 Jan; 26 (5): 2317-22.
[185] Chen Q, Zhao W, Fung Y. Determination of acrylamide in potato crisps by capillary electrophoresis with quantum dot-mediated LIF detection. Electrophor 2011 May; 32 (10): 1252-7.
[186] Celiz MD, Colón LA, Watson DF, Aga DS. Study on the Effects of Humic and Fulvic Acids on Quantum Dot Nanoparticles Using Capillary Electrophoresis with Laser-Induced Fluorescence Detection. Environ Sci Technol 2011 Apr; 45 (7): 2917-24.

CHAPTER 2

Materials and Methods

1. Introduction

In this chapter the instruments and the experimental methods used to implement the research activities carried out under the scope of this thesis, are exposed. Aiming at assuring a better understanding of the developed work, a brief and general description is provided for the used analytical techniques. The parameters and/or information provided by each of these techniques and their relationship with the work progress are also highlighted. Moreover, the general procedures for the preparation of solutions and the description of the devices used to assemble the flow systems, with a particular emphasis on their features, operation mode and control, are also presented. Finally, this chapter also describes the fundamental aspects related to the optimization of the proposed methodologies and the statistical treatment used to assess the quality of the obtained results.

2. UV/Vis spectrophotometry

This technique, along with fluorescence spectroscopy, is fundamental for the study of semiconductor nanocrystals, especially to evaluate and characterize their optical properties.

As it was already explained previously, quantum dots absorption spectra reveals the position and the energy associated to the first excitonic transition. This crucial data is extremely helpful for the determination of the nanoparticle size and molar extinction coefficient (ε). This possibility was firstly demonstrated in the work of Yu at al [1] that proposed an experimental model for the determination of these parameters for CdSe, CdS and CdTe quantum dots. For CdTe, by plotting the wavelength corresponding to the maximum of the first transition, nanoparticles size could be determined by the following expression,

$$D = \left(9.8127 \times 10^{-7}\right)\lambda^3 - \left(1.7147 \times 10^{-3}\right)\lambda^2 + \left(1.0064\right)\lambda - \left(194.84\right) \quad \text{Equation 1}$$

At the same time the relationship between size and ε was described as,

$$\varepsilon = 3450\Delta E\left(D\right)^{2.4} \quad \text{Equation 2}$$

where ΔE is the transition energy corresponding to the first absorption peak (expressed in eV). Knowing ε the molar mass is easily determined by measuring the absorbance of a

known concentration solution and by applying the Lambert-Beer law. All measured quantum dots solutions were freshly prepared in water. To prevent deviations of the Lambert-Beer law the solutions for the determination of size and extinction molar coefficient were prepared at appropriate concentration values, with an absorbance never superior to 0.1. For all the measurements a Jasco V-660 (Easton, USA) spectrophotometer and a Perkin Elmer (Waltham, MA, USA) Lambda 45 UV/VIS spectrophotometer were used.

3. Fluorescence spectroscopy

Since quantum dots are semiconductor nanoparticles able to absorb and emit light, fluorescence spectroscopy is one of the most important techniques for the investigation of their properties. A quantum dots emission spectrum can furnish assorted information (Figure 1). First of all, the red shift of the emission maximum is a clear symptom of the nanoparticle growth and this fact might be used to control the synthetic process. Other important data, deducible by spectrum analysis, is the FWHM.

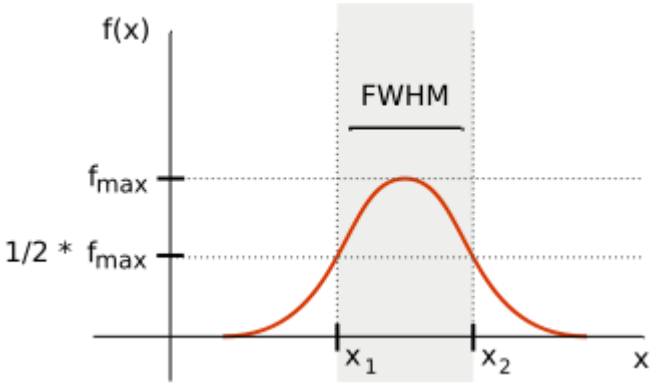

Figure 1 - Example of FWHM in a quantum dots spectrum.

One of the most challenging aspects in quantum dots synthesis is to obtain the narrower particle size distribution, because most of their properties are influenced by size. FWHM is a parameter strongly affected by size dispersion of NC population and tends to increase for higher dispersion. Fluorescence spectroscopy is also used for quantum yield determination, a type of information much more interesting than the absolute fluorescence value in what concerns the study of the properties of these materials. Absolute fluoresce measurements were used in the works presented in chapter x and y for the determination of chlorhexidine and N-acetyl-cysteine. Usually analytical techniques

involving quantum dos and fluorescence measurements are based in reactions that result in a quenching of the nanoparticle emission. The novelty of those works was that for the first time, instead of a fluorescent quenching phenomenon, the interaction between the analyte and the nanocrystals produced a significant enhancement of the emission intensity. An important particularity of the application of this detection technique with QDs concerns the selection of suitable nanoparticles concentration in order to avoid inner filter effects. This is especially true for the bigger quantum dots which, because of their size, can significantly diffract light even at very low concentrations producing a PL emission lower than expected.

For monitoring of the synthesis process (chapter 3) as well as for chlorhexidine (chapter 6) and N-acetyl-L-cysteine (chapter 5) determination an optical fiber spectrofluorometer (USB 4000-FL, Ocean Optics, Dunedin, USA) equipped with premium-grade fibers (QP1000-2-UVVIS, Ocean Optics, Dunedin, USA) and a LS-450 pulsed light source and a CUV-UV Holder, was used. The excitation maximum at 395 nm was guaranteed by using a LED-395 (Ocean Optics, Dunedin, USA) as source.

Fluorescence spectra for QDs characterization and FWHM quantification were recorded with a PerkinElmer LS-50B (Waltham, MA, USA) and a Jasco FP-6500 (Easton, USA) luminescence spectrometer.

4. Quantum yield measurement

The absolute emission quantum yields were measured at room temperature using a quantum yield measurement system C9920-02 from Hamamatsu with a 150 W Xenon lamp coupled to a monochromator for wavelength discrimination, an integrating sphere as sample chamber and a multi channel analyzer for signal detection. Three measurements were made for each sample so that the average value is reported. The method is accurate to within 10 %. Excitation wavelength was fixed at 400nm. All the quantum dots samples analyzed were freshly prepared in water, and the solution absorbance was around 0.1 at 400nm. For the quantum dots immobilized in glass (chapter 7) a water dispersion was used for the measurements in order to avoid oxidation of the nanoparticle by contact with the atmospheric oxygen.

5. Fourier transformed infrared spectroscopy (FTIR)

FTIR is an absorption analytical technique that can be used to identify chemical compounds and substituent groups. When a sufficiently energetic quanta of infrared light interacts with a target molecule capable to absorb it, it promotes the vibration of the molecule along its bond. Chemical bonds have specific frequencies at which they vibrate corresponding to discrete energy levels, so the frequency can be associated to a particular bond type.

A Fourier transform instrument, differently from a classical transmission infrared spectrophotometer, is based on a Michelson Interferometer and all the wavelengths are measured at the same time. The interferogram resulting from this measure is then transformed in a transmittance or absorbance spectrum by Fourier transform.

This technique was used in the works presented in the chapter 5, to determine the nature of the interaction between N-acetyl-L-cysteine and QDs, and in chapter 7 to prove the covalent nature of the QDs linking to aminated glass. In this works an ATI Mattson Genesis series (software: WinFirst v. 2.10) spectrophotometer and a Perkin-Elmer Spectrum BX FTIR, were used, respectively. For both works the assayed samples were homogeneously dispersed in KBr (≈ 2% wt). Structure of the bonds was confirmed by data available in literature. For the work presented in chapter 7 was necessary to perform a 2nd derivative and spectrum subtraction in order to identify the presence of the formed imine band.

6. X-ray diffraction

X-ray diffraction is a non-destructive analytical technique predominantly used for the phase identification of a crystalline material and is a common technique for the study of quantum dots crystal structures and atomic spacing.

The ordered structure of crystals produces a coherent scattering of the x-rays, which can be observed at specific angles diffracted from the sample depending of the material lattice constant. A crystal lattice is a regular three-dimensional distribution (cubic, rhombic, etc.) of atoms in space. Because of their regular arrangement, the atoms form a series of parallel planes separated from one another by a distance *d*, dependent from the nature of the material. In X-ray diffraction the incident radiation induces on the sample an accelerated movement of the electrons. This movement creates a wave with the same wavelength of incident radiation, a process called consistent dispersion [2]. As a

consequence of the regular atom arrangement coherent dispersion is enhanced in certain directions and cancelled in others due to interference effects, as pictured in figure 2.

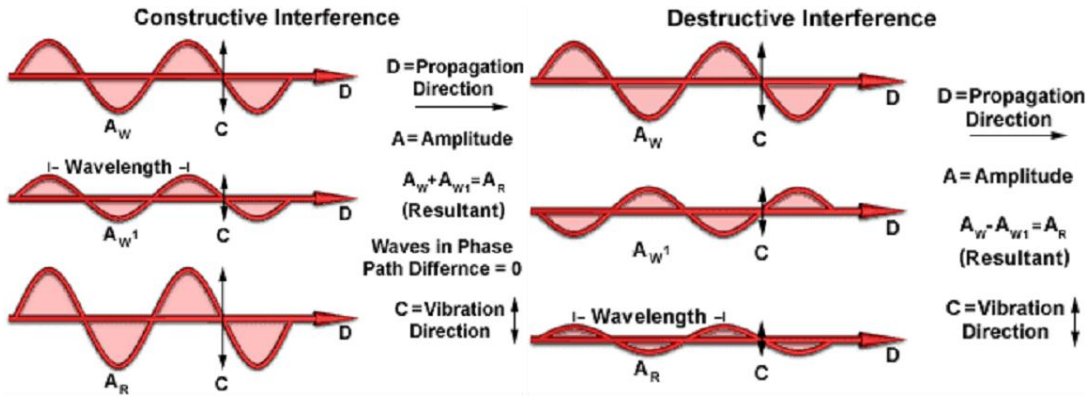

Figure 2. Example of constructive and destructive interferences in X-ray.

If one imagines a monochromatic X-ray beam with wavelength *lambda* projected onto a crystalline material at an angle *theta*, diffraction occurs only when the distance travelled by the rays reflected from successive planes differs by a complete number *n* of wavelengths (figure 3) and satisfies the Bragg law,

$$n\lambda = 2d \sin\theta \qquad \text{Equation 3}$$

that relates the wavelength of the incident electromagnetic radiation (λ) with the diffraction angle and the lattice spacing (*d*) in the crystalline sample.
By scanning the sample through a range of 2θ angles, all possible diffraction directions of the lattice should be attained due to the random orientation of the powdered material.

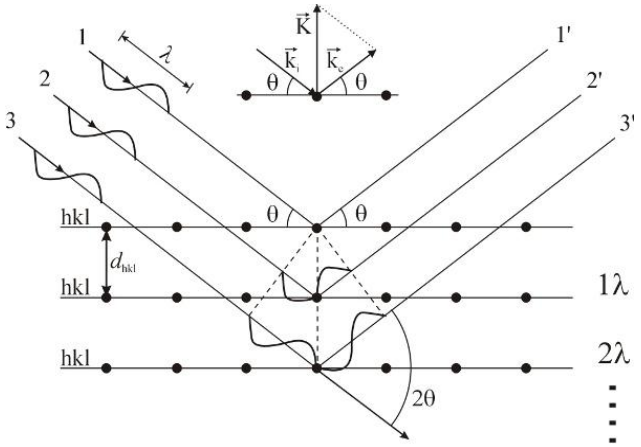

Figure 3. Representation of the X-ray diffraction by crystal surface of thickness d in the direction perpendicular to its plane.

X-ray diffractometers consist of three basic elements: an X-ray tube, a sample holder and an X-ray detector. X-rays are generated in a cathode ray tube by means of heating a filament to produce electrons. These are accelerated towards a target material by applying a voltage. When the bombarding electrons have sufficient energy to dislodge inner shell electrons of the target material characteristic X-ray spectra are produced. Filtering, by using foils or crystal monochromators, is required to produce monochromatic X-rays needed for diffraction. Copper is the most common target material for single-crystal diffraction, with CuK_α radiation = 1.5418Å. These X-rays are collimated and directed onto the sample. As the sample and detector are rotated, the intensity of the reflected X-rays is recorded. When the geometry of the incident X-rays impinging the sample satisfies the Bragg Equation, constructive interference occurs and a peak in intensity occurs (Figure 4).

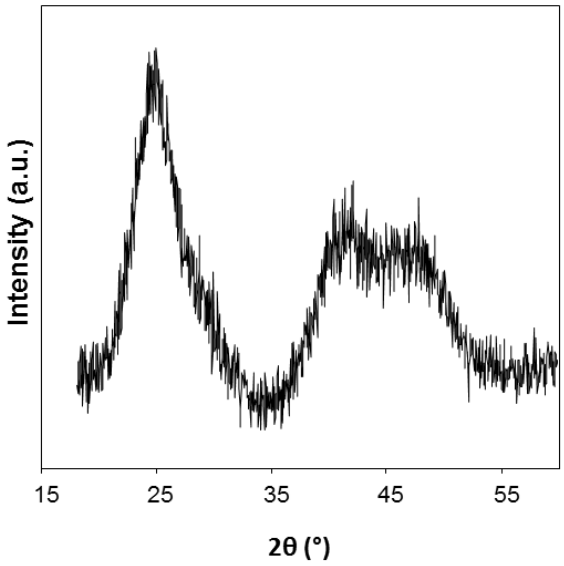

Figure 4. Typical diffraction pattern for CdTe quantum dots.

By analyzing the line profile, more specifically the FWHM of the peak, it is possible to also determine the crystallite size (Chapter 3). With this propose, and between the existing methods, the Scherrer Equation [3] is one of the most commonly used;

$$\tau = \frac{K\lambda}{\beta \cos\theta} \qquad \text{Equation 4}$$

where K is the shape factor, λ is the X-ray wavelength, β is the line broadening at FWHM in radians, and θ is the Bragg angle.

In this work powder X-Ray Diffraction was performed using a Philips X'Pert X-ray MPD diffractometer pe to confirm the formation of CdTe nanocrystals and to determine the existence of impurities or additional monolayers with different cell-unit size/structure. Scherrer Equation was also applied to confirm the crystallite size.

7. Transmission electron microscopy (TEM)

A detailed structural and morphological characterization of nanoparticles can be achieved using transmission electron microscopy (TEM). In a TEM microscope a beam of electrons is forced to pass through a sample, and then an image is formed, magnified and directed to appear on a photographic film or detected by a sensor such as a CCD camera. The electrons beam penetrates the sample and gives information about its morphology, size or structure. Electrons are emitted from a field emission gun and focused by means of magnetic lenses. A final lens sets the sample either on the image or on the focal plane. In the first case a magnified image of the sample is obtained at the CCD camera. On the contrary, when the sample is focused on the focal plane an image of the reciprocal space is taken and electron diffraction can be performed. TEM was used primarily to validate QDs size obtained with other microscopic/spectrophotometric techniques.

8. Atomic force microscopy (AFM)

AFM is a powerful technique for visualizing and measuring nanometer scale features.
It provides a 3D image at the nanoscale by measuring the forces existing between a sharp probe and a surface at a distance ranging between 0.2 and 10nm [4]. This probe is placed at the end of a cantilever, and the intensity of forces between the probe and the surface is dependent on both the *spring constant* of the cantilever and the distance from the surface. This force is described by the Hooke Law's,

$$F = -kx \qquad \text{Equation 5}$$

where k is the spring constant and x the cantilever deflection.

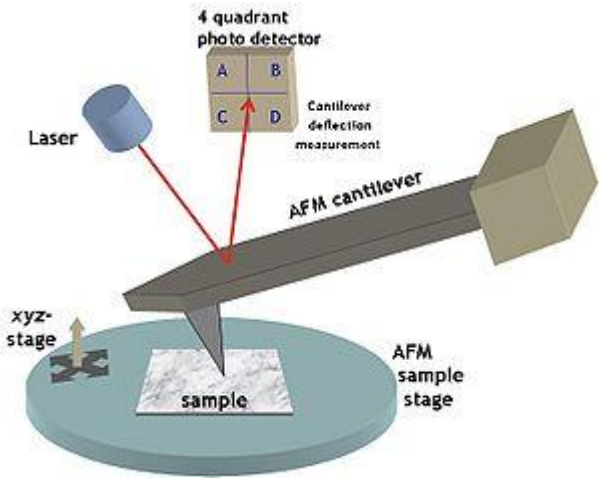

Figure 5. Simple representation of atomic force microscopy.

The probes are normally made of Si or Si_3N_4 and can have different sizes, shapes and lengths. The movement of the probe on the sample surface is generally controlled by piezoelectric scanners and feedback loops, and the deflection is usually measured by means of a laser (Figure 5). This is pointed at the back of the cantilever and reflected towards a photodiode detector that measures the cantilever bending during the scanning of the sample. In AFM there are three primary imaging modes:

i) contact mode: the tip scans the sample in close contact with the surface. The force on the tip results from repulsive Van der Waals forces. When the spring constant of the cantilever is less than surface one, the cantilever bends. Using feedback loops the cantilever deflection can be maintained constant. This way the force between the tip and the scanned surface does not change and the image can be acquired.

(ii) tapping mode: the cantilever tip oscillates at the sample surface with its resonant frequency contacting the surface at the bottom of its swing. By maintaining a constant oscillation amplitude a constant tip-sample interaction is maintained and an image of the surface is obtained.

(iii) non-contact mode: in this case the probe does not contact with the sample surface but oscillates on the fluid layer naturally existing upon it. Changes on the amplitude of this oscillation due to attractive Van der Waals forces can be monitored using a feedback loop.

The relatively easy and fast sample preparation makes this technique really useful for size determination of quantum dots nanoparticles. In this work AFM was used for the studies presented in Chapters 4 and 8. Samples were prepared by drying onto freshly cleaved mica substrates from diluted aqueous solutions. AFM measurements were made using an AFM Workshop TTAFM instrument in vibrating (intermittent contact) mode. A small (15 >μm) scanner and low gains were used to ensure high resolution. Probes from AppNano (ACT)

with resonant frequency of around 300 kHz were used. Images were analysed using Gwyddion software.

9. Fluorescence microscopy

A fluorescence microscope is similar to an ordinary optical microscope but equipped with some features that enhance its capabilities to highlight the emission of a fluorophore present in the sample [5]. A fluorescence microscope uses a high intensity light source which excites a fluorescent species in a sample of interest. This fluorescent species, in turn, emits a lower energy light of a longer wavelength that produces the magnified image (Figure 6).

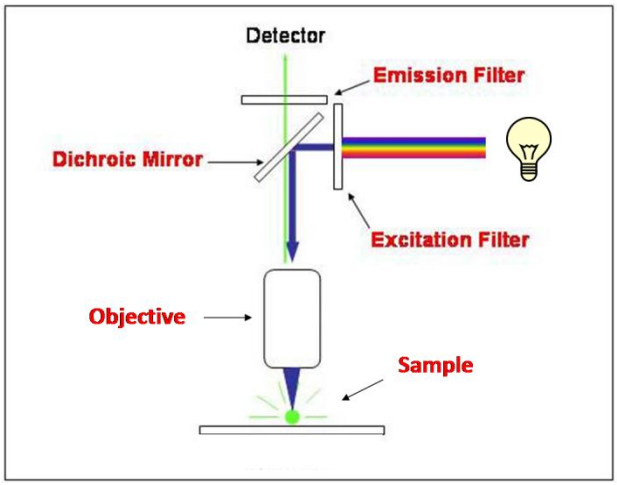

Figure 6. Schematic representation of a fluorescence microscope.

For the selection of incident radiation a excitation filter is used. The fluorescence emitted from the sample is separated from the much brighter excitation light in a second filter (emission filter). The majority of the fluorescence microscopes used nowadays, including the one used in these experiments, are epi-fluorescence microscopes. This means that both the excitation and the observation of the fluorescence occur above the sample. Fluorescence microscopy was performed to prove the conjugation of quantum dots on aminated glass beads surface (chapter 7). With this purpose a system composed by an inverted epifluorescence microscope (Eclipse TE300, Nikon, Tokyo, Japan) equipped with 10X air objectives, a monochromator (Polychrome II; TILL Photonics, Martinsried, Germany), a CCD camera (C6790; Hamamatsu Photonics, Hamamatsu, Japan), and a computer with analysis software (Aquacosmos 2.5; Hamamatsu Photonics) was used.

10. Flow apparatus and instrumentation

10.1. Flow manifold based on the multipumping concept

In the following sections the fundamental components of the flow systems, based on the multipumping concept, developed in the different analytical determinations carried out under the scope of this thesis will be discussed in detail. The devices and components used in the assemblage of the referred flow systems will be also described.

10.2. Propelling and insertion devices

For propelling and insertion of sample and reagent solutions in the developed analytical systems, solenoid micro-pumps were used. The same devices were exploited for the continuous monitoring of the QDs synthesis. The solenoid micro-pumps were purchased from Bio-Chem Valve Inc. (Boonton, USA) and exhibited different stroke volumes namely 10, 25 and 50 µL (models 120SP1210, 120SP1225 and 120SP1250 respectively). Those micro-pumps had a cylindrical configuration and reduced dimensions (Figure 7).

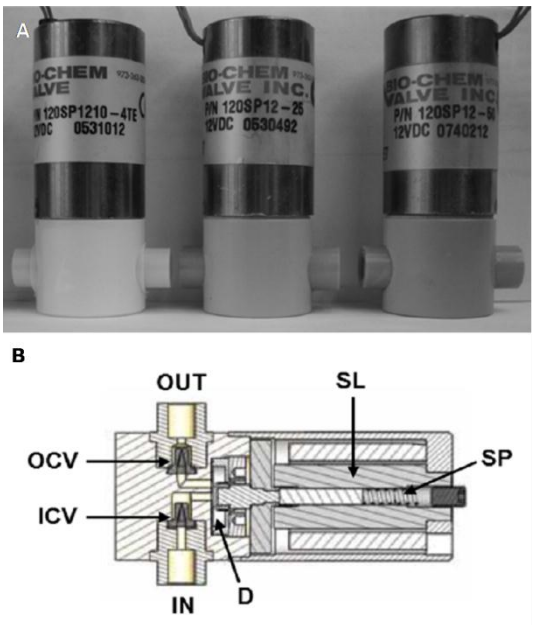

Figure 7 – A. Solenoid micro-pumps; B Schematic representation of solenoid micro-pumps cross section (adapted from [6]). ICV, inlet check valve; OCV, outlet check valve; D, diaphragm; SL, solenoid; SP, spring

The functioning of the micro-pump is based on the displacement of a flexible diaphragm operated by a solenoid. In the inactive state the diaphragm is maintained closed by means of an inner spring mechanism. When the solenoid is energized the diaphragm open, permitting the entry of fluid into the pump chamber through the inlet check valve. Simultaneously the outlet check valve is closed. In the subsequent step the solenoid is de-energized and the spring forces the diaphragm to the close. At this point a determined volume of fluid is dispensed through outlet check valve and simultaneously the inlet check valve is closed [6].

A peristaltic pump Minipulse 2 purchased by Gilson Inc. (Middleton, USA) was used for the automatization of the quantum dots synthesis (chapter 3). This pump consisted on a rotating head that exhibit several spinning rollers. The flow is generated when the head rotates and squeezes the rollers onto a flexible tube. Because of the high temperature and the high reactivity of the NaHTe solution a fluoroelastomer flexible tube was used.

10.3. Tubing and other manifold components

All tubing used to connect the different components of the multipumping flow systems was made of polytetrafluoroethylene (Omnifit), with 0.8 mm of internal diameter. End-fittings and connectors were also used. The reactors with different length were also made with PTFE tubes of 0.8 mm i.d. Laboratory made acrylic (Perspex®) connectors were used as confluences in order to connect the tubes to one another and to other parts of the system. Confluences with different configurations namely in triple (Y-shaped) or in quadruple (usually in the shape of an arrowhead) were used.

For NaHTe transfer during the synthesis automatization PTFE tube of 1 mm i.d. was employed.

10.4. Detection systems

As it was previously referred, for the fluorimetric determinations described in Chapter 5 and 6, as well as for the synthesis monitoring (chapter 3), an Ocean Optics optical fibers (QP1000-2-UVVIS, Ocean Optics, Dunedin, USA) spectrofluorometer (USB 4000-FL, Ocean Optics, Dunedin, USA) equipped with a LS-450 light source and a CUV-UV Holder, was used. The excitation maximum at 395 nm was guarantee using a LED-395 (Ocean Optics, Dunedin, USA) as source. In all works an Hellma flow cell (8µL inner volume, 10

mm optical path) was used. The flow manifold described in Chapter 4 used a A Camspec CL-2 (Leeds, UK) luminometer equipped with a 60μL inner volume flow cell.

10.5. Computer control and data acquisition

The developed analytical flow systems were fully controlled by means of a microcomputer, through home-made software, allowing the selection and adjustment of all analytical parameters that conditioned the performance of the flow systems. The automatic control of the active devices used in the different flow systems was accomplished by an Intel Pentium® based microcomputer. A home-made power drive based on a ULN2003 chip (chapter 5) or a CoolDrive (Nresearch, West Caldwell, NJ, USA) (chapters 3, 4 and 6) was used for the actuation of solenoid micro-pumps. This is a crucial component of a MPFS because it provides the electric current required for the activation of the solenoids. The developed flow systems were controlled by means of home-made software developed in Visual Basic (chapter 3, 5 and 6) or Quick Basic 45 (chapter 4). The connection between the microcomputer and the power drive was always established through the parallel LPT1 port.

The analytical signals obtained in the determination described in Chapter 4 were registered by means of a model L250E Linseis chart recorder which was coupled to the detection system. In the analytical determinations performed in Chapters 5 and 6 the data acquisition was accomplished by using the Spectrasuite software version 2007 (OceanOptics, Dunedin, USA). The same program was used for the data acquisition in chapter 3.

10.6. Additional Instrumentation

According to the required precision, reagents were weighed in a Mettler Toledo (Mettler-Toledo International Inc., Columbus, USA) AG 285 analytical balance (precision of 1×10^{-5}), Kern (Balingen, Germany) ABT 120-5 DM analytical balance (precision of 1×10^{-6}), Kern ACJ/ACS 80-4 (precision of 1×10^{-5}) and Kern 440-35N balance (precision of 1×10^{-2} g). The solutions were agitated by a Falc - F60 electromagnetic stirrer with heating option. To degas the solutions a VWR USC 100T5 (VWR International, Radnor USA) ultrasonic bath was used. Solutions pH was measured using a combined glass pH electrode (Crison 52-02, Crison Instruments, Alella, Spain) and a Crison model GLP 22 milivoltimeter. The calibration of the combined electrode was daily performed with commercial standards of

pH = 4.00 (Riedel-de Haën, 33543), pH = 7.00 (Riedel-de Haën, 33546) and pH = 9.00 (Merck, 9889). For the synthesis of quantum dots magnetic stirrers with heating IKA C-MAG HS 7 equipped with sensor IKA ETS-DS were employed (IKA-Werke GmbH & Co., Staufen, Germany). With the same propose were used heating mantles from JP Selecta (Abrera, Spain) coupled to a digital controller Omron E5CC and a thermo couple probe from OMEGA (Stamford, USA). A centrifuge Jouan BR4 multifunction (Thermo Fisher Scientific Inc.) and Centurion K_2 Series were used for the separation of precipitated quantum dots. Precipitated nanoparticles were dried under vacuum by using a V-700 vacuum pump (Buchi, Flawil Switzerland). Jasco LC-NET II/ADC high performance liquid chromatograph furnished with a PU-2080 Plus Intelligent pump, a Waters XTerra™ RP_8 3.9 mm × 150 mm column and a MD-2015 Plus multiwavelength detector was used to perform the refence methods in chapter 4 and 5.

10.7. Statistical evaluation of results

In the analytical determinations described in Chapters 5, 6 and 7, the analytical signal, corresponding to the drug concentration under evaluation, was calculated as a function of the average of a set of measures obtained by consecutive insertions of the same sample. The final concentration was calculated by interpolation of the obtained analytical signal intensity in the calibration curve established for each methodology. If required and for accuracy assessment the results obtained from the developed methodologies were compared with those provided by the reference procedures and paired t-tests were applied.

The t value was calculated from the formula $t = \frac{\bar{x}}{s}\sqrt{n}$, where $\bar{x}$ and s are the mean and the standard deviation, respectively. The number of degrees of freedom of *t* was n – 1. The *t* value calculated when compared to the reference *t* value (P = 0.05), for a significance level of 95 %, allowed to confirm the agreement between the two methods when the null hypothesis is verified [7].

For size determination of quantum dots in AFM and TEM at least 100 nanoparticles were measured and the value presented is the mean of all the particles counted.

References

[1] Yu WW, Qu L, Guo W, Peng X. Experimental determination of the extinction coefficient of CdTe, CdSe, and CdS nanocrystals. Chem Mater 2003 Apr; 15(14):2854-60.

[2] Cullity BD. Elements of X-Ray Diffraction, Addison-Wesley, 1978.

[3] Scherrer P. "Bestimmung der Grösse und der Inneren Struktur von Kolloidteilchen Mittels Röntgenstrahlen, Nachrichten von der Gesellschaft der Wissenschaften, Göttingen," *Mathematisch-Physikalische Klasse*, Vol. 2, 1918, pp. 98-100.

[4] Jalili N, Laxminarayana K. A review of atomic force microscopy imaging systems: application to molecular metrology and biological sciences. Mechatronics 2004 ;14 () 907-945.

[5] Bradbury S, Evennett, P. *Fluorescence microscopy, Contrast Techniques in Light Microscopy*. Oxford: BIOS Scientific Publishers, Ltd. 1996.

[6] Bio-Chem valve solenoid operated micro-pump. Available in: https://www.biochemfluidics.com/pdf/micro-pump-brochure.pdf

[7] Miller JN, Miller JC. Statistics and Chemometrics for Analytical Chemistry. 4th ed. GreatBritain: Pearson Education; 2000.

CHAPTER 3

Automated Aqueous Synthesis of CdTe-MPA Capped Quantum Dots

Automated Aqueous Synthesis of CdTe-MPA Capped Quantum Dots

Christian Frigerio and JoãoL.M. Santos
University of Porto, REQUIMTE, Faculty of Pharmacy, Dept Chem Sci, Lab Appl Chem, P-4050-313 Porto, Portugal.
† *Correspondence author:* joaolms@ff.up.pt

Abstract

Despite the enormous progresses already attained in the improvement of QDs photochemical properties, the poor synthesis reproducibility is an unsolved hindrance and has remained an elusive issue. At the same time, growth rate influence on the final optical properties of the synthesized QDs was not entirely ascertained. Herein, automatization of CdTe-MPA QDs aqueous synthesis was implemented allowing fast growing of the nanocrystals while assuring high reproducible controlled conditions for the entire synthetic process. The effects of the growth rate on the population dispersion and quantum yield (QY) have been investigated. Experimental results pointed that fast growth rate, avoiding Ostwald ripening regime, could produce narrower populations of bigger QDs (>3 nm). Lower growth showed the same effect for smaller nanocrystals (< 3 nm).
The QY result also influenced by the growth rate with respect to QDs size, but only before reaching the maximum QY value and not in absolutes terms. Under the assumption of stoichiometric crystals, the extinction coefficient per mole (ε) at 3.1eV and the molar mass of QDs were calculated and was found to be dependent on the nanocrystal size by exponential dependence.

Keywords

Quantum dots, CdTe, 3-mercaptopropionic acid, automatization, molar extinction coefficient

1. Introduction

In the last two decades the research on colloidal semiconductor nanocrystals (quantum dots or QDs) has experienced a huge development, both in terms of the preparation of new materials and their utilisation in a broad range of application, largely due to their incomparable size-dependent photochemical properties (Alivisator 1996). The exceptional and distinctive tunable properties of QDs has rendered them attractive tools for application in optoelectronic and photovoltaic devices (Robel et al 2006, McDonald et al 2005), in telecommunication networks (Kovalenko et al 2006), in bioimaging (Alivisator 2004, Ruedas-Rama et al 2012) as well as in an variety of analytical applications (Frigerio et al 2012).

The synthetic routes used to prepare QDs have always been subject to a great interest as these could determine most of the nanocrystals properties. In a broad perspective QDs synthesis could be included in two main groups: organometallic synthesis and aqueous synthesis. Organometallic synthesis is the most used approach to produce high quality QDs (Donega et al 2005). These are synthesized in organic solvents and have hydrophobic surface ligands that difficult a direct application in biological applications and in water-based analytical procedures. Different strategies were developed to modify the QDs surface chemistry in order to ensure solubilisation in water (Yang and Clapp 2011) but the great majority of these modifications impaired nanocrystal optical characteristics resulting in a pronounced decrease of quantum efficiency (Yang and Clapp 2011).

More recently direct aqueous synthetic routes have been proposed, in particular for CdTe QDs, getting a significant attention because they are simpler, safer and less expensive than the organometallic ones and the synthesized QDs are intrinsically soluble in water not requiring any additional post-synthesis treatment. The most common method for synthesizing water-soluble QDs, namely CdTe QDs, is by resorting to hydrophilic capping ligands. Thiol-containing stabilizing molecules (thioglycerol, thioglycolic acid, 3-mercaptopropionic acid, glutathione, etc) have been extensively used to ensure the surface passivation and to provide stability, solubility and surface functionality. Since the first work published in this field (Rajh et al 1993) remarkable progresses have been accomplished in the improvement of this synthetic approach, including the implementation of microwave (He et al 2006 and 2007, Duan et al 2009, Li et al 2005, Song et al 2010, Dong et al 2012) hydrothermal (Zhang et al 2003, Yang et al 2006, Yang et al 2008, Liu et al 2012) and photochemical aqueous synthesis (Liu et al 2012, Gao et al 2012). Comprehensive studies were also carried out on the assessment of the influence of

precursor concentration (Zhao et al 2007, Li et al 2007, Feteha et al 2012, Deng et al 2006), nature of thiol capping agents (Silva et al 2012, Zheng et al 2007, Zhang et al 2009), pH (Liu et al 2009, Li et al 2006) and temperature (Guo et al 2005, Khalavka et al 2010). This extensive research has boosted the application of QDs in analytical chemistry where they could be used as luminescent biolabels advantageously replacing hazardous radioactive markers or poor stability fluorescent or chemiluminescent organic dyes, as well as multicoloured photoluminescent probes in environmental and pharmaceutical analysis, with enhanced selectivity and sensitivity.

Despite the enormous progresses already attained in the improvement of QDs photochemical properties, the poor synthesis reproducibility is an unsolved hindrance and has remained an elusive issue. At the same time, growth rate influence on the final optical properties of the synthesized QDs was not entirely ascertained and required further investigation. In the present work aqueous synthetic process was automatized and continuously monitored by using a flow based approach. A model based on experimental results was also proposed for molar mass and molar extinction coefficient determination.

2. Experimental

2.1. Materials

Tellurium powder (200 mesh, 99.8%), sodium borohydride ($NaBH_4$, 99%), cadmium chloride hemi(pentahydrate) ($CdCl_2 \cdot 2.5H_2O$, 99%) were purchased from Sigma–Aldrich (St. Louis, MO, USA); 3-mercaptopropionic acid (MPA, 99%) and absolute ethanol (99.5%) were obtained from Fluka (St. Louis MO, USA) and Panreac (Barcelona, Spain), respectively. Standard solution for Cd determination was purchased by Merk.

2.2. Methods

2.3. Synthesis of Te precursor NaHTe

For the preparation of telluride precursor (NaHTe) a modified literature method was used (Fang et al 2008). Briefly, a certain amount of tellurium powder was placed in a two-neck flask with an excess of $NaBH_4$. All the air in the system was removed with a N_2 flow,

followed by the addition of 10 mL of ultra pure water, previously deoxygenated. The reaction mixture was heated at 80 ºC for 30 min under continuous N2 flow until no solid Te was visible and the solution turned dark violet. The obtained NaHTe fresh solution was readily and thoroughly transferred into a second flask for nanocrystals synthesis.

2.4. Synthesis of CdTe NCs

The developed synthetic route was similar to Zou et al (2008) with some modifications. In general, 0.2 mmol of CdCl2 solution and 0.34 mmol of MPA solution ([Cd]:[MPA] molar ratio 1:1.7) were mixed in a 40 mL solution and pH was adjusted to 11.8 by addition of 1.0 M NaOH solution under stirring. The solution was placed in a three-necked flask and deoxygenated for 30 minutes with a N2 flow. Freshly prepared NaHTe solution with variable concentration was added to the Cd precursor solution at room temperature. The reaction mixture was then refluxed at 100 ºC under atmospheric conditions with a condenser attached. Synthesis timing started when NaHTe transfer was completed.

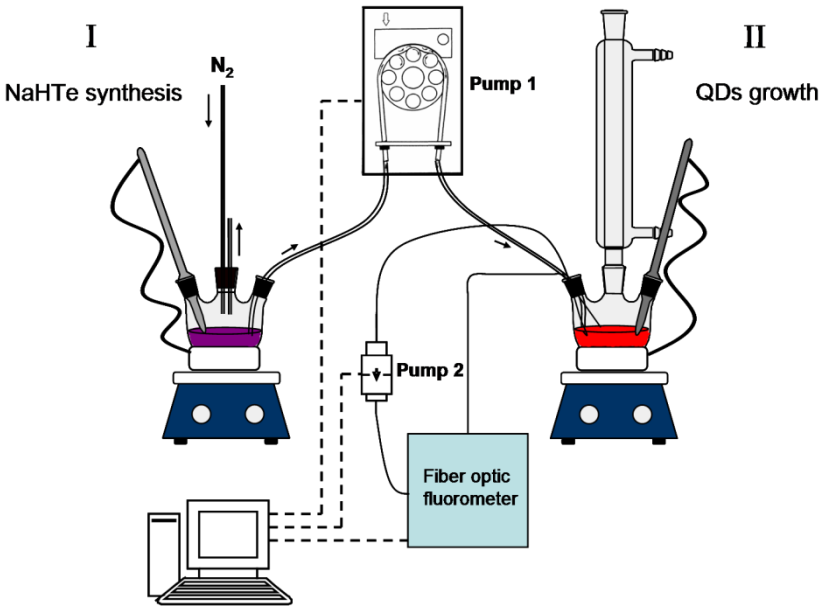

Figure 1. General schematic representation of the automated synthesis system. Pump 1: peristaltic pump used for the transfer of NaHTe from the first (I) to the second stage (II). Pump 2: solenoid micro-pump used for the real-time control of the synthesis. Dashed lines: computer controlled devices. Solid lines: recirculation circuit for real-time synthesis monitoring by means of a computer controlled fiber optic fluorometer.

2.5. Automatization

The flow manifold pictured in figure 1 was used in all synthesis. For the automatization of the process a peristaltic pump (Pump 1) was used for the introduction of deoxygenated water in the first synthetic stage and for the transfer of NaHTe into the second stage. Rotation of the pump head promoted the squeezing of the spinning rollers onto a flexible fluoroelastomer tube producing a solution flowing stream. The volume of solution injected or transfer was determined by means of controlling the pump rotation speed and time. The simultaneous synthesis of 2 QDs, in two parallel processes, was achieved simply by splitting the NaHTe solution into two fractions upon control of the peristaltic pump activation time and by using a y-shaped confluence. Connections between the two vessels were assured by polytetrafluoroethylene (PTFE) tubing (1mm i.d.). The synthetic process was continuously monitored by a recirculation circuit including a solenoid micro-pump (Pump 2) with a 10μL stroke volume used to propel the solution. In this case the tubing was also made of PTFE but with a lower internal diameter (0.8mm) in order to minimise the circulating volume avoiding its cooling. During recirculation the solution flowed through a continuous flow cell and its emission spectra were recorded in real time with a fiber optical spectrofluorometer. A PC was used to control the recirculation routine by means of dedicated software developed in Visual Basic, which enabled to operate the solenoid pumps by means of the LPT parallel port. The system was implemented in a computer equipped with a PC-LAB card model PCL-711 B (Advantech, Taipei, Taiwan) analogical/digital interface card used to operate and control de peristaltic pump. A homemade power drive based on the ULN2003 chip was used to operate the solenoid micro-pumps. The data acquisition was accomplished by using the Spectrasuite software version 2007 (OceanOptics, Dunedin, USA).

2.6. Characterization

Solution pH was measured using a pH meter Crison GLP 22. Real-time control of the synthesis was performed with a fiber optical (Ocean Optics, QP1000-2-UV-VIS) spectrofluorometer (Ocean Optics USB 4000-FL, Light Source LS-450) equipped with a 8 μL inner volume flow cell (176.753-QS, Hellma). The excitation maximum at 395 nm was guaranteed using the LED-395 source. UV-vis spectra were obtained on a Jasco V-660 spectrometer and PL spectra on a Jasco FP-6500 spectrofluorometer. The absolute emission quantum yields were measured at room temperature by using a C9920-02 quantum yield measurement system from Hamamatsu with a 150 W Xenon lamp coupled to a monochromator for wavelength discrimination, an integrating sphere as sample

chamber and a multi channel analyzer for signal detection. Three measurements were made for each sample so that the average value is reported. The method is accurate to within 10 %. Samples for atomic force microscopy (AFM) were prepared by drying onto freshly cleaved mica substrates from diluted aqueous solutions. AFM measurements were made using an AFM Workshop TTAFM instrument in vibrating (intermittent contact) mode. A small (15 >μm) scanner and low gains were used to ensure high resolution. Probes from AppNano (ACT) with resonant frequency of around 300 kHz were used. Images were analysed using Gwyddion software. Transmission electron micrographs (TEM) were taken on a JEOL JEM-1400 at an acceleration voltage at 100 kV. X-Ray powder diffraction (XRD) was measured by wide-angle X-ray scattering, using a Siemens D5005 2808 X-ray powder diffractometer equipped with graphite monochromated high-intensity Cu-Kα radiation (1.54178Å). XRD samples were prepared by depositing NC powder on a piece of Si (100) wafer. Jouan BR4I refrigerated centrifuge was used for QDs separation. Cadmium concentration was measured atomic absorption spectroscopy (AAS) using a Perkin Elmer 3100 atomic absorption spectrometer.

3. Results and discussion

3.1. Rapid and reproducible synthesis

Previous works (Zou et al 2008) have referred that the adjustment of pH up to 11.5 and the increment in precursor concentration can lead to extremely fast synthesis of CdTe-MPA QDs, especially when compared to the traditional synthetic route. In a typical automated synthesis the transfer of the first stage synthesized NaHTe into the second stage flask, which already contained the cadmium precursor (CdCl2) and the thiol molecule (MPA), produced a colour change in the CdCl2/MPA solution that turned yellow-orange but without showing any luminescence. When heating the solution a green fluorescence appeared as the temperature reaches 80°C and the solution turns red, a symptom of initiation of crystal growth. With the prolongation of reaction the fluorescence maximum and the absorption wavelength corresponding to the first transition shifted to longer wavelengths and the crystal size increased as showed in figure 2. Under the reaction conditions exploited in this work QDs emitting from green (515 nm) to NIR (810 nm) were synthesized. The absorbance spectra showed a well defined first excitonic transition that tended to lose its definition with increasing size. This phenomenon can be due to a weaker quantum confinement effect of the bigger QDs. Powder X-ray diffraction (p-XRD)

patterns for CdTe NCs (Fig. S1 of ESI†) confirmed the characteristic peaks of zinc blend cubic CdTe, which are broadened due to the finite crystalline size. For bigger NCs the prolonged heating yielded a partial degradation of the organic thiol promoting the liberation of sulphur that formed a monolayer of CdS on the QDs surface, as indicated by the small but progressive shift of the XRD reflections toward the position corresponding to cubic CdS. The overview TEM image (Figure S2) and AFM scan (Figure S3) illustrates the formation of nearly spherical and well dispersed CdTe NCs with an average size around the diameter calculated by Yu et al (2003).

For comparison purposes the same synthesis conditions (relative molar ratios for [Cd]:[Te]:[MPA]) of 1:0.1:1.7, respectively) and pH 11.8, were maintained for both the manual and the automated approaches. As it could be seen in figure 3, with the manual synthesis a faster NC growth was achieved although a lower reproducibility is clearly perceptible. On the other hand, using the automated route a lower growth rate was observed but with a huge improvement in terms of synthesis reproducibility. Similar results were verified during the assessment of a wide range of [Cd]:[Te] molar ratios, even for very high values, as shown in figure 3.

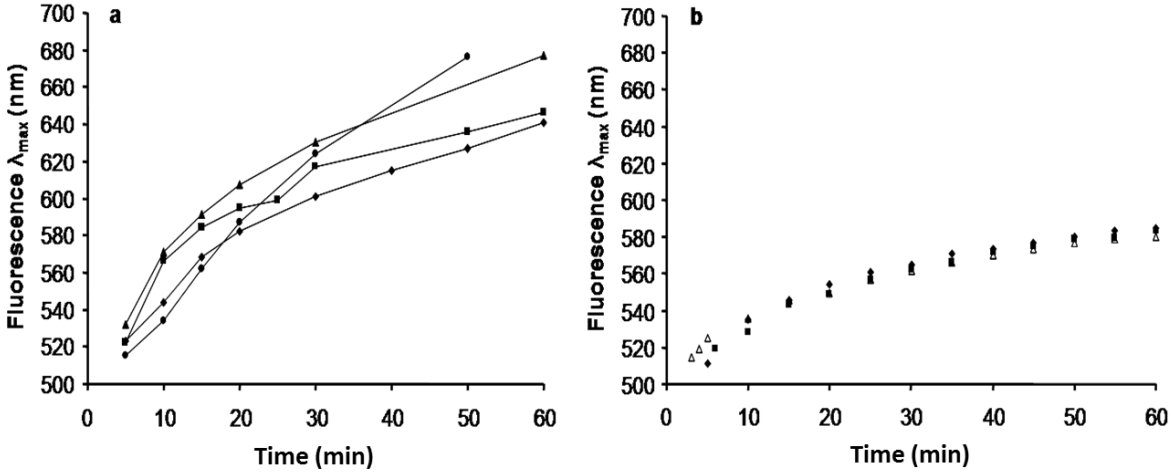

Figure 2. a) Temporal evolution of CdTe PL peak on “manual” (a) and automated (b) synthesis under the same conditions (([Cd]:[Te]:[MPA] molar ratio of 1:0.1:1.7, respectively), pH 11.8).

The automatization focused primarily in two sensitive steps of the synthesis: (i) the handling of the reagents used for the synthesis of NaHTe; (ii) the NaHTe transfer from the first into the second synthetic stage. The differences in the growth rate observed for the manual and automated techniques can be explained by an increase in the efficiency of these steps. NaHTe is extremely susceptible to oxidation by oxygen forming a black insoluble precipitate. It is anticipated that during the manual transfer a fraction of NaHTe

precipitates since the commonly used syringes do not entirely prevent contact with air as it happened with the automated system. For the same reason, during the manual introduction of deoxygenated water into the flask, for the synthesis of NaHTe, a small amount of air can enter the flask with the consequent partial oxidation of the tellurium powder. The partial loss of NaHTe observed in the referred transfer process or during its preparation would lessen the amount available for the second synthesis stage and would therefore affect the real [Cd]:[Te] molar ratio, promoting a faster growth. Because the magnitude of this loss is unpredictable the manual synthesis results more difficult to standardize. This problem is solved when these steps are carried out in a controlled environment without operator's intervention in an automated, therefore more reproducible, way.

3.2. Study of growth rate influence on nanocrystals size dispersion

One of the main goals in quantum dots synthesis is the production of a population of nanocrystals with a low size-dispersion. The organic synthesis permits the preparation of quantum dots with a very narrow size distribution, with an emission peak full width at half maximum (FWHM) of about 30 nm (Yu at al 2003). In the aqueous synthesis narrowing the size dispersion is more difficult mainly because the temperature is lower than the one used in the organometallic approach, which turns the nucleation stage slower compromising the focusing regime efficiency (Rogach 2008).

In this work it was decided to vary the [Cd]:[Te] precursors molar ratio in order to enhance growth rate. Four different [Cd]:[Te] ratios were used: 10:1, 20:1, 30:1, 40:1, and their influence on the synthetic process is showed in figure 3. As it was expected, the growth rate increased with the increase in the molar ratio, as previously described by Zou et al (2008). However, the obtained resulted showed that to achieve a growth rate similar to that of the cited work, higher molar ratios would have to be used. Once again, this discrepancy is explained by the more efficient transfer of Te precursor, and therefore a lower oxidation extent (or no definite oxidation).

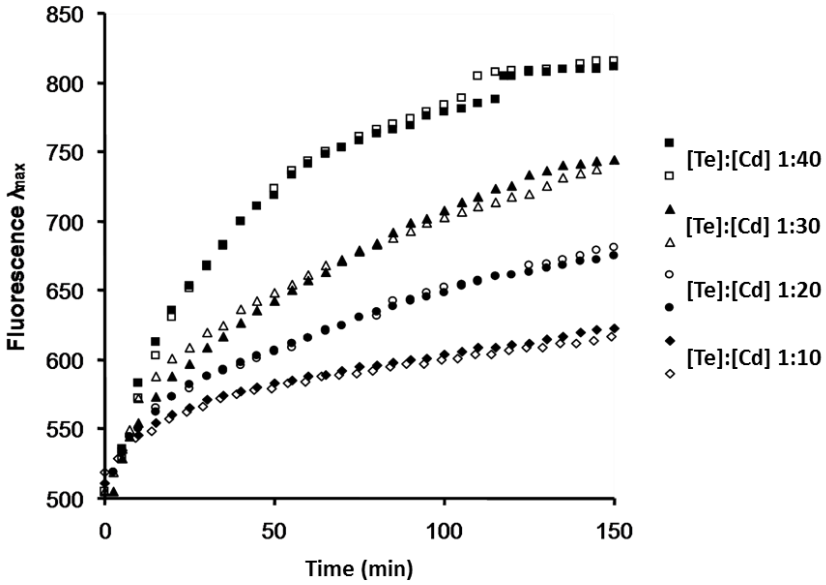

Figure 3. Temporal evaluation of CdTe QDs synthesized with different [Cd]:[Te] molar ratios. To highlight reproducibility the graphic shows two syntheses for every molar ratio used.

In previous studies only partial information on the influence of growth rate on population dispersion was gathered. For each studied molar ratio, aliquots of QDs solution were taken at different synthesis interval. After removal of excess reactant, by precipitation, photoluminescence spectrum was recorded and the full width at half maximum (FWHM) was measured.

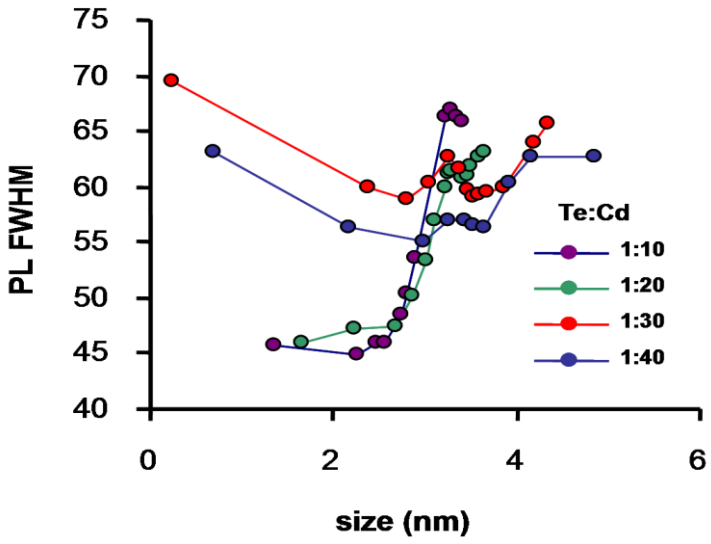

Figure 4. PL FWHM of different QDs series synthesized with variable [Te]:[Cd] ratios.

Upon evaluation of obtained results (Figure 5) it is evident that growth rate influences size dispersion and different focusing and defocusing tendencies are discernible. Lowest values of FWHM were found for lower growth rates (molar ratios [Cd]:[Te] of 10:1 and 20:1) but only for smaller QDs. A fast broadening of the PL spectrum occurs when the NCs approach a certain size (≈ 2.6 nm). For [Cd]:[Te], 10:1 molar ratio the FWHM reaches 66.85 nm for QDs of 3.36 nm. Around this size it is evident a peak on the size dispersion for all ratios. Above it there is a small dispersion decrease (focusing) followed by another defocusing phase. For the highest studied molar ratios (30:1, 40:1) the initial dispersion is relatively higher (69.58 for [Cd]:[Te] , 30:1) but the synthesis proceeded in a focusing regime until about 3 nm. Overall, it is noticeable that, as a function of size, different molar ratios could be used to manage QDs population dispersion. For higher ratios larger QDs (> 3 nm) resulted less dispersed probably because the time needed for their synthesis is not enough to entering in the Ostwald ripening regime. Smaller dots (< 3 nm) focusing is possible by using lower ratios.

3.3. Growth rate influence on the nanocrystals quantum efficiency

The emission efficiency of a fluorophore is normally expressed in terms of quantum yield (QY), the ratio between the number of absorbed and emitted photons. According to results found in literature, for MPA capped CdTe QDs the highest achieved QY were between 0.15 and 0.4 for the “fast recipe” route and between 0.1 and 0.32 for the “normal” route (Zou et al 2008). By using microwave synthesis, higher QY of about 0.4-0.6 and of 0.68 were reported by Li et al (2005) and by He et al (2006), respectively. It is important to emphasise that QY value is strongly affected by crystal quality: low crystallinity result in a greater number of defects and surface traps that can compromise the radiative relaxation of the electrons from the conduction to the valence band. A fast NC growing is considered a prejudicial condition for the formation of highly perfect structures (Rogach 2008). The influence of the growth rate on the QY was assessed by measuring the QY values of selected QDs grown at different rates by varying the cadmium:tellurium molar ratio. Figure 5 pictured the variation of QY according to NCs size being distinguishable an exponential relationship between these two parameters, until the attainment of the maximum QY value. After this value (0.53 at 4.18 nm for [Cd]:[Te], 20:1) QY approaches stabilisation or a slight decrease occurred for larger sizes.

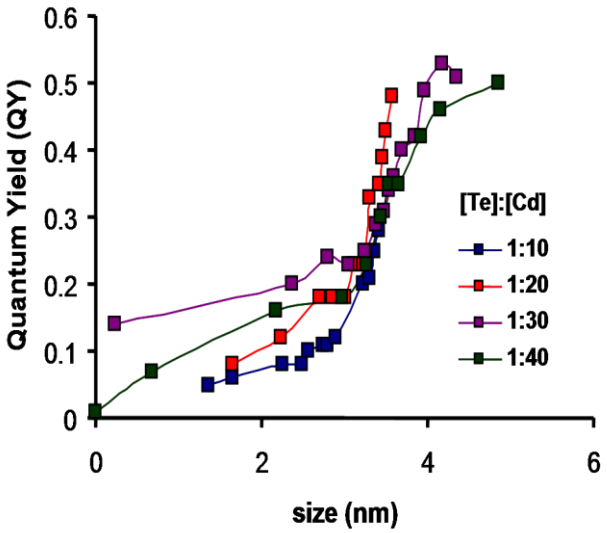

Figure 5. Influence of the [Te]:[Cd] ratio on the QY.

On the other hand, for lower molar ratios a higher slope was evident. Taking into account specific sizes, such as (≈3.6 nm), it is noticeable that the highest QY (0.48) was achieved with [Cd]:[Te], 20:1. For sizes between ≈ 3.2 and 3.5 nm all four assayed molar ratios yielded similar QY. On the contrary, for smaller QDs (≈ 1 up to ≈ 3 nm) the differences between QY are significant and the use of a higher molar ratio permitted the synthesis of more perfect nanocrystals. QDs with size greater than 3.6 nm were synthesized only at high cadmium:tellurium ratio and the data showed that for a 30:1 ratio the QY decreased after attaining the maximum for 4.18 nm, while for [Cd]:[Te], 40:1 this maximum seems to shift towards larger QDs (> 4.85 nm). This means that the QDs QY can be influenced by the growth rate with respect to QDs size only before reaching the maximum QY value and not in absolutes terms. This will depend on the slope of the variation of the QY versus size because, under the studied conditions, the absolute QY maximum seems to be independent of growth rate.

3.4. Molar Extinction Coefficient and molar mass of particles

The molar extinction coefficient (ε) of semiconductor nanocrystals is a parameter of great practical importance, being very useful when considering their application. The QDs molar mass is also a fundamental data, especially when NCs are used as photoluminescent labels. Few articles proposed experimental models for the determination of extinction coefficients of CdTe QDs, being the most important one the work developed by Yu et al (2003). This model was established for QDs synthesized by the organometallic route,

which afforded narrow size distributions and the production of QDs with size larger than 3.5 nm. The population dispersion is a parameter that strongly influences ε at the first transition maximum, especially enhancing the error associated to its calculation (Yu et al 2008, Moreels et al 2007). To avoid this error it is possible to determine ε at a wavelength lower than the one corresponding to the first excitonic transition, where ε is no longer influenced by size dispersion (Moreels et al 2007). Furthermore, the hydrothermal aqueous synthesis allows preparing QDs smaller than 3.5 nm, which are not included on the existing models.

Aiming at constructing our model different QDs samples were submitted to several cleaning steps, to guarantee the removal of possible interfering species. Subsequently, several solutions at known concentrations were prepared and the Cd concentration was measured by atomic absorption spectrometry (after sample digestion). Assuming a stoichiometric nanocrystal, a [Cd]:[Te], 1:1 ratio was established and the total mass of CdTe in solution was calculated. Because CdTe QDs have a near spherical shape, the number of atoms in each QDs was given by the equation 1;

$$A = \frac{4\pi}{3}\left(\frac{r}{a}\right)^3 \quad (1)$$

where r is the radii of the QDs (calculated by Yu et al 2008), and a is the lattice constant for CdTe.

By knowing A, the QDs core mass (QDcore m) and the number of QDs in solution were then calculated. The mass corresponding to the MPA capping was calculated taking into consideration the total mass of QDs in solution and the estimated total CdTe mass.

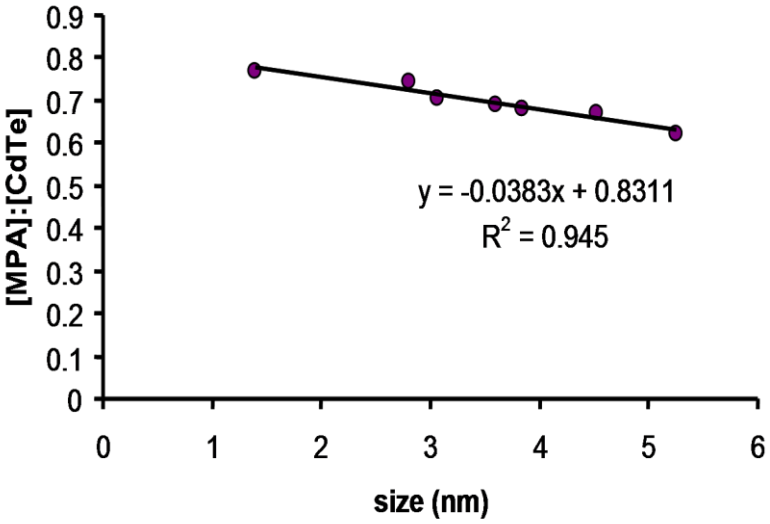

Figure 6. [MPA]:[CdTe] molar ratio for different size QDs, assuming a stoichiometric crystal. The obtained equation was employed in molar mass calculation.

The molar ratio [MPA]:[CdTe], showed in figure 7, was found to be size dependent and tended to decrease with the increase in the NCs size. The equation representing the observed linear relationship (R2 = 0.945) could be used for the calculation of the molar mass upon relating [MPA]:[CdTe] variation with the increase in nanocrystal size. The molar mass can be then calculated by using the equation 2;

$$\mathrm{M} = \frac{\left(QD_{core}m + \left(QD_{core}m \times \left(-0.0383d + 0.8311\right)\right)\right) \times NA}{1000} \qquad (2)$$

where $QD_{core}m$ is the nanoparticle core mass, d the QD diameter, NA the Avogadro's number. Plotting M versus nanocrystal diameter an exponential relationship could be obtained (Equation 3),

$$\mathrm{M} = 6657.8d^{1.9501} \qquad (3)$$

The molar extinction coefficient was determined by the Beer-Lambert law (Equation 4),

$$A = \varepsilon dC \qquad (4)$$

where *A* was the absorbance at 3.1eV (400 nm) of the same solution used for AA, *C* the molar concentration of the NC in the solution and *l* was fixed to 1 cm.

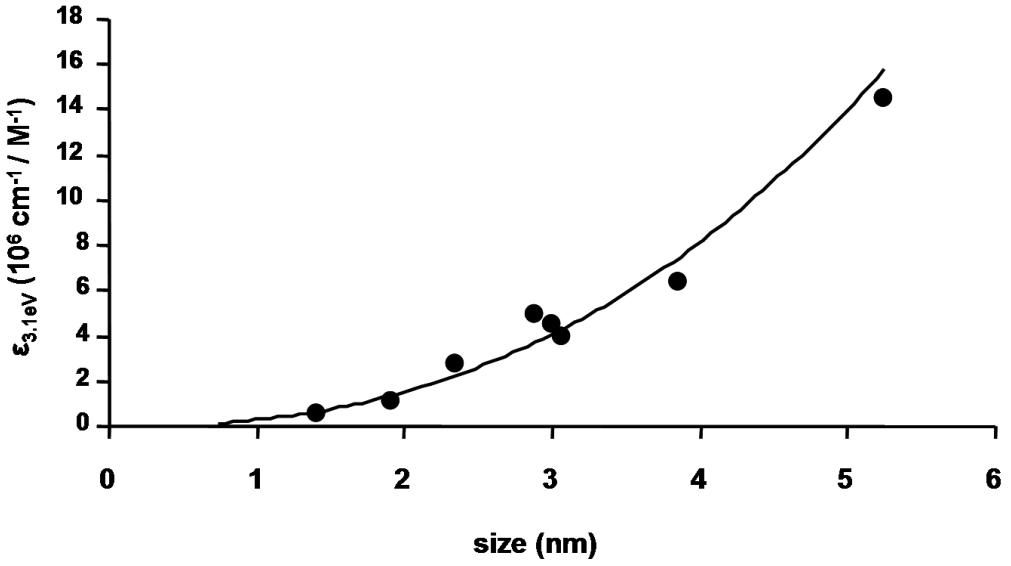

Figure 7. Graphical representation of the extinction molar coefficient variation with the size.

By graphical representation of ε with respect to size (Figure 8) an exponential relationship was verified (Equation 5),

$$\varepsilon = 284175 d^{2.422} \quad (5)$$

where *d* is the QD diameter in nm.

4. Conclusions

The automatization of CdTe-MPA QDs aqueous synthesis was implemented allowing fast growing of the nanocrystals while assuring high reproducible controlled conditions for the entire synthetic process. This, when combined with the utilisation of high [Cd]:[Te] precursor molar ratios in order to enable high growth rate similar to those available in literature, demonstrated that developed approach assured a efficient management of precursor concentration, in particular for NaHTe. The influence of the growth rate on the population dispersion was also studied, showing how for higher ratios larger QDs (> 3 nm)

resulted less dispersed probably because the time needed for their synthesis is not enough to entering in the Ostwald ripening regime. Smaller dots (< 3 nm) focusing is possible by using lower ratios.

The QY also result influenced by the growth rate with respect to QDs size, but only before reaching the maximum QY value and not in absolutes terms. This will depend on the slope of the variation of the QY versus size because, under the studied conditions, the absolute QY maximum seems to be independent of growth rate

By assuming stoichiometric crystals an experimental model was created to calculate the QDs molar mass and the molar extinction coefficient only by its optical characteristics. Differently from the already existing in literature, the proposed model avoids the population dispersion influence, and included nanocrystals with diameter less to 3.5 nm.

References

Alivisatos AP. (1996) Semiconductor Clusters, Nanocrystals, and Quantum Dots. Science 271:933-937.

Alivisatos AP. (2004) Nat. Biotechnol. 22:47–2252.

Deng D, Qin Y, Yang X, Yu J, Yi Pan Y. (2006) The selective synthesis of water-soluble highly luminescent CdTe nanoparticles and nanorods: The influence of the precursor Cd/Te molar ratio. J. Cryst. Growth, 296: 141–149.

Donega CdM, Liljeroth P, Vanmaekelbergh D (2005) Physicochemical evaluation of the hotinjection method, a synthesis route for monodisperse nanocrystals. Small 1: 1152–1162.

Dong C, Ren J. (2012) Water-soluble mercaptoundecanoic acid (MUA)-coated CdTe quantum dots: one-step microwave synthesis, characterization and cancer cell imaging. J Luminesc.,27: 199–203.

Duan J, Song L, Zhan J. (2009) One-Pot Synthesis of Highly Luminescent CdTe Quantum Dots by Microwave Irradiation Reduction and Their Hg^{2+}-Sensitive Properties. Nano. Res., 2: 61-68.

Feteha M, Ebrahim S, Soliman M, Ramdan W, Raoof M. (2012) Effects of mercaptopropionic acid as a stabilizing agent and Cd:Te ion ratio on CdTe and CdHgTe quantum dots properties. J. Mater. Sci.: Mater. Electron., 23:1938–1943.

Frigerio C, Ribeiro DSM, Rodrigues SSM, Abreu VLRG, Barbosa JAC, Prior JAV, Marques KL, Santos JLM. (2012) Application of quantum dots as analytical tools in automated chemical analysis: A review. Anal. Chim. Acta 735:9–22.

Gao X, Wu J, Wei X, He C, Wang X, Guob G, Pu Q. (2012) Facile one-step photochemical synthesis of water soluble CdTe(S) nanocrystals with high quantum yields. J. Mater. Chem., 22: 6367-6373.

Guo J, Yang W, Wang C. (2012) Systematic study of the photoluminescence dependence of thiolcapped CdTe nanocrystals on the reaction conditions. J. Phys. Chem. B, 109: 17467–17473.

He Y, Lu H, Sai L, Lai W, Fan Q, Wang L, Huang W. (2006) Synthesis of CdTe Nanocrystals through Program Process of Microwave Irradiation. J. Phys. Chem. B, 110 (27): 13352-13356.

He Y, Sai L, Lu H, Hu M, Lai W, Fan Q, Wang L, Huang W. (2007) Microwave-Assisted Synthesis of Water-Dispersed CdTe Nanocrystals with High Luminescent Efficiency and Narrow Size Distribution. Chem. Mater., 19:359-365.

Khalavka Y, Mingler B, Friedbacher G, Okrepka G, Shcherbak L, Panchuk O. (2010) Influence of temperature on the synthesis of thiol-stabilized CdTe nanoparticles in aqueous solutions. Phys. Status Solidi A, 207: 370-374.

Kovalenko MV, Kaufmann E, Pachinger D, Roither J, Huber M, Stangl J, Hesser G, Schaffler F, Heiss W. (2006) Colloidal HgTe nanocrystals with widely tunable narrowband gap energies: from telecommunications to molecular vibrations. J. Am. Chem. Soc., 128: 3516–3517.

Li L, Qian H, Ren J. (2005) Rapid synthesis of highly luminescent CdTe nanocrystals in the aqueous phase by microwave irradiation with controllable temperature. Chem Commun., 4: 528–530.

Li L, Qian H, Fang N, Ren J. (2006) Significant enhancement of the quantum yield of CdTe nanocrystals synthesized in aqueous phase by controlling the pH and concentrations of precursor solutions. J. Luminesc., 116: 59-66.

Li M, Ge Y, Chen Q, Xu S, Wang N, Zhang X. (2007) Hydrothermal synthesis of highly luminescent CdTe quantum dots by adjusting precursors' concentration and their conjunction with BSA as biological fluorescent probes. Talanta, 72: 89-94.

Li Y, Jing L, Qiao R, Gao M. (2011) Aqueous synthesis of CdTe nanocrystals: progresses and perspectives. ChemComm 47:9293–9311.

Liu M, Zhao H, Chen S, Wang H, Quan X. (2012) Photochemical synthesis of highly fluorescent CdTe quantum dots for "on–off–on" detection of Cu(II) ions. Inorg. Chim. Acta, 392:236-240.

Liu Y, Yu J. (2009) Selective synthesis of CdTe and high luminescence CdTe/CdS quantum dots: The effect of ligands. J. Coll. Interf. Sci., 333:690–698.

McDonald SA, Konstantatos G, Zhang S, Cyr PW, Klem EJD, Levina L, Sargent EH. (2005) Solution-processed PbS quantum dot infrared photodetectors and photovoltaics. Nat. Mater., 4:138-142.

Moreels I, Lambert K, De Muynck D, Vanhaecke F, Poelman D, Martins JC, Allan G, Hens Z. (2007) Composition and Size-Dependent Extinction Coefficient of Colloidal PbSe Quantum Dots. Chem. Mater., 19, 6101–6106.

Rajh T, Micic OI, Nozik AJ (1993) Synthesis and characterization of surface-modified colloidalcadmium telluride quantum dots. J. Phys. Chem. 97: 11999–12003.

Robel I, Subramanian V, Kuno M, Kamat PV. (2006) Quantum dot solar cells. Harvesting light energy with CdSe nanocrystals molecularly linked to mesoscopic TiO2 films. J. Am. Chem. Soc., 128, 2385-2393.

Rogach AL. (2008) Semiconductor Nanocrystals Quantum Dots Synthesis, Assembly, Spectroscopy and Applications. Vien: Springer-Verlag.

Ruedas-Rama MJ, Waltersb JD, Ortea A. (2012) Hall E.A.H., Fluorescent nanoparticles for intracellular sensing: A review. Anal. Chim. Acta 751:1– 23.

Silva FO, Carvalho MS, Mendonça R, Macedo WAA, Balzuweit K, Reiss P, Schiavon MA. (2012) Effect of surface ligands on the optical properties of aqueous soluble CdTe quantum dots. Nanosc. Res. Lett., 7: 536.

Song Q, Ai X, Topuria T, Rice PM, Alharbi FH, Bagabas A, Bahattab M, Bass JD, Kim H, Scott JC, Miller RD. (2010) Microwave-assisted synthesis of monodispersed CdTe nanocrystals. Chem. Commun., 46: 4971–4973.

Yang R, Yan Y, Mu Y, Ji W, Li X, Zou M, Fei Q, Jin Q. (2006) A Rapid and Facile Method for Hydrothermal Synthesis of CdTe Nanocrystals Under Mild Conditions. J. Nanosci. Nanotechnol., 6: 215–220.

Yang W, Li W, Dou H, Sun K. (2008) Hydrothermal synthesis for high-quality CdTe quantum dots capped by cysteamine. Mat. Lett., 62: 2564–2566.

Yu WW, Qu L, Guo W, Peng X. (2003) Experimental Determination of the Extinction Coefficient of CdTe, CdSe, and CdS Nanocrystals. Chem. Mater., 15, 2854-2860.

Zhang H, Wang L, Xiong H, Hu L, Yang B, Li W. (2003) Hydrothermal synthesis for high-quality CdTe nanocrystals. Adv. Mater., 15: 1712–1715.

Zhang Y, Zhang H, Ma M, Guo X, Wang H. (2009) The influence of ligands on the preparation and optical properties of water-soluble CdTe quantum dots. Appl. Surf. Sci., 255: 4747-4753.

Zhang Y, Clapp A. (2011) Overview of Stabilizing Ligands for Biocompatible Quantum Dot Nanocrystals. Sensors, 11:11036-11055.

Zhao K, Li J, Wang H, Zhuang J, Yang W. (2007) Stoichiometric Ratio Dependent Photoluminescence Quantum Yields of the Thiol Capping CdTe Nanocrystals. J. Phys. Chem. C, 111, 5618-5621.

Zheng Y, Gao S, Ying JY. (2007) Synthesis and Cell-Imaging Applications of Glutathione-Capped CdTe Quantum Dots. Adv. Mater., 19: 376–380.

Zou L, Gu Z, Zhang N, Zhang Y, Fang Z, Zhu W, Zhong X. (2008) Ultrafast synthesis of highly luminescent green- to near infrared-emitting CdTe nanocrystals in aqueous phase J. Mater. Chem., 18: 2807–2815.

Supporting information

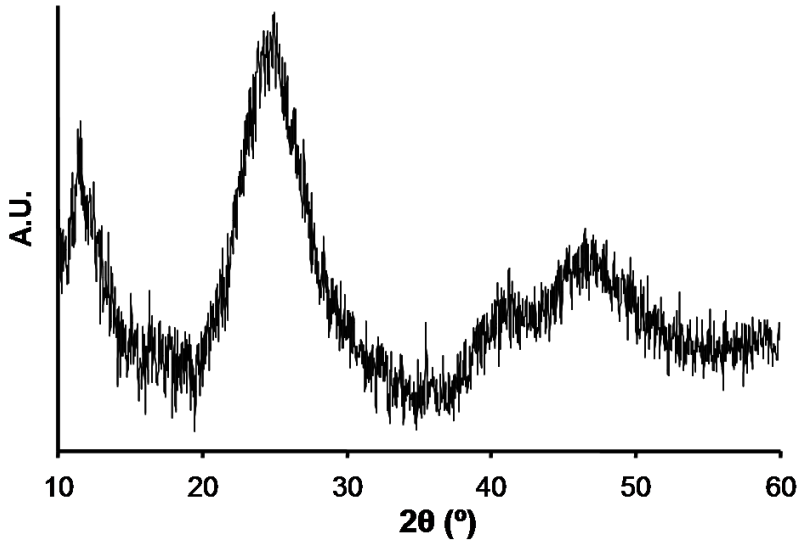

S1. p-XRD of 2.3 nm CdTe-MPA QDs.

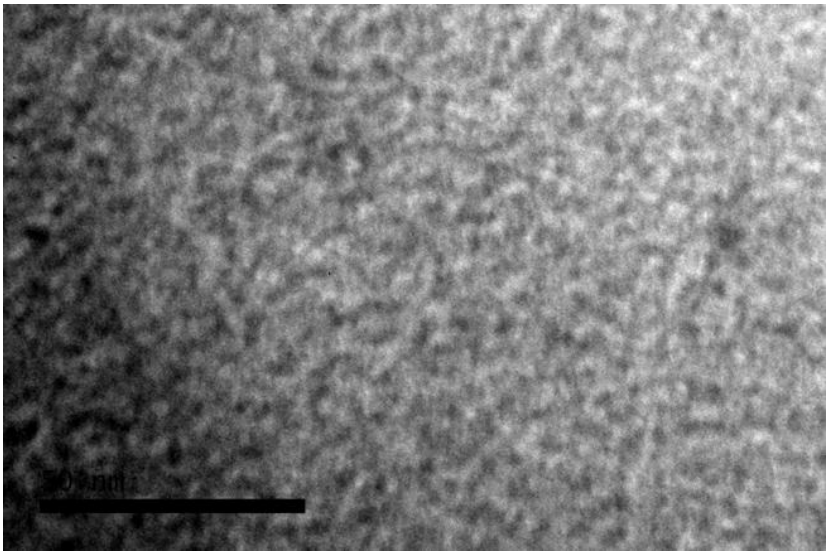

S2. TEM image of 3.1 nm CdTe-MPA QDs.

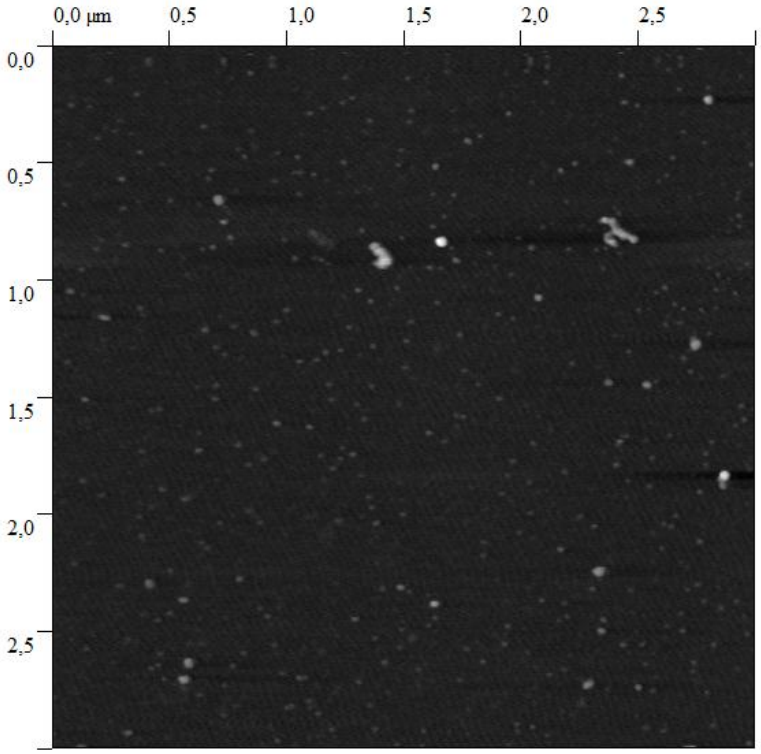

S3. AFM image of 3 nm CdTe-MPA QDs.

CHAPTER 4

Cadmium telluride nanocrystals as luminescent sensitizers in flow analysis

Talanta 84 (2011) 1314–1317

Contents lists available at ScienceDirect

Talanta

journal homepage: www.elsevier.com/locate/talanta

Cadmium telluride nanocrystals as luminescent sensitizers in flow analysis

Paula R. Fortes[a], Christian Frigerio[b], Cristina I.C. Silvestre[b], João L.M. Santos[b], José L.F.C. Lima[b], Elias A.G. Zagatto[a,*]

[a] Centre for Nuclear Energy in Agriculture, University of São Paulo, P.O. Box 96, Piracicaba 13400-970, Brazil
[b] REQUIMTE, Departamento de Química, Faculdade de Farmácia, Universidade do Porto, Rua Aníbal Cunha 164, Porto 4099-030, Portugal

Abstract

A fully automated multipumping flow system (MPFS) using water-soluble CdTe quantum dots (QD) as sensitizers is proposed for the chemiluminometric determination of the anti-diabetic drugs gliclazide and glipizide in pharmaceutical formulations. The nanocrystals acted as enhancers of the weak CL emission produced upon oxidation of sulphite by Ce(IV) in acidic medium, thus improving sensitivity and expanding the dynamical analytical concentration range. By interacting with the QD, the two analytes prevented their sensitizing effect yielding a chemiluminescence quenching of the Ce(IV)–SO_3^{2-}–CdTe QD system. The pulsed flow inherent to MPFS assured a fast and efficient mixing of all solutions inside the flow cell, circumventing the need for a reaction coil and facilitating the monitoring of the short-lived generated chemiluminescent species. QD crystal size, concentration and spectral region for measurement were investigated.

Keywords: CdTe; Quantum dots; Chemiluminescence; Multipumping flow system; Pharmaceutical formulations

1. Introduction

In recent years CdTe quantum dots (QD) size-tunable optical properties, broad absorption and narrow emission bands as well as good photostability have made them more attractive than conventional organic fluorophores as luminescent molecular probes [1]. As the optical properties of CdTe QD strongly depend on the nature of their surface, modifications of the later with functional groups or biomolecules and the interactions that it could establish with specific analytes can result in dramatic changes in these properties [2]. Therefore, fluorescence or chemiluminescence (CL) based chemical sensing involving CdTe QD have been developed for different chemical species such as ascorbic acid [3], ATP, folic acid and l-cysteine [4], phenolic compounds and H_2O_2[5], as well as heavy metals such as Hg(II) [6], Ag(I) [7] and Cu(II) [8].

In most CdTe QD applications, the detection is based on signal quenching, although more recently attention has been focused on signal enhancing, mainly associated to QD ability to sensitize distinct chemiluminescent systems [9] and [10]. Sensitized chemiluminescence is an expeditious strategy to exploit CL reactions with low quantum efficiencies for analytical purposes. The weak produced energy is transferred to a sensitizer, usually an organic fluorophore with high quantum yield, which is able to amplify it. Any species that selectively interacts with the fluorophore could quench the CL emission. In general, nanocrystal materials exhibiting high quantum yields, tunable emission spectra, long photoluminescence decay times and a low susceptibility to photobleaching, could advantageously replace these organic fluorescent molecules.

Analogously to semiconductor materials, theories concerning the electronic energy levels, bands conduction, bands of separation and valence bands are also applicable to QDs. In relation to the Bohr excitation radius, a difference should be emphasized. It is well known that the dimensions of a semiconductor, usually with a >10 nm diameter, are larger than the Bohr radius of excitation, condition that defines its electronic energy levels. As the dimensions of the QDs are comparatively smaller (usually 1.5–6.0 nm), its diameter is close to the radius of excitation Bohr. In this way, the larger the diameter of the QDs, the lower Bohr excitation radius, thus reducing the energy emitted. On the other hand, as the diameter of the QDs decreases, higher the energy is needed to excite it, and therefore, a higher energy is released when it returns to its ground state [11].

CdTe QD analytical applications have been almost exclusively based on discrete approaches that rely on both manual handling of all involved solutions (nanodots included) and manual measurements. The related methods present critical shortcomings namely a higher consumption of solutions, poor reproducibility and repeatability, and susceptibility to inaccuracy setbacks; moreover, they are laborious and time-consuming.

Some of the generated or measured species are short-lived ones, thus very difficult to be handled under discrete conditions. MPFS [12] exhibited operational characteristics that enable to overcoming all the above mentioned drawbacks, along with a low cost of implementation and operation and high analytical efficiency.

In MPFS, multiple solenoid micro-pumps are the core and exclusive active components of the analytical system being accountable for multiple tasks including solutions insertion, propelling, mixing and commuting. Moreover, the disorganized sample/reagent solutions proximity inside the MPFS pulsed flow leads to improved mixing conditions thus efficient homogenisation of the reaction zone. Consequently, length of the reaction coil can be reduced, thus minimising sample dispersion. This aspect becomes more evident under limited dispersion conditions. This characteristic makes MPFS particularly attractive for applications in situations requiring a fast sample/reagent mixing, as is the case of measurements of short-lived species yielding chemiluminescence emissions. Gliclazide [13] and glipizide [14] are sulfonylurea hypoglycemic drugs with general free radical scavenging properties [13] and antioxidant activity [14]. These anti-diabetics species are usually determined by liquid chromatography [15], [16] and [17] and, to the best of our knowledge, were never quantified by chemiluminescence.

The aim of this work was then to develop a MPFS for the chemiluminometric determination of these compounds which, by interacting with the CdTe QD, prevent their sensitizing action yielding a chemiluminescence quenching of the Ce(IV)-SO_3^{2-}-CdTe QD system.

2. Experimental

2.1. Samples, standards, reagents

All solutions were prepared with water from a Milli-Q system (specific conductivity <0.1 μS cm^{-1}) and chemicals of analytical reagent grade quality. Reagents were not subjected to any further purification.

A 0.01 mol L^{-1} $(NH_4)_2Ce(NO_3)_6$ (Sigma, St. Louis MO, USA) solution was daily prepared by dissolving the appropriate amount in 0.15 mol L^{-1} H_2SO_4.

A 5.0×10^{-4} mol L^{-1} Na_2SO_3 (Fluka, St. Louis MO, USA) solution was also daily prepared.

For the CdTe QD synthesis, 1.6×10^{-3} mol of sodium borohydride (Sigma, St. Louis MO, USA), 0.4×10^{-3} mol Te, 200 *mesh* (Sigma, St. Louis MO, USA), 4.0×10^{-3} mol of cadmium chloride (Sigma, St. Louis, MO, USA), $1{,}7 \times 10^{-3}$ mol of 3-mercaptopropionic

acid (MPA) (Fluka, St. Louis MO, USA) and absolute ethanol (Panreac, Barcelona, Spain) were used. For adjusting the alkalinity of the reaction medium, a 1.0 mol L^{-1} NaOH solution was used.

The stock standard solutions were prepared by dissolving the appropriate amounts of glipizide or gliclazide (Sigma, St. Louis MO, USA) in 2.0 mL of 0.1 mol L^{-1} NaOH and filling the volume up to 100.0 mL with water. Working standard solutions (0.0–100.0 mg L^{-1} glipizide or gliclazide) were prepared from dilutions of the corresponding stock solutions with water.

The sample preparation was carried out according to the British Pharmacopoeia [18]. To this end, 20 tablets containing glipizide were powdered and homogenised. A 15-mg aliquot was sampled and transferred to a 25-mL flask with 0.5 mL of 0.1 mol L^{-1} NaOH and 20 mL of water. The solution was stirred during one hour and the volume was made up with water. The resulting solution was filtered and an aliquot of 5.0 mL was transferred to 50 mL flask and diluted with water.

Twenty tablets containing gliclazide were powdered and after homogenisation, 0.8 g were weighed and suspended in 200 mL of acetonitrile and kept under constant stirring for one hour. Thereafter, the formed suspension was filtered and transferred to a 200-mL flask. The volume was then completed with a 2:3 (v/v) acetonitrile/water solution.

2.2. Apparatus

A Camspec CL-2 (Leeds, UK) luminometer equipped with a 60 µL-inner volume flow cell was used for chemiluminescence measurements. Four 120SP solenoid micro-pumps (Bio-Chem Valve Inc., Boonton NJ, USA) delivering 10-µL per stroke were used as fluid propeller devices. They were operated through a CoolDrive (NResearch, West Caldwell NJ, USA) power driver and a PCL-711B interface card from Advantech (Munich, Germany) and Quick Basic 4.5 software. The flow manifold was build-up with PTFE tubing (i.d. = 0.8 mm) and end-fittings, and acrylic confluence points.

The reference method for gliclazide determination was carried out by using a Jasco LC-NET II/ADC high performance liquid chromatograph furnished with a PU-2080 Plus Intelligent pump, a Waters XTerra™ RP_8 3.9 mm × 150 mm column and a MD-2015 Plus multiwavelength detector. The reference method for glipizide determination was carried out by UV spectrophotometry (274 nm) by using a Jasco, V-660 UV–vis spectrophotometer with a quartz cuvette (inner volume = 100 µL, optical path = 10 mm).

2.3. Synthesis of CdTe QD

MPA-capped CdTe QD were synthesized as described by Yu et al. [19] with some modifications. Briefly, the reaction between $NaHB_4$ and Te powder was carried out in N_2 saturated water, inside a 50 mL flask at 80 °C for 30 min, under constant stirring. The resulting NaHTe solution was transferred to another 100-mL flask containing 4.0×10^{-3} mol $CdCl_2$ and 6.8×10^{-3} mol MPA in a 100 mL N_2 saturated water solution. The pH of the solution was adjusted to 11.5 with a f 1.0 mol L^{-1} NaOH solution. The Cd^{2+}:Te^{2-}:MPA molar ratio was fixed as 1:0.1:1.7. The CdTe QD size was tuned by varying the heating time.

Purification of QD was performed by precipitation in absolute ethanol. The obtained precipitate was re-dissolved in deionised water. The synthesis concentration was maintained, and the diameter of CdTe QD was calculated as [20]:

$$D=(9.8127\times10^{-7})\lambda^3-(1.7147\times10^{-3})\lambda^2+(1.0064)\lambda-194.84 \quad (1)$$

where D is the diameter of the nanocrystals (nm); λ is the wavelength corresponding to maximal absorbance (see Table 1).

Table 1. Characteristics of the CdTe QD employed.

Quantum dots	λ Emission max. (nm)	Diameter (nm)
A	630	3.34
B	542	1.84
C	554	2.66
D	659	4.41

2.4. Method

The oxidation of sulphite by Ce^{4+} in acidic medium yields a weak chemiluminescent emission, which can be enhanced in the presence of sensitizers or fluorophore

compounds. Several compounds can be used, and special attention has been given to QD due to their high quantum yields. The probable reaction mechanism is shown in Eqs. (2), (3), (4), (5) and (6), and the radiation emission is probably due to the formation of excited molecules of sulphur dioxide which, during the reaction, transfer this energy to the QD [10].

$$Ce^{4+} + HSO_3 \rightarrow HSO_3 + Ce^{3+} \quad (2)$$

$$2HSO_3 \rightarrow S_2O_6^{2-} + 2H^+ \quad (3)$$

$$S_2O_6^{2-} \rightarrow SO_4^{2-} + SO_2 * \quad (4)$$

$$SO_2 * + CdTeQD \rightarrow SO_2 + (CdTeQD)* \quad (5)$$

$$(CdTeQD)* \rightarrow CdTeQD + hv \quad (6)$$

In the presence of gliclazide and glipizide, which exhibited radical scavenging and/or antioxidant activity (CdTeQD)* is deactivated and the CL emission (*hv*) is reduced proportionally to the concentration of these compounds allowing their quantification.

2.5. Flow diagram

The MPFS [21] was operated as follows (Fig. 1). Initially, P_1 and P_2 pumps were operated, allowing the R_1 and R_2 reagent streams to merge together at the confluence point, letting the reaction to proceed inside the flow cell. Baseline reflected then the weak chemiluminescent emission of the reaction (sulphite oxidation by Ce^{4+} in acidic medium). Sample and CdTe QD introduction were accomplished by turning P_3 and P_4 on. As the reactions yielding Ce^{4+}–SO_3^{2-}–CdTe QD, and the subsequent light emission, were too fast, the reagents and the sample were fully mixed inside the detector by simultaneously operating all four micro-pumps P_1–P_4. The chemical reaction took place inside the detector and the CL emission was monitored. After insertion of the sample and QD selected volumes, P_3 and P_4 were turned off while P_1 and P_2 remained under operation to carry out the established reaction zone towards waste.

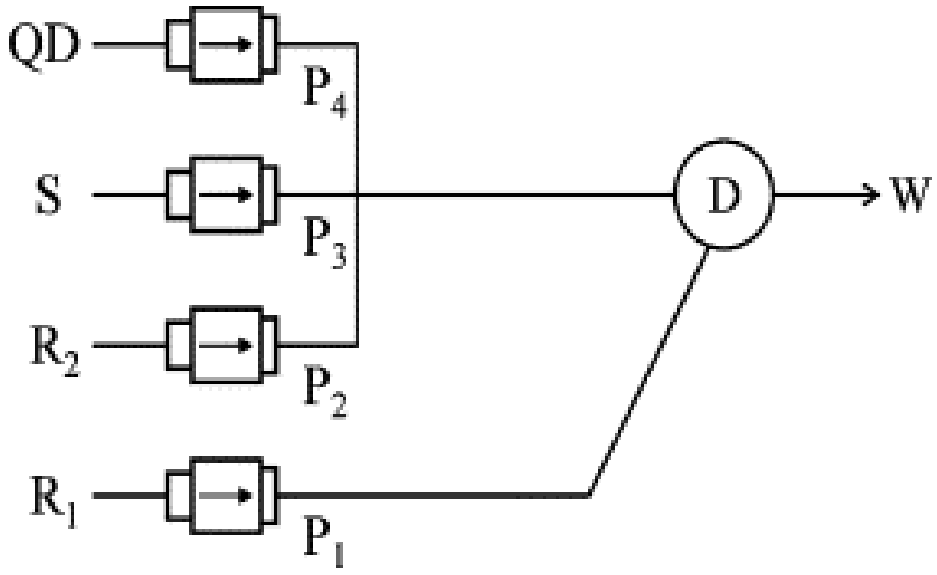

Fig. 1. Flow diagram of the MPFS for determination of glipizide and gliclazide. P_i = solenoid pumps; R_1: 0.01 mol L^{-1} Ce in 0.15 mol L^{-1} H_2SO_4; R_2: 5.0×10^{-4} mol L^{-1} Na_2SO_3; R_3: 5.0 mg L^{-1} CdTe QD; S: sample; D: detector; W: waste.

3. Results and discussion

As the involved reactions are fast and produced short-lived species, the distance between the solutions confluence point and the detector is an important factor for system design. A reduction of the analytical signal was observed when this distance was higher than 10 cm. On the other hand, an efficient solutions mixing was crucial to attain a good repeatability. Since the pulsed flow produced by micro-pumps assured this latter requirement, the tube length was kept at the minimum size as to enable the physical attachment of the flow manifold to the detector; therefore all solutions were mixed within the detector flow cell. Another parameter that directly affects mixing and reaction development is the flow rate. In MPFS it is determined by the frequency of micro-pump and the stroke volume. It was observed that the CL emission increased up to a pulse interval of 0.15 s (for all micro-pumps) and subsequently decreased. This pulse interval corresponded to a flow rate of about 4 mL min^{-1}.

Regarding influence of sulphite concentration, the analytical signal exhibited a pronounced increase up to a concentration value of 5.0×10^{-4} mol L^{-1} and then approached stabilisation; moreover, no differences in analytical signals related to the standards of the same analyte were observed below 1.0×10^{-2} mol L^{-1} SO_3^{2-}. In relation to Ce^{4+} concentration, concentrations lower than 5.0×10^{-3} mol L^{-1} Ce led to a reduction of

ca 30% in the intensity of the analytical signal and the linearity of the analytical curve was worse when compared with the intensities related to concentrations of 1.0×10^{-2} mol L^{-1} Ce. For higher concentrations, a 70% reduction in analytical signals was observed. Both analytes showed similar behaviour. Reagents R_1 and R_2 where then selected as 0.01 mol L^{-1} Ce e 5.0×10^{-4} mol L^{-1} Na_2SO_3, respectively.

The Ce^{4+} solution in sulphuric medium is stable, but acidity plays a pronounced influence on the development of the chemical reactions. This influence was evaluated within 0.05 and 0.40 mol L^{-1} H_2SO_4. By increasing the acidity in R_1, a proportional reduction in the analytical signal was observed. On the other hand, for concentrations within 0.05 and 0.10 mol L^{-1} H_2SO_4 the repeatability of the analytical signals was impaired, resulting in measurement uncertainties within 10 and 15%. Aiming at both sensibility and repeatability, the concentration of H_2SO_4 was selected as 0.15 mol L^{-1}.

As the reagents and the sample were mixed within the detectors flow-cell, the flow rate and the sample volume were selected in order to provide enough time for the reaction development and thus a suitable sensitivity. A 160% increment in the analytical signal was noted when the flow rate was increased from 2.0 to 4.0 mL min^{-1}. Flow rates beyond this later value led to a proportional decrease in the analytical signal. The flow rate was selected as 4.0 mL min^{-1}.

By increasing the sample volume within 50 and 200 μL, an increase in the emitted radiation was noted, and for volumes higher than 250 μL double peaks was recorded, probably due to the lack of reagents in the central portion of the sample zone. The sample volume was then selected as 200 μL.

Different sized QD (Table 1) were selected for evaluating the analytical performance related to the sensitivity and repeatability of the analytical signal. The nanodots with greater size (A, D) although promoting a decrease in the CL emission, both for gliclazide and glipizide, did not provide an adequate sensitivity. For smaller QD (B, C), a pronounced CL quenching was observed, especially for QD C. Effectively, the monitored CL intensity showed a decrease of about 400% as the analytes concentration increased (Fig. 2). This aspect can be explained by considering that the energy generated in the chemical reaction probably corresponds to the excitation energy required by the QDs C. In fact, the more energy from the chemical reaction corresponds to the excitation energy required by the QDs, the higher its efficiency and more intense the radiation emitted [22]. The quenching effect was clearly dependent of the QD size and can be explained in terms of the radical scavenging and/or antioxidant activity of the anti-diabetic drugs or due to surface interactions between the QD particle and the analyte.

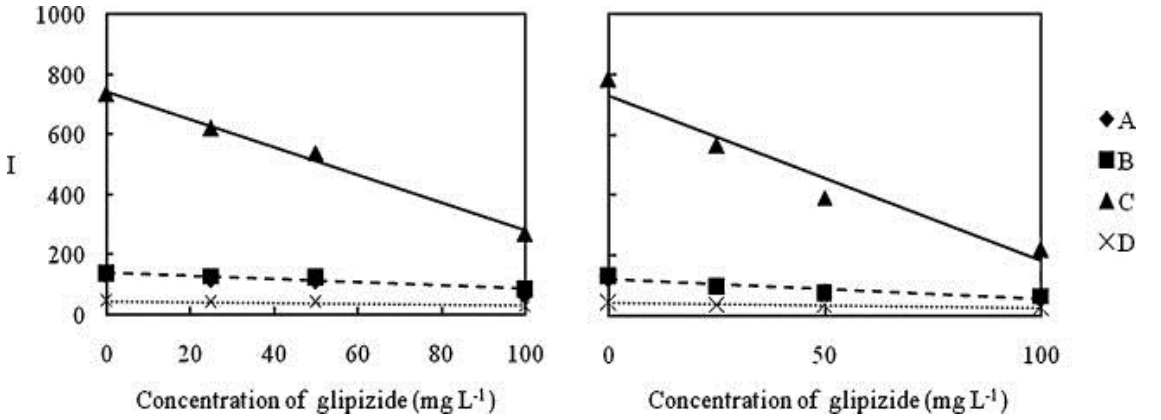

Fig. 2. Performance of CdTe QD. (A) 3.34 nm; (B) 1.84 nm; (C) 2.66 nm; (D) 4.41 nm diameter.

It is well know that size and shape of the QD may affect either the photochemical properties or the reactivity of the particle [23] and [24], especially if there is a direct interaction between the two chemical species. The analytical signal increased with increasing QD concentrations, but for the highest concentrations the repeatability was impaired, resulting in a relative standard deviation of >10%. Use of 1.58×10^{-6} mol L^{-1} CdTe QD solution led to reproducible signals (r.s.d. ~1.0%). The CdTe QDs concentration was then fixed as 1.58×10^{-6} mol L^{-1}, which assured a compromise between sensitivity, analytical dynamical concentration range and precision, with relative standard deviations for the measurements estimated as 1.41% and 1.68% for gliclazide and glipizide, respectively.

Once optimized, the MPFS system was applied to the determinations of gliclazide and glipizide in pharmaceutical formulations. The system showed good analytical figures of merit such as a linear range within 18.0 and 100.0 mg L^{-1}, coefficient correlation (r) of 0.973 and 0.996, equation $Y = -5.489\,x + 729.1$ and $Y = -4.613\,x + 742.1$, r.s.d. of 1.41 and 1.68, LQ (10σ) of 12.8 and 18.0 mg L^{-1} and LOD (3σ) of 2.9 and 6.3 mg L^{-1} for gliclazide and glipizide, respectively. The evaluation of the interfering effect of the excipients present in the formulations: magnesium stearate, anhydrous colloidal silica, lactose and calcium carbonate, showed no interfering effect up to a 100-fold excipient/analyte molar ratio. The proposed system is characterized by a sampling rate of 150 h^{-1}, meaning a sample and QD consumption of 200 μL per determination.

The analytical results were satisfactory (Table 2), and in agreement with those obtained by the reference method, with relative deviations lower than 3.8%. A Student's paired *t-test* confirmed that there were no significant statistical differences at a 95% level (estimated $t = 0.088$; tabulated $t = 2.571$).

Table 2. Comparative results. Data obtained by the developed MPFS and by the reference method.

Samples	Dosage (mg/tablet)	Proposed system (MPFS)	Reference method	R.D. (%) [a]
Gliclazide Winthrop	80	80.5 ± 0.2	80.0	0.6
Gliclazide Generis	80	82.5 ± 0.06	79.9	3.1
Gliclazide KRKA	30	31.1 ± 0.05	29.8	3.8
Gliclazide Ratiopharm	30	29.9 ± 0.2	30.0	−0.3
Gliclazide Alter	30	30.3 ± 0.04	30.1	1.1
Diamicron LM (gliclazide)	30	30.5 ± 0.07	29.9	1.7
Minidiab Pfizer (glipizide)	5	5.0 ± 0.01	5.0	0.5

a relative deviation (expressed in percentage) of the proposed method in relation to the reference method.

4. Conclusions

The feasibility of implementing CdTe QD in a multi-pumping flow system for the determinations of gliclazide and glipizide in pharmaceutical formulations was demonstrated. CdTe QD can be advantageously used as chemiluminescence sensitizers enabling the chemiluminometric determination of compounds that have the potential or interacting with the nanodots affecting their photochemical properties and/or reactivity. The mixing capacity and high automation level of MPFS provide an expeditious way of implementing reaction schemes involving nanoparticles and the generation of short-lived species that are difficult to monitor in discrete methodologies.

Acknowledgements

The authors thank CAPES (proc.197/2008), FAPESP (proc. 06/03859-9) and FCT for financial support (project PTDC/QUI-QUI/105514/2008) under COMPETE/QREN/FEDER. C. Frigerio thanks FCT for the PhD grant (SFRH/BD/47651/2008).

References

[1] X. Wang, M.J. Ruedas-Rama, E.A.H. Hall, Anal. Lett. 40 (2007) 1497–1520.
[2] M. Gao, S. Kirstien, H. Mohawald, A.L. Rogach, A. Kornowski, A. Eychmuller, H. Weller, J. Phys. Chem. B 102 (1998) 8360–8363.
[3] Y. Chen, X. Yan, Small 5 (2009) 2012–2018.
[4] Y. Wang, J. Zheng, Z. Zhang, C. Yuan, D. Fu, Colloid Surf. A 342 (2009) 102–106.
[5] J. Yuan, W. Guo, E. Wang, Anal. Chem. 80 (2008) 1141–1145.
[6] Y. Xia, C. Zhu, Talanta 75 (2008) 215–221.
[7] A. Zheng, J. Chen, H. Li, C. He, G. Wu, Y. Zhang, H. Wei, G. Wu, Microchim. Acta 165 (2009) 187–194.
[8] S. Lai, X. Chang, C. Fu, Microchim. Acta 165 (2009) 39–44.
[9] Z.P. Wang, J. Li, B. Liu, J.H. Li, Talanta 77 (2009) 1050–1056.
[10] C. Sun, B. Liu, J. Li, Talanta 75 (2008) 447–454.
[11] S.M. Reimann, M. Manninen, Rev. Mod. Phys. 74 (2002) 1284–1336.
[12] J.L.M. Santos, M.F.T. Ribeiro, J.L.F.C. Lima, A.C.B. Dias, E.A.G. Zagatto, Anal. Chim. Acta 600 (2007) 21–28.
[13] N.A. Scott, P.E. Jennings, J. Brown, J.J. Belch, Eur. J. Pharmacol. 208 (1991) 175–177.
[14] S. Tuzun, F.K. Girgin, E.Y. Sozmen, G. Mentes, B. Ersoz, Exp. Toxicol. Pathol. 51 (1998) 436–441.
[15] S.H. Kim, J. Lee, T. Yoon, J. Choi, D. Choi, D. Kim, S.W. Kwon, Biomed. Chrom. 23 (2009) 1259–1265.
[16] S. AbuRuz, J. Millership, J. McElnay, J. Chrom. B 817 (2005) 277–286.
[17] G.-X. Ling, J. Sun, J.-L. Tang, X.-D. Xu, Y.-H. Sun, Z.-G. He, Anal. Lett. 39 (2006) 1381–1391.
[18] British Pharmacopoeia. v. 1, The Stationery Office, London, 2005.
[19] W.W. Yu, L.-H. Qu, W.-Z. Guo, X.-G. Peng, Chem. Mater. 15 (2003) 2854–2860.
[20] L. Zou, Z. Gu, N. Zhang, Y. Zhang, Z. Fang, W. Zhu, X. Zhong, J. Mater. Chem. 18 (2008) 2807–2815.
[21] J.L.F.C. Lima, J.L.M. Santos, A.C.B. Dias, M.F.T. Ribeiro, E.A.G. Zagatto, Talanta 64 (2004) 1091–1098.
[22] J.R. Lakowicz, Principles of Fluorescence Spectroscopy, Springer, New York, 2006.
[23] Y.-S. Xia, C. Cao, C.-Q. Zhu, Chin. J. Chem. 25 (2007) 1836–1841.
[24] T. Uematsu, T. Waki, T. Torimoto, S. Kuwabata, J. Phys. Chem. C 113 (2009) 21621–21628.

CHAPTER 5

Evaluation of acetylcysteine promoting effect on CdTe nanocrystals photoluminescence by using a multipumping flow system

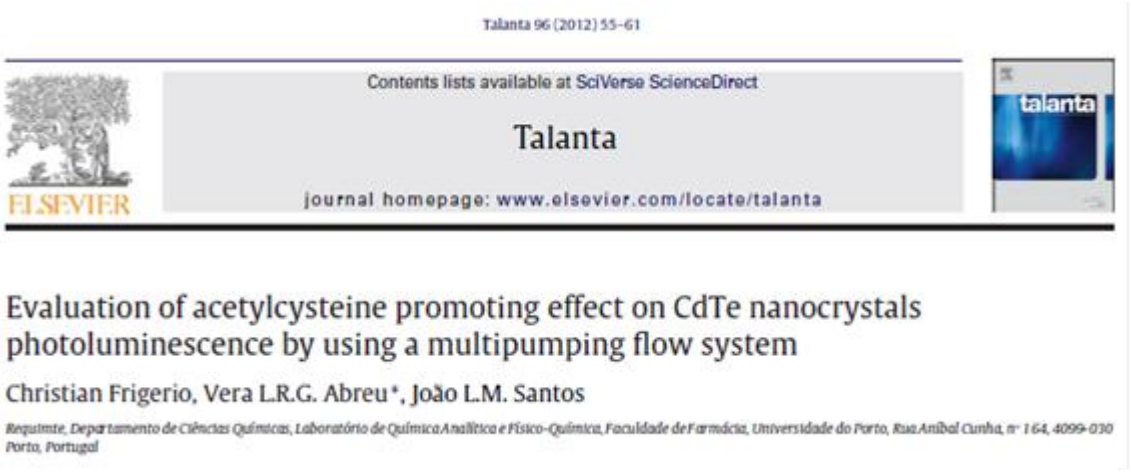
Talanta 96 (2012) 55–61

Contents lists available at SciVerse ScienceDirect

Talanta

journal homepage: www.elsevier.com/locate/talanta

Evaluation of acetylcysteine promoting effect on CdTe nanocrystals photoluminescence by using a multipumping flow system

Christian Frigerio, Vera L.R.G. Abreu*, João L.M. Santos

Requimte, Departamento de Ciências Químicas, Laboratório de Química Analítica e Físico-Química, Faculdade de Farmácia, Universidade do Porto, Rua Aníbal Cunha, nº 164, 4099-030 Porto, Portugal

Abstract

A simple and straightforward quantification method integrated in a fully automated multi-pumping flow system (MPFS) using water-soluble mercaptopropionic acid (MPA)-capped CdTe quantum dots (QDs) was implemented for the fluorescence quantification of *N*-acetyl-l-cysteine (NAC) in pharmaceutical formulations. The developed approach was based on NAC ability to establish surface interactions that result in enhanced nanocrystals fluorescence intensity, proportional to analyte concentration. Size and concentration of QDs, ageing, composition, concentration and pH of the buffer solution revealed to have a noticeable effect on the enhancing efficiency affecting sensitivity and linear working range of the methodology. Under the optimal conditions, a linear working range was obtained for NAC concentrations ranging from 50 to 750 μmol L^{-1} (r = 0.9978), with good precision (r.s.d. < 1.6%; n = 5) and a sampling rate of about 75 hr^{-1}. The detection limit (LOD) was approximately 1.6 μmol L^{-1}. The method was applied to pharmaceutical preparations and the results revealed good agreement with those obtained by the reference procedure with relative deviations between −2.1 and +4.2%. Advantages of the new procedure include speed, low consumption of reagents, minor waste generation, requiring also much less work than the recommended HPLC method. The mechanism for luminescence enhancement of CdTe QDs is discussed. FT-IR spectra revealed that sulphydryl groups of NAC have a high affinity with the nanocrystals.

Keywords

CdTe; Quantum dots; Nanocrystals; Fluorescence; Multipumping flow system

1. Introduction

Colloidal nanocrystals, often referred to as quantum dots (QDs), have gained increasing interest over the past decade to their unique properties such as size-tunable optical properties, wide absorbance range, narrow emission, strong fluorescence intensity and excellent photostability [1]. Although QDs have been widely used in biolabeling and bioimaging [2], a new area has recently emerged in which QDs are used in the development of fluorescence sensors for analytical applications [3]. In this regard, in literature there is already a reasonable amount of published methodologies concerning analytical quantification procedures for detection macromolecules such as proteins and nucleic acids, as well vitamins, heavy metals, etc., involving surface interactions with these nanocrystals [4], [5], [6] and [7]. So far, development of fluorescence sensing schemes for analytical applications using quantum dots has been almost exclusively based on discrete approaches (manual sample handling and measuring). These approaches present critical drawbacks namely high consumption of solutions, complex and laborious sample preparation procedures, poor reproducibility and repeatability and are time-demanding; manual handling is also more prone to errors. Continuous flow-based techniques, as expeditious solutions to overcome these drawbacks, are finding their way into quantum dots analytical exploitation. Sequential injection analysis (SIA) [8] and flow injection analysis (FIA) [9], [10] and [11] approaches, using fluorescence and chemiluminescence detection, respectively, have been proposed. Fortes et al. [12] developed a multipumping flow system (MPFS) for the determinations of glicazide and glipizide in pharmaceutical formulations using CdTe quantum dots as chemiluminescence sensitizers. A single interface flow analysis (SIFA) system was implemented for the assessment of chemical oxygen demand by using CdTe nanocrystals as radical generators for organic matter photodegradation [13]. These works showed that quantum dots photoluminescence could be significantly influenced by changes on QDs surface charge or ligands that affect electron–hole recombination. Direct binding of the analyte on the QDs surface could, for instance, induce a change on the fluorescence response resulting in either a enhancing or a quenching effect.

N-Acetyl-l-cysteine (*N*-acetyl-2-amino-3-mercaptopropionic acid, NAC), is an acetyl derivative and one of the homologs of the l-cysteine, being a biologically active compound owing to the crucial role in biological systems [14]. NAC is also used as a pharmaceutical drug due to its importance as a mucolytic agent used to reduce the viscosity of pulmonary secretions in respiratory diseases among other potential applications mainly due to its antioxidant action [15]. For the determination of NAC in pharmaceutical formulations, the United States Pharmacopeia [16] recommends high-performance liquid chromatography

(HPLC) whereas the Brazilian Pharmacopeia [17] describes a titrimetric procedure. Nevertheless, based on the-on-going research of the quality control analyses of NAC-containing pharmaceuticals, several alternatives of flow-injection procedures have been developed with different detection systems via spectrophotometric [18] and [19], chemiluminescence [20], potentiometric [21], amperometric [22], voltammetric [23], etc. Moreover, SIA has also been reported in the quantification of this analyte as another alternative of flow analysis with different detection systems such as fluorimetric [24] and spectrophotometric [25]. Although the development of those conventional flow systems permitted to overcome most of the shortcomings associated to the commonly used chromatographic methods, recently developed MPFS [26] and [27] has provided additional features and brought important advantages in terms of analytical application such as ease and simplicity of assemblage, operation and control, compact and straightforward configuration increasing versatility and minimizing solutions consumption, high mixing capacity, etc. Based on the exclusive utilization as active components of multiple solenoid actuated micropumps of very small size it is possible to assure a very simplified configuration of the flow system due to the different task they could be accountable for including sample and reagents insertion and propelling, the implementation of different strategies for solutions mixing and reaction zone establishment. Moreover, the characteristic pulsed flow ensures an effective sample/reagent mixing leading to a better and a faster reaction zone homogenization and thus improved analytical signal.

The aim of this work was to study the surface interactions between *N*-acetyl-l-cysteine and CdTe nanocrystals and, as a consequence of the pronounced fluorescence enhancement observed, to develop a simple and fast automated analytical methodology for its determination in pharmaceutical formulations providing a high analytical sensitivity and a wide dynamic working range. Due to the versatility, efficiency and feasibility guaranteed by the MPFS, important analytical parameters such as solution volumes and flow rate, reactor length, size and concentration of the QDs, buffer and sample pH, as well as QDs ageing time were evaluated for their repercussion on analytical sensitivity and reaction rate.

2. Experimental

2.1. Apparatus

For fluorescence measurement an optical fiber (QP1000-2-UV-VIS, Ocean Optics, Dunedin, USA) spectrofluorometer (USB 4000-FL, Ocean Optics, Dunedin, USA)

equipped with a LS-450 light source and a CUV-UV Holder, was used. The excitation maximum at 395 nm was guarantee using the LED-395 (Ocean Optics, Dunedin, USA) as source. The designed flow manifold comprised three 120SP (Bio-Chem Valve Inc. Boonton, NJ, USA) solenoid actuated micro-pumps, which were of the fixed displacement diaphragm type, two of them (P_1 and P_3) were dispensing 10 μL per stroke while P_2 was dispensing 20 μL per stroke. All connections, depicted in Fig. 1, were made of PTFE tubing (0.8 mm i.d.) with lab-made end-fittings and confluence connectors. The holding coil (*L*) was serpentine-shaped in configuration and was 60 cm long. A 8 μL inner volume flow cell (176.753-QS, Hellma) completed the flow system.

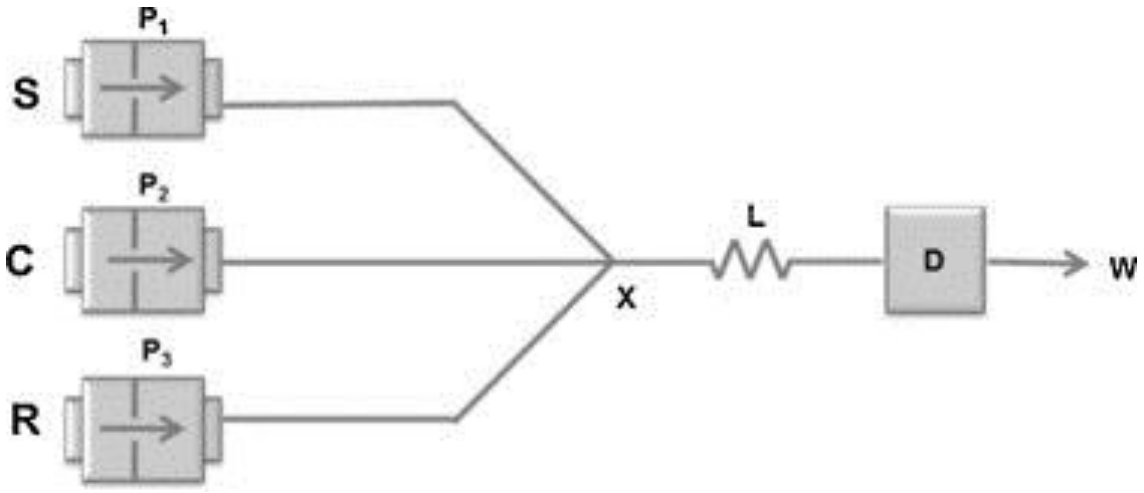

Fig. 1. Multipumping flow manifold for the determination of *N*-acetyl-l-cysteine. P_1 and P_3: solenoid micro-pumps (10 μL per stroke); P_2: solenoid micro-pump (20 μL per stroke); *X*: confluence point; *L*: reactor (60 cm); D: Fluorimeter detector (λ_{exc} = 395 nm, λ_{em} = 522–524 nm), *W*: waste; *S*: sample in 6 mmol L^{-1} acetate buffer at pH 5.2; *C*: Carrier (water); *R*: 5 μmol L^{-1} CdTe QDs.

A PC was used to control the flow system by means of dedicated software built in Visual Basic, which enabled to operate the solenoid pumps by RS-232 C serial binary data signals. The system was implemented in a computer equipped with a PC-LAB card model PCL-711 B (Advantech, Taipei, Taiwan) interface card. A homemade power drive based on the ULN2003 chip was used to operate the solenoid micro-pumps. The data acquisition was accomplished by using the Spectrasuite software version 2007 (OceanOptics, Dunedin, USA). Absorbance spectra for the characterization of the synthesized QDs were measured on a Jasco V-660 spectrophotometer. Fluorescence measurements were carried out with a PerkinElmer LS-50B luminescence spectrometer. QDs centrifugation was performed with a ThermoElectron Jouan BR4I refrigerated centrifuge. FT-IR spectra were

obtained on an ATI Mattson Genesis series (software: WinFirst v. 2.10) spectrophotometer in KBr pellets (cm^{-1}). All pH measurements were made with a Model pH-meter GLP 22 (Crison, Allela, Spain). The absolute emission quantum yields were measured at room temperature using a quantum yield measurement system C9920-02 from Hamamatsu with a 150 W xenon lamp coupled to a monochromator for wavelength discrimination, an integrating sphere as sample chamber, and a multichannel analyzer for signal detection. Three measurements were made for each sample so that the average value is reported. The method is accurate to within 10%.

2.2. Samples, standards and reagents

All solutions were prepared with water from Millipore Q system (conductivity ≤ 0.1 μs cm^{-1}) and analytical grade chemicals. A 4 mmol L^{-1} *N*-acetyl-l-cysteine (Sigma–Aldrich. Chemie GmbH, Steinheim, Germany) standard solution was prepared by dissolving 13 mg in 20 mL of deionized water and kept in the refrigerator.

For the preliminary studies, several NAC solutions were tested by using various buffers with different pH. Based on this, 500 μmol L^{-1} NAC was diluted with different concentrations following buffers: Na_2HPO_4/NaH_2PO_4, citric acid/Na_2HPO_4, boric acid/NaOH and sodium acetate/acetic acid [28], adjusted to different pH values. Within the range of 3.6–8, depending on the pH range of each buffer, the luminescence intensity variation ΔF (%), calculated according to Eq. (3), was evaluated. For further studies reported in this paper, the acetate buffer with pH from 3.4 to 5.9 was the selected one as described in the optimization section.

After optimization, the working NAC standards ranging from 50 to 750 μmol L^{-1} were prepared, on a daily basis, by appropriate dilution of the above stock solution. An appropriate volume of 6 mmol L^{-1} acetate/acetic acid buffer solution at pH 5.2 was transferred to those flasks containing the aforementioned working NAC standards.

Six commercially available pharmaceutical samples, one in granulated form and five in liquid form containing NAC were analyzed according to the proposed procedure. No pre-treatment was required for any of the liquid samples prior to analysis. For the granulated form, this was accurately weighed, dissolved in water and filtered. For the remaining five samples, a known amount of each sample already diluted was transferred to a volumetric flask of 10 mL. Afterwards, to those flasks were transferred 300 μL of 0.2 mol L^{-1} acetate/acetic acid buffer solution at pH 5.2, filling the volume up to the mark with deionized water. The amounts of sample were defined in accordance to the labeled NAC contents of the assayed samples.

For the synthesis of the CdTe quantum dots, tellurium powder (200 mesh, 99.8%), sodium borohydride ($NaBH_4$, 99%), cadmium chloride hemi(pentahydrate) ($CdCl_2 \cdot 2.5H_2O$, 99%) were purchased from Sigma–Aldrich (St. Louis, MO, USA); 3-mercaptopropionic acid (MPA, 99%) and absolute ethanol (99.5%) were obtained from Fluka (St. Louis MO, USA) and Panreac (Barcelona, Spain) respectively.
QDs solutions were prepared by dissolving a certain amount of the dried nanocrystals in ultrapure water and used directly.

2.3. Synthesis of CdTe QDs

Three different diameters of MPA-capped CdTe QDs were synthesized as described by Zou et al. [29] with some modifications. Briefly, the first stage consists on the reduction process of tellurium with $NaBH_4$ in N_2 saturated water to produce NaHTe. After all tellurium has been consumed, the resulting solution was transferred into a second flask containing 4.0×10^{-3} mol of $CdCl_2$ and 6.8×10^{-3} mol of MPA in 100 mL N_2 saturated solution. The pH of the solution was adjusted to 11.5 with a 1.0 mol L^{-1} NaOH solution. The molar ratio of Cd^{2+}:Te^{2-}:MPA was fixed at 1:0.1:1.7. The size of CdTe QDs was controlled by changing the refluxing time.
To purify CdTe QDs, these were precipitated in absolute ethanol to remove the contaminants and the precipitate was subsequently separated by centrifugation, vacuum dried, kept in amber flasks and protected from light, for posterior use. The particle size of the synthesized QDs was calculated by the following expression Eq. (1)[30]:

$$D=(9.8127\times10^{-7})\lambda^3-(1.7147\times10^{-3})\lambda^2+(1.0064)\lambda-(194.84) \quad (1)$$

where D is the diameter (nm) and λ (nm) the wavelength of maximum absorbance corresponding to the first excitonic absorption peak of the crystal.
To facilitate the preparation of the QDs solutions was also necessary to calculate the molar weight of the different sized nanocrystals. This was carried out by establishing firstly the extinction coefficient (ε) by using the expression Eq. (2)[30]:

$$\varepsilon=3450\Delta E(D) \quad (2)$$

where ΔE is the transition energy corresponding to the first absorption peak and the unit is in eV. Knowing ε it was simple to reach the molar mass by measuring the absorbance of a known concentration solution and by applying the Lambert–Beer law.
In order to reach the desired molar concentration of QDs, a certain amount of the dried nanocrystals was dissolved in ultrapure water.

Table 1. Data corresponding to the diameter, λ emission max., quantum yield (%), and concentrations of the nanocrystals used in this work.

Diameter (nm)	λ Emission max. (nm)	Quantum yield (QY%)	Concentration (μmol L^{-1})
1.87	≈523	8	2.5; 5; 10
3	≈574	29	1.25; 2.5; 5
3.8	≈647	35	1.25; 2.5; 5

2.4. Manifold and MPFS procedure

The analytical flow manifold pictured in Fig. 1, comprised three solenoid micro-pumps (P_1, P_2, P_3) which were responsible for the individual insertion and propulsion of sample and reagent solutions. P_1 and P_3 were responsible of the insertion of the sample and QDs solution, respectively, whereas P_2 pumped the carrier stream and simultaneously was responsible for the establishment of the baseline. The versatility provided by the actuation of the micropumps allowed controlling at once the sample and reagent volumes, flow rate and the sequence and timing of sample insertion and reaction zone establishment. The developed analytical cycle began after all flow tubing had been filled with the corresponding solutions. After this first step, the baseline was established by repeated actuation of P_2 used to propel the water (as carrier) toward waste while P_1 and P_3 remained switched off. Subsequently, sample was inserted by simultaneous actuation of P_1 and P_3 for a pre-set number of pulses, generating a flowing stream (at confluence point X) resulting from the merging of QDs and sample aliquots, which were directed to fill the reactor L. These solutions when flowing throughout L establishing a reaction zone that by actuating P_2 and keeping P_1 and P_3 deactivated permitted the reaction zone to be carried out toward the detector generating an analytical signal whose magnitude was proportional to the NAC concentration. The fluorescence emission was monitored at 395 nm (λ_{em} = 522–524 nm).

3. Results and discussion

3.1. Sampling strategy, sample volume and flow rate

Aiming at the maximization of the analytical signal, some optimization studies involving physical and chemical parameters were carried out using the univariate method (Table 2). This was attained by using the QDs with a size of 3 nm at a concentration of 5 μmol L^{-1} in water and a 500 μmol L^{-1} NAC solution also in water.

Table 2. Range of values used in dimensioning the MPFS system, and selected operating conditions for the NAC determination using 1.87 nm CdTe QDs.

Parameters	Evaluated range	Selected value
Sample volume (μL)	[30–80]	60
QDs volume (μL)	[30–80]	60
Carrier stream volume (μL)	[1000–1600]	1200
Reactor length (cm)	[25–85]	60
QDs/sample flow rate (mL min^{-1})	[1.2–3]	2
Carrier flow rate (mL min^{-1})	[2,3]	2.4
Acetate buffer concentration (mol L^{-1})	[0.001–0.008]	0.006
pH range	[5,6]	5.20
QDs ageing time (days)	[1–6]	2
QDs concentration (μmol L^{-1})	[2.5; 5; 10]	5

Even though initial studies showed that the use of a reactor did not show a relevant influence on the analytical signal, the length of the serpentine reaction coil was assessed between 0 and 85 cm, by using an insertion of 6 pulses for both the sample and the reagent. The results demonstrated that there was a slight increase on the analytical signal up to 25 cm, although for longer coils the signal slightly dropped probably because of an increase in sample dispersion. As a compromise between repeatability and sample dispersion for the subsequent assays a reactor of 60 cm length was selected. Different sampling strategies, such as merging zones, binary sampling and the insertion of a unique sample volume were exploited and it was verified that merging of sample and reagent zones was the most suitable strategy as it provided enhanced repeatability and sensitivity, and a more stable baseline. Moreover, it assured lower reagent consumption and higher

sampling rates. Taking into account the sample volume, the obtained results demonstrated an improvement in sensitivity up to 6 pulses of sample solution (60 μL of sample, 120 μL for reaction zone) and a subsequent stabilization for higher values, at a flow rate of 1.2 mL min^{-1}. The influence on the peak height of stopping the flow was also examined for halting periods of 30–120 s and the results showed that the signal was not affected by any of the stop periods.

Another relevant parameter in system design was the flow rate which is determined by the pulse frequency and can affect not only the reaction development but also the sample throughput. The flow rate of sample and QDs solutions was assessed in the range of 1.2–3 mL min^{-1}. The magnitude of the analytical signal seemed not to be influenced by the flow rate because the analytical signal remained practically unchanged over all tested values although the repeatability decreased for the higher flow rates. Aiming at a compromise between sampling rate and repeatability, a flow rate of 1.2 mL min^{-1} was selected for the further experiments. Considering the flow rate of the carrier, a value of 2.4 mL min^{-1} was selected since it decreased the time required for the analysis without compromising precision.

3.2. CdTe QDs and acetate buffer

Preliminary studies revealed that NAC interacted with MPA-capped CdTe quantum dots in slightly acidic medium yielding a fast fluorescence enhancement. The emitted light intensity was directly related to the amount of NAC in the sample and depended on the pH and concentration of buffer solution and on its composition. Nevertheless, the CdTe QDs solution had a noteworthy impact on the analytical signal, regarding its concentration, size and even the ageing time. Given the extensive range of chemical and physical variables affecting analytical signal magnitude that have emerged during this work, a fully automated MPFS was implemented for automating the optimization procedure and the subsequent determinations due to its high analytical efficiency and speed, ease of parameters adjustment as well as its high reproducibility and repeatability which facilitates the study of a set of reaction conditions that otherwise would be very tedious, laborious and time-consuming to accomplish.

A factor that was found to promote CdTe fluorescence, even in the absence of NAC, was the buffer solution. Knowing this, in all experiments the fluorescence intensity arising from the interaction between the acetate buffer solution and the QDs was used as the blank reading. The evaluation of the fluorescence enhancing effect, ΔF (%), was made

through the ratio between the fluorescence emission of the sample solution (F_s) and of the blank (F_0) according to the Eq. (3):

$$\Delta F(\%) = \frac{F_0 - F_s}{F_s} \times 100 \quad (3)$$

All experimental conditions were optimized in order to obtain the highest ΔF (%).
Regarding the chemical optimization, the magnitude of the analytical signal was observed to be strongly affected by the QDs size, age, pH, composition and concentration of the buffer. A study of the effect of such variables on the analytical sensitivity allowed achieving the optimal conditions and also to understand some phenomena occurring on the surface of the QDs. By using two different sizes of the nanodots, and two concentrations for each size, some work was done to study the impact on the ΔF (%) of diluting NAC in buffer solutions of distinct composition and concentration, over a wide range of pH, already described in the experimental section. After an extensive evaluation of the obtained results, the acetate buffer was selected for the succeeding optimization assays due to two main reasons. The first reason is that when the NAC solutions were slightly acidified, independently of the type of buffer, an increase of luminescence intensity was observed. Quite the opposite, when NAC solutions were made more alkaline, no changes on signal magnitude were noticed. This result is particularly interesting because the generality of the analytical procedures available in literature using QDs capped with carboxylic acids, such as MPA, tended to avoid acidic pH. The main reason is that at acidic pH the surface negative charge of QDs decreases and these tend to aggregate and precipitate. Since the referred analytical procedures are discrete ones reaching a stable reading under these conditions is very difficult. On the contrary, when using a flow-based methodology (like MPFS) all measurements are carried out at the same reproducible reaction time (determined by flow rate and reaction coil length), which did not require the attainment of a stable reading. Therefore the exploitation of stability detrimental reaction conditions, which would be forbidden in a batch method, is possible in flow analysis. The second reason is that under the selected range of low pH, it was also possible to see a greater increase of the signal ΔF (%) when acetate buffer was used in comparison with other buffers. Furthermore, this buffer seemed not to interfere with the QDs/NAC interaction. Another variable that revealed to affect ΔF (%) was the concentration of acetate buffer solution. At pH in the range 3.4–5.9, concentration values between 1 and 7 mmol L^{-1} were assayed being the highest analytical signal difference observed for 6 mmol L^{-1} which was then selected for the posterior experiments.

By using the previously selected variables, three sizes of QDs (1.87, 3 and 3.8 nm), each one at three different concentrations, were evaluated in terms of fluorescence intensity, reactivity, repeatability and reproducibility. Two distinct ranges of concentrations were established according to the QDs size: for the bigger sizes (3 and 3.8 nm), the influence of QDs concentration was evaluated from 1.25 to 5 μmol L^{-1} while for the smaller ones (1.87 nm) the QDs concentration was studied between 2.5 and 10 μmol L^{-1}. It was observed that for former the analytical signal increased up to 2.5 μmol L^{-1} and then decreased while for the later it increased until 5 μmol L^{-1} followed by a drop. This could be explained by the fact that when the concentration reached higher values it led to a decrease of fluorescence mainly due to the inner filter effect as a result of re-absorption of emitted radiation. The concentration and diameter of QDs were therefore of utmost importance affecting QDs reactivity and the sensitivity of NAC determination. After a detailed and extensive study on the evaluation of the fluorescence response of the various QDs sizes with the corresponding concentrations, the highest sensitivity (higher ΔF (%)) was verified with the 1.87 nm nanodots. Although these nanoparticles were observed to be less fluorescent than the two other sizes, they exhibited a higher reactivity. A possible explanation is that they present a greater number of surface defects that can coordinate with the different groups of the NAC, which also justifies the lower quantum yield QY%, when compared to the bigger QDs (Table 1), thus the evidently lower fluorescence.

After establishing the concentration of acetate buffer and dot size (1.87 nm) the pH was readjusted between 5 and 5.9 (the fluorescence signal remained almost constant for a pH down to 4.9 but the solution stability markedly decreased). Another variable that was considered in the assessment of the optimization variables was the quantum dots solutions ageing. We have noticed differences on the variation of the fluorescence signal in terms of photostability/reactivity whether fresh solutions of the QDs or old ones (with some days of age) were used. For this reason a study was carried out to evaluate the fluorescence response according to the age of the QDs solutions. QDs concentrations of 2.5 and 5 μmol L^{-1} were studied over six days within the pH range already selected. Subsequently, for each day of ageing, the fluorescence intensity variation for each concentration of the QDs was observed to vary randomly over the pH range. After some repetitions, the concentration of 5 μmol L^{-1} was estimated to be the optimum value according to those parameters of validation given by an increase of approximately 78% on the fluorescence signal at pH of 5.21 in the second day of ageing (Fig. 2). Nevertheless, for the concentration of 2.5 μmol L^{-1}, an increase of approximately 47% on the analytical signal at pH 5.78 in the second day of ageing was observed as the highest value. As perceived by the results, the fluorescence emission of CdTe QDs demonstrated to be pH-sensitive with the ageing time and with the concentration of the quantum dot. Since the

final decision was influenced by compromise between analytical sensitivity and wide range of linearity, a calibration curve was plotted for both concentrations. After an evaluation of the calibration curves, the concentration of 5 μmol L^{-1} was the applied one, since lower detection limit (LOD) was efficiently reached as well wider linear working range. In the graph of Fig. 2 is only plotted the influence of the pH on the analytical signal over three days of QDs age for the selected concentration of 5 μmol L^{-1}. Under the optimized experimental conditions a linear range for NAC concentrations within 50 and 750 μmol L^{-1} was defined.

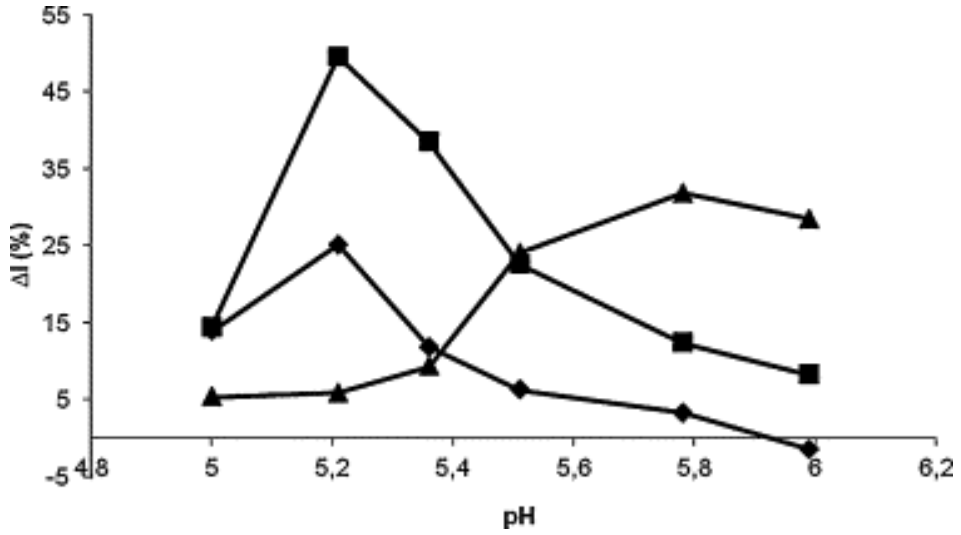

Fig. 2. Influence of the pH on the analytical signal over three days of QDs ageing time for a fixed concentration of *N*-acetyl-l-cysteine: 500 μmol L^{-1} and for a fixed concentration of acetate buffer: 6 mmol L^{-1}. (♦) 1st day; (■) 2nd day; (▲) 3rd day.

3.3. Interferences

The interfering effect of several substances usually present in the pharmaceutical formulations such as excipients, like benzalkonium chloride, sodium benzaoate and sodium chloride was assessed. Samples containing NAC at a fixed concentration of 13 mg L^{-1} (corresponding to 80 μmol L^{-1}) and increasing concentrations of the excipient (up a 100-fold molar ratio) were analyzed by the developed methodology. A compound was considering as non-interfering if the analytical signal variation was ±3% when compared to the one obtained in its absence. The results (Table 3) showed that under the system operating conditions, no interfering effect was observed.

Table 3. Interfering effect of excipients on the developed methodology.

Interference	Tolerance limit [a]
Benzalkonium chloride	25
Sodium benzoate	50
Sodium chloride	100 [b]

a 80 μmol L^{-1} *N*-acetyl-l-cysteine added; b The highest value tested.

3.4. Analysis of pharmaceutical formulations

After system optimization, the proposed procedure was applied to the determinations of NAC in pharmaceutical formulations. By using a 5 μmol L^{-1} QDs solution a linear working range for NAC concentrations between 50 and 750 μmol L^{-1} was obtained. The calibration curve was expressed by the equation (Eq. (4)):

$$\Delta F = 66.315C + 100.87 \quad (4)$$

in which ΔF was the *delta* of fluorescence intensity and C was the logarithm of NAC concentration, in μmol L^{-1}, with a correlation coefficient of 0.998 (n = 5). The precision of the MPFS system was also satisfactory as corroborated by the r.s.d. < 1.6%, n = 5. The detection limit and the quantification limit (LOQ) were calculated according to Skoog et al. [31] using the following expression: LOD = $3\sigma/b$ and LOQ = $10\sigma/b$, where σ is the standard deviation of 20 measurements of the blank and b is the slope of the analytical curve. The LOD and the LOQ were 1.6 and 5.3 μmol L^{-1}, respectively; these results demonstrate the sensitivity of the proposed MPFS spectrofluorimetric procedure. The sampling frequency was about 75 hr^{-1}, with the consumption of 60 μL of both sample and QDs solution per determination. This represents a noteworthy improvement regarding the official method that requires 20 min for the determination of just one sample.

For assessing the accuracy of the results furnished by the developed procedure, the same 6 commercial pharmaceutical formulations containing NAC were analyzed according to the reference procedure recommended by the United States Pharmacopeia which relies on a HPLC methodology [16]. The results, summarized in Table 4, revealed a good agreement between both methods, with relative deviations between −2.1 and 4.2%. In addition, a paired Student's *t*-test [32] confirmed that there were no statistical differences

($t_{estimated}$ = 1.083, $t_{tabulated}$ = 2.571) between the results obtained by both procedures, for a confidence level of 95% (n = 3).

Table 4. Results obtained in the determination of *N*-acetyl-l-cysteine in pharmaceutical preparations.

Samples	**Concentration declared (mg)**	**Amount found** [a]	**R.D.(%)** [b]	
		Developed methodology	**Reference method**	
Fluimucil 2% [c]	20	21 ± 4	20.1 ± 0.2	2.1
Fluimucil 4% [c]	40	42 ± 2	41 ± 4	2.0
Tirocular [c]	40	39 ± 3	40 ± 2	−1.3
Fluimucil injectable [c]	100	103 ± 4	102 ± 1	1.5
Fluimucil 20%(injectable) [c]	200	196 ± 3	200 ± 1	−2.1
Fluimucil (granule) [d]	200	203 ± 3	212 ± 3	4.2

a Mean ± $t_{0.05}$ (Student's t-test) × $(S/\sqrt{n})$.

b Relative deviation of the developed methodology with respect to the reference procedure; c mg *N*-acetyl-l-cysteine per mL; d mg *N*-acetyl-l-cysteine per sachet.

3.5. Proposed mechanism of interaction between QDs and NAC

In order to better understand the response characteristics of CdTe QDs to NAC molecules some batch assays involving steady-state fluorescence spectroscopy measurements and FT-IR were carried out by applying the reaction conditions already used in flow. For the photoluminescence emission studies, two different solutions of QDs were prepared (2.5 μmol L^{-1} CdTe QDs in 3 mmol L^{-1} acetate buffer at pH 5.2 and 2.5 μmol L^{-1} CdTe QDs in 3 mmol L^{-1} acetate buffer at pH 5.2 with 250 μmol L^{-1} NAC), and the results were compared (Fig. 3). For both solutions no significant shift of the emission spectra was observed. However, the fluorescence intensity of QDs changed reasonably. With the addition to a solution of 2.5 μmol L^{-1} CdTe QDs in 3 mmol L^{-1} acetate buffer at pH 5.2 of 250 μmol L^{-1} NAC, an increase of approximately 35% was verified in comparison to the blank (in the absence of NAC). This fluorescence enhancement is clearly lower than the 78% increase in luminescence intensity obtained with MPFS (for identical reaction

conditions) confirming that the applied flow-based methodology is undoubtedly an advantageous expeditious way of implementing reactions of this type.

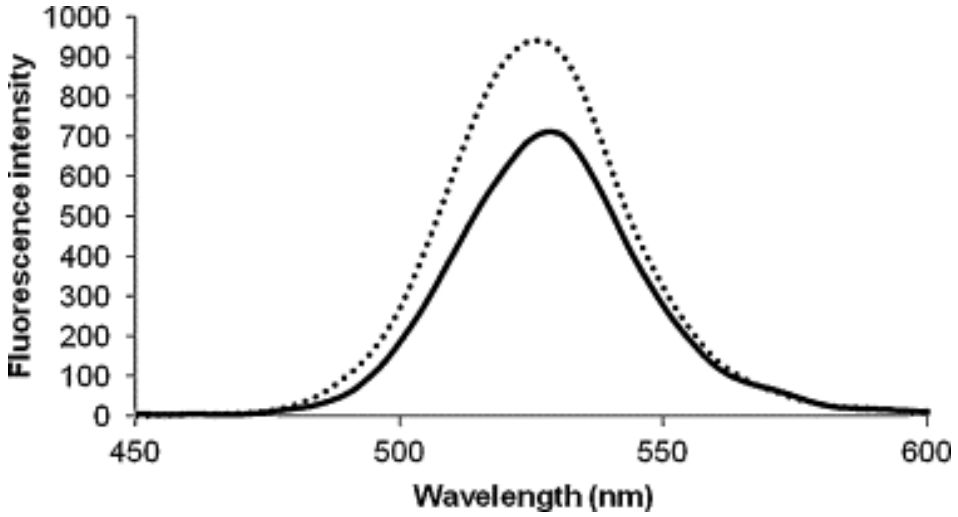

Fig. 3. Fluorescence enhancement of CdTe QDs upon addition of 250 μmol L^{-1} NAC in pH 5.2;(solid line) 2.5 μmol L^{-1} CdTe QDs in 3 mmol L^{-1} acetate buffer at pH 5.2; (dashed line) 2.5 μmol L^{-1} CdTe QDs in 3 mmol L^{-1} acetate buffer at pH 5.2 with 250 μmol L^{-1} NAC.

By comparing the FT-IR spectrum of two solutions obtained after lyophilization, one containing 250 μmol L^{-1} NAC and another one with 2.5 μmol L^{-1} CdTe QDs in 3 mmol L^{-1} acetate buffer at pH 5.2 with 250 μmol L^{-1} NAC it was possible to gather additional information that helped to understand the interactions that may happen on the surface of the dots resulting in enhanced fluorescence emission. *N*-Acetyl-l-cysteine is a weak acid containing three important functional groups: thiol (sulfhydryl), amine and carboxylic acid. In order to identify whether some of these groups could be bonded to the surface of QDs, FT-IR measurements were performed and the spectra are displayed in Fig. 4. The thiol group has a high affinity for binding heavy metals [33] and the results obtained with the FT-IR spectra seemed to reinforce this finding. In fact, the disappearance of the entire NAC S–H band (2550–2678 cm^{-1}) upon interaction with the dots surface can be explained by complexation of incompletely bounded cadmium ions (Cd^{2+} surface traps) which contributed to improve dots passivation inducing a quantitative modification of the optical properties. These results showed to be a good evidence for the remarkable enhancement emissions of CdTe QDs promoted by NAC. Even though it has been demonstrated that the interaction cadmium–thiol strongly depends on the pH, the diameter of the QDs was clearly an aspect affecting the fluorescence increase. Effectively, luminescence

enhancement was much more prominent in the case of smaller sized QDs, compared to larger ones, despite their initial low fluorescence emission. As it was already mentioned, QDs with a diameter of about 1.87 nm showed a lower QY% when compared with the other nanoparticles assayed. This happens because smaller sized QDs have a greater surface to core atoms ratio and therefore most of the electronic defects or dangling bonds are localized on the surface [34]. As it was referred, those traps are Cd^{2+} ions located on the QDs surface that did not complete all their allowed bonds. Molecules like NAC bind to those sites effectively removing the traps states [35] and increasing the intensity of emission. Albeit the experimental results suggested that the enhancement effect is mainly due to the binding of the thiol group to surface defects sites, the participation of other functional groups of NAC was not entirely rejected since they are all prone to coordinate cadmium ions. Furthermore, a slight acidic medium seems to facilitate the reaction between NAC and Cd^{2+} sites. This can be probably attributed to the only "partial" protonation of MPA carboxylic groups at the QDs surface. These groups when dissociate conferred a negative charge to the nanoparticles surface that ensures the stability in solution. On the other hand, this charged layer can difficult the diffusion of negatively charged analytes into the QDs surface and subsequently prevents the establishment of interaction with the reactive sites existing on it. If we compare the carboxylic acidic group pK_a of the two involved molecules (pK_a MPA = 4.34; pK_a NAC = 4) at pH 5.2, MPA will be more protonated than NAC. Thus, NAC has a easier surface access and a more strong tendency to react with Cd^{2+}[36]. This assumption was validated by the results obtained when NAC solution was acidified with HCl at pH 5.2, which provided a 35% enhancement, similar to the one obtained with acetate buffer. Despite of this, a lack of efficiency and reproducibility would hinder the reliability and efficacy of the HCl method. Moreover, this procedure would be more complex and time consuming since we would have to guarantee the uniformity of pH for all standards and samples.

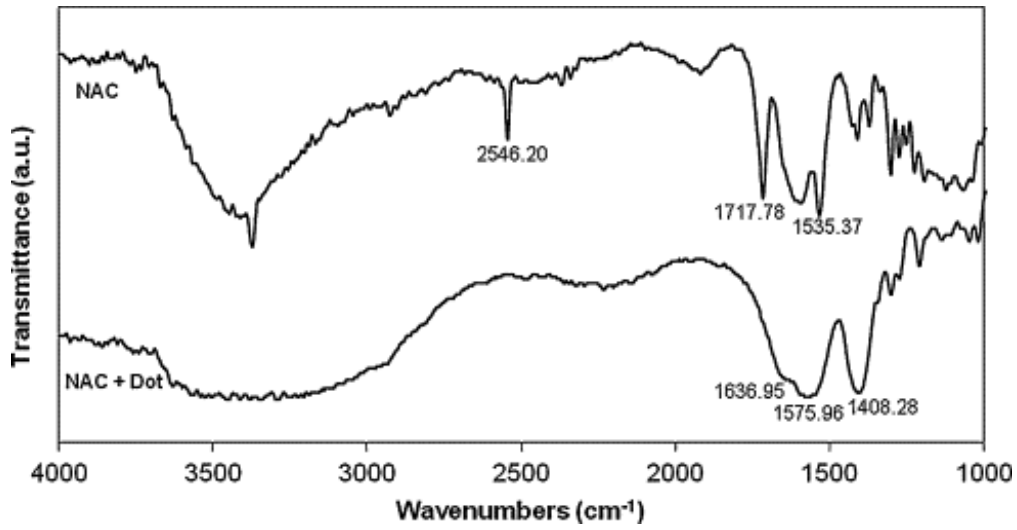

Fig. 4. Infrared spectra of *N*-acetyl-l-cysteine (NAC) and the interaction of NAC with MPA–CdTe QDs under the optimized conditions.

4. Conclusions

The feasibility and robustness of implementing CdTe QDs in a multipumping flow system for the fluorimetric determination of NAC in pharmaceutical formulations was demonstrated. The use of such nanosensors constitutes a noteworthy contribution for the success and efficiency of the proposed methodology regarding other available alternatives. Due to the extended range of variables to be optimized, the multipumping flow methodology allowed a simplification of the entire process and the gathering of the ideal conditions in a simple and fast way. The pulsed flowing stream generated by micro-pump actuation not only permitted the attainment of very stable flow rates but it also imparted a fast homogeneous mixing which contributed to improve the interactions development. Furthermore, the use of the merging zones strategy was of great benefit as it enabled the reduction of the time required for the analysis as well as the reagent consumption.

Additionally, in comparison with the reference procedure, the proposed system proved to fill many of the gaps left by those former methodologies which always require high volume of reagents, often hazardous for the environment, expensive equipment and time-consuming sample handling operations. Good repeatability, a wide linear working range, low limits of detection and quantification, low consumption of reagents and a high sampling frequency were easily achieved with the proposed method. These results point out the potential use of water-soluble CdTe QDs as pharmaceutical drugs probes by pH modulation of the analyte solutions. In conclusion, the effect of luminescence

enhancement of CdTe nanoparticles when NAC is added in a slight acidic medium was much more pronounced for the QDs of smallest size. Due to the their reduced size, a great number of local surface-trap states become more accessible to coordination by the thiol groups of NAC as proved by FT-IR measurements.

Acknowledgment

The authors are grateful to Fundação para a Ciência e Tecnologia (FCT) for the financial support under the project PTDC/QUI-QUI/105514/2008.

References

[1] A.P. Alivisatos, Science 271 (1996) 933–937.
[2] P. Alivisatos, Nat. Biotechnol. 22 (2004) 47–52.
[3] J.M. Costa-Fernández, R. Pereiro, A. Sanz-Medel, Trends Anal. Chem. 25 (2006) 207–218.
[4] Y. He, P. Yin, H. Gong, J. Peng, S. Liu, X. Fan, S. Yan, Sens. Actuators B 157 (2011) 8–13.
[5] T. Zhang, X. Sun, B. Liu, Spectrochim. Acta Part A 79 (2011) 1566–1572.
[6] Z. Chen, X. Ren, X. Meng, D. Chen, C. Yana, J. Ren, Y. Yuan, F. Tang, Biosens. Bioelectron. 28 (2011) 50–55.
[7] J. Chen, A. Zheng, Y. Gao, C. He, G. Wu, Y. Chen, X. Kai, C. Zhu, Spectrochim. Acta Part A 69 (2008) 1044–1052.
[8] N. Butwonga, T. Noipa, R. Burakham, S. Srijaranai, W. Ngeontae, Talanta 85 (2011) 1063–1069.
[9] S. Kanwal, Z. Traore, C. Zhao, X. Su, J. Lumin. 130 (2010) 1901–1906.
[10] H. Chen, R. Li, L. Lin, G. Guo, J.-M. Lin, Talanta 81 (2010) 1688–1696.
[11] S. Kanwal, X. Fu, X. Su, Microchim. Acta 169 (2010) 167–172.
[12] P.R. Fortes, C. Frigerio, C.I.C. Silvestre, J.L.M. Santos, J.L.F.C. Lima, E.A.G. Zagatto, Talanta 84 (2011) 1314–1317.
[13] C.I.C. Silvestre, C. Frigerio, J.L.M. Santos, J.L.F.C. Lima, Anal. Chim. Acta 699 (2011) 193–197.
[14] D. Voet, J.G. Voet, Biochemistry, 2nd ed., John Wiley & Sons, New York, 1995, p. 1236.
[15] Index Merck, 12th ed., 1996, p.16.
[16] USP 28/NF 23, The United States Pharmacopeial Convention, Inc., 2005, pp. 46–47.
[17] Brazilian Pharmacopoeia, third ed., Organizac¸ ão Andrei Editora S.A, São Paulo, Brazil, 1997.
[18] A.L.D.T. Fornazari, W.T. Suarez, H.J. Vieira, O. Fatibello, Acta Chim. Slov. 52 (2005) 164–167.
[19] W.T. Suarez, H.J. Vieira, O. Fatibello-Filho, J. Pharm. Biomed. Anal. 37 (2005) 771–775.
[20] A. Waseem, M. Yaqoob, A. Nabi, Luminescence 23 (2008) 144–149.
[21] M. Kolar, D. Dobcnik, Die Pharmazie 58 (2003) 25–28.
[22] M.H. Pournaghi-Azar, F. Ahour, J. Electroanal. Chem. 622 (2008) 22–28.
[23] I.S. da Silva, M.F.A. Araújo, H.A. Ferreira, J.J.G. Varela Jr., S.M.C.N. Tanaka, A.A. Tanaka, L. Angnes, Talanta 83 (2011) 1701–1706.

[24] P.D. Tzanavaras, T.D. Karakosta, J. Pharm. Biomed. Anal. 54 (2011) 882–885. [25] P.D. Tzanavaras, C.K. Zacharis, D.G. Themelis, Anal. Lett. 43 (2010) 1889–1901. [26] R.A.S. Lapa, J.L.F.C. Lima, B.F. Reis, J.L.M. Santos, E.A.G. Zagatto, Anal. Chim. Acta 466 (2002) 125–132.
[27] J.L.M. Santos, M.F.T. Ribeiro, A.C.B. Dias, J.L.F.C. Lima, E.E.A. Zagatto, Anal. Chim. Acta 600 (2007) 21–28.
[28] D.D. Perrin, B. Dempsey, Buffers for pH and Metal Ion Control, Chapman and Hall, London, 1974, Appendices, pp. 123–157.
[29] L. Zou, Z. Gu, N. Zhang, Y.Z. Fang, W. Zhu, X.J. Zhong, Mater. Chem. 18 (2008) 2807–2815.
[30] W.W. Yu, L. Qu, W. Guo, X. Peng, Chem. Mater. 15 (2003) 2854–2860.
[31] D.A. Skoog, F.J. Holler, T.A. Nieman, Principles of Instrumental Analysis, 5th ed., Thomson Brooks/Cole, 1997.
[32] J.C. Miller, J.N. Miller, Statistics and Chemometrics for Analysis Chemistry, 4th ed., Pearson Education, England, 2000, pp. 48–50.
[33] D. Baker, G. Czarnecki-Maulden, J. Nutr. 117 (1987) 1003–1010.
[34] D. Hayes, O.I. Micic, M.T. Nenadovic, V. Swayambunathan, D. Meisel, J. Phys. Chem. 93 (1989) 4603–4608.
[35] T. Dannhauser, M. O'Neil, K. Johansson, D. Whitten, G. McLendon, J. Phys. Chem. 90 (1986) 6074–6076.
[36] S. Xu, C. Wang, H. Zhang, Z. Wang, B. Yang, Y. Cui, Nanotechnology 22 (2011) 315703.

CHAPTER 6

Determination of chlorhexidine by induced fluorescence enhancement of MPA-capped CdTe quantum dots

Journal of Fluorescence
Determination of chlorhexidine by induced fluorescence enhancement of MPA-capped CdTe quantum dots
--Manuscript Draft--

Determination of chlorhexidine by induced fluorescence enhancement of MPA-capped CdTe quantum dots

Christian Frigerio, Vera L.R.G. Abreu, João A.C. Barbosa, S. Sofia M. Rodrigues, João L.M. Santos.

Requimte, Laboratory of Applied Chemistry, Faculty of Pharmacy, Porto University
Rua Jorge Viterbo Ferreira 228, 4050-313 Porto, Portugal

Abstract

In this work the fluorescence enhancement that water-soluble CdTe quantum dots (QDs) capped with 3-Mercaptopropionic acid (MPA) exhibit in the presence of a biguanide compound, chlorhexidine, was investigated. Acting as an electron-donor ligand chlorhexidine was able to interact with the defects (mid-gap energy traps) on the QDs surface improving the surface passivation and the fluorescence emission. The accomplished fluorescence enhancement was used as the sensing strategy for the implementation of an analytical methodology for the determination of chlorhexidine in pharmaceutical formulations.

The developed approach was implemented by resorting to a fully automated multipumping flow systems, which improved the versatility and analytical potential provided by QDs enabling to overcome some of the shortcomings associated with the commonly used batch procedures. Different sized QDs were synthesised and evaluated. A chlorhexidine analytical working range for concentrations between $0.05x10^{-3}$ and $0.5x10^{-3}$ mol L^{-1} was verified with a sampling throughput of about 63 samples hr^{-1}. The obtained results were in good agreement with those furnished by the reference method (RD% < ±4.77). A mechanism for the enhancing phenomenon is proposed.

Keywords: CdTe; Quantum dots; Fluorescence; Chlorhexidine; Multipumping flow system; flow analysis.

1. Introduction

Colloidal semiconductor nanocrystals, also known as quantum dots (QDs), have been finding many new analytical applications. Initially developed as molecular probes for utilisation in biomaging [1], in biotargeting [2] and drug delivery [3], QDs are being researched for organic and inorganic analyte determination mostly taking advantage of their peculiar photoluminescent (PL) properties [4]. In fact, the longer luminescence lifetimes, molar extinction coefficients, photostability, high quantum yield, broad excitation bandwidths and narrow size-tuned emission spectra along with a large surface-to-volume ratio, surface functionality, a relatively low cost and a high chemical flexibility make them attractive luminescent tools for implementing selective and sensitive analytical methodologies. In this regard, QDs have been used in environmental analysis [5], in the determination of pesticides [6] and heavy metals [7], pharmaceuticals [8], etc.

Quantum dots luminescence is very sensitive to micro-environmental changes because the luminescence intensity and wavelength is determined not only by the nanocrystals size but also by their surface characteristics. Effectively, in small crystals a high percentage of the atoms, approximately 56% in 3-nm QDs, are at the surface [9]. Organic ligands coordinated to the QDs surface not only serve as passivators, as a means to increase solution stability preventing aggregation, but are also involved in electron transfer processes (as donors or acceptors) to or from dangling bonds incompletely coordinated, affecting the optical properties of QDs, namely the luminescence lifetime and quantum yield. External ligands interacting with the capping (passivating) layer or with the surface imperfections (traps) would alter electro-hole recombination and thus the photoluminescence response. A panoply of viable operating principles could be therefore devised to signal and relay the presence of a target analyte with a marked luminescence change. These mechanisms generally transduce a recognition event into a measurable signal by relating a sensor-target association with an electron or energy transfer process.

Previous works have referred that amino compounds could present “antiquenching” effect [10] as a consequence of a quantum yield enhancement. These compounds could act as passivators of the QDs surface suppressing nonradiative recombination at surface vacancies [11]. Biguanides were already identified as strongly chelating ligands that bind readily to a variety of metals, such as copper, zinc, cobalt, and manganese [12]. They could therefore interact with incompletely coordinated Cd^{2+} on the surface of CdTe quantum dots improving luminescence emission.

Chlorhexidine, N',N''''-hexane-1,6-diylbis[N-(4-chlorophenyl)(imidodicarbonimidic diamide)] (Fig 1), is an antiseptic drug with a biguanidic structure active against Gram-negative and Gram-positive bacteria. Several methods, recently reviewed [13], have been

proposed for chlorhexidine determination in pharmaceuticals and biological samples. These methods include chromatography [14-17], fluorimetry [18], UV/Vis spectrophotometry [19] and capillary electrophoresis [20]. A flow-based extraction-spectrophotometric method was also proposed [21]. The official method of the European [22] and Bristish [23] Pharmacopoeias is a non-aqueous titrimetric method.

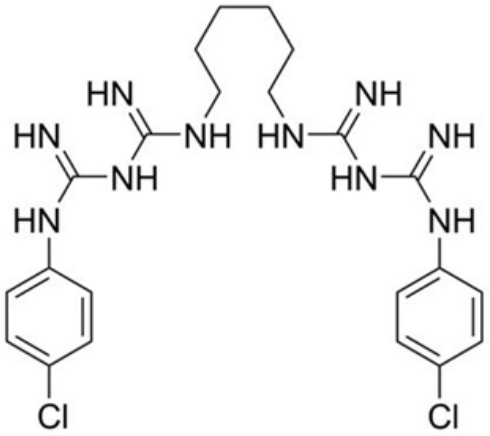

Figure 1 - Chlorhexidine structure.

Most of the available analytical methodologies relying on the utilisation of QDs as chemosensors are based on batch approaches displaying no or a low automation level in what concerns sample handling, reaction implementation and measurements execution. They are thus generally characterized by high consumption of sample and reagents solutions, exhibit low versatility in terms of analytical parameters adjustment and reconfiguration, poor reproducibility and repeatability, are laborious and time-consuming, and are more prone to operational errors. Moreover, they require equilibrium conditions for the attainment or reproducible readouts, which in many circumstances could prevent the evaluation or utilisation of more drastic reaction conditions as they could derange QDs stability impairing detection. Multipumping Flow Systems (MPFS) [24] represent a computer controlled continuous flow-based technique providing a fully automated operation of the analytical system [25] that comprehends not only solutions handling, mixing and reaction zone implementation but also analytical signal acquisition and processing and system performance real-time adjustment. Based on the individual actuation of multiple solenoid micro-pumps that are accountable for all solutions insertion, commutation and propelling, being the only active elements of the entire flow manifold, they generate a pulsed-flowing stream that ensure fast mixing and fast reaction development [26]. MPFS are consequently well suited for the implementation of sensing

schemes based on QDs nanotechnology, even enabling, due to the very short residence time, the exploitation of extreme reaction conditions that otherwise would be unpractical.
In this work we took advantage of the ability of biguanides to chelate metals, in this case to chelate incompletely coordinated Cd^{2+} on the surface of CdTe quantum dots ensuring up to a 160% fluorescence enhancement, to develop an automated multi-pumping flow methodology for chlorhexidine determination.

2. Materials and methods

2.1. Samples, standards and reagents

All solutions were prepared with water from a Milli-Q system (specific conductivity <0.1μS cm^{-1}) and chemicals of analytical reagent grade quality.
3-Mercaptopropionic acid (MPA, 99%) was purchased from Fluka (St. Louis, USA). Sodium borohydride ($NaBH_4$, 99%), tellurium powder (200 mesh, 99.8%), cadmium chloride hemi(pentahydrate) ($CdCl_2$, 99%), Chlorhexidine digluconate 20% (w/v) solution were purchased from Sigma (St. Louis, MO, USA) and used without further treatment. Ethanol (99.5%) was purchased from Panreac (Barcelona, Spain).
Standard solutions of Chlorhexidine digluconate were daily prepared by suitable dilutions with ultrapure water.
Two commercially available pharmaceutical samples, a solid form and a liquid form containing chlorhexidine digluconate were analysed according to the proposed procedure. No special pre-treatment was required for the liquid samples prior to analysis, just a dilution in order to reach a chlorhexidine digluconate concentration of $0.267x10^{-3}$ mol L^{-1}. For the solid form, three tablets were accurately weighed and powdered. A certain amount of powder was dissolved in water to make a solution at $0.2\ x10^{-3}$ mol L^{-1} of chlorhexidine digluconate

2.2. Apparatus

The developed multi-pumping flow system comprised three fixed-diaphragm solenoid actuated micro-pumps (Bio-Chem Valve Inc., Boonton, NJ, USA) (two of the micro-pumps dispensing a stroke volume of 10μL and the third one a stroke volume of 20μL), and a modular optical-fibre spectrofluorimeter from Ocean Optics (Dunedin, MA, USA)

consisting on USB4000-FL detector, a LS-450 power source equipped with a LED emitting at 395nm , and a 8 μL internal volume flow-cell. Reaction coils were made of PTFE tubing (0.8mm i.d.). Homemade end-fittings, a four way confluence point and connectors were also used [27].

For the QDs characterization absorption spectra were collected using a Perkin Elmer (Waltham, MA, USA) Lambda 45 UV/VIS spectrophotometer and the emission spectra was obtained with a luminescence spectrometer Perkin Elmer (Waltham, MA, USA) LS50B. A ThermoElectron (Waltham, MA, USA) Jouan BR4I refrigerated centrifuge was used for QDs separation. X-ray powder diffraction (XRD) studies of the nanocrystals were carried out by using a Philips X'Pert X-ray MPD diffractometer (Cu Kα radiation). XRD data were collected at a scan rate o 40.0 s for step at step intervals of 0.04º.

A computer was used for system control, the software being developed in Microsoft Visual Basic 6.0. The computer was equipped with a PC-LABCard model PCL-711B (Advantech, Cincinnati, OH, USA) interface card. A CoolDrive (NResearch Inc., West Caldwell, NJ, USA) power drive was used to operate the solenoid micro-pumps. Analytical signals were computer recorded and processed by using Spectra Suite software version 2007 (OceanOptics, Dunedin, MA, USA).

2.3. Synthesis of CdTe-MPA quantum dots

MPA-capped CdTe QDs were synthesized as described by Zou L. *et al.* 2008 [28] with some modifications. Briefly, NaHTe solution was prepared by the reaction between $NaHB_4$ and Te powder in N_2 saturated water. CdTe QDs was synthesized adding freshly prepared NaHTe into a second flask containing 4.0 x 10^{-3} mol of $CdCl_2$ and 6.8 x 10^{-3} mol of MPA in a 100 mL N_2 saturated solution. The pH of the $CdCl_2$ and MPA solution was adjusted to 11.5 by addition of 1 mol L^{-1} NaOH. The molar ratio of Cd^{2+}/Te^{2-}/MPA was fixed at 1:0.1:1.7. Precursors were converted into nanocrystals by refluxing the mixture at 100ºC under open air conditions and the CdTe QDs size was tuned by varying the heating time.

The solutions obtained were precipitated with ethanol, in order to remove the excess of precursors, centrifuged and finally the QDs were dried and stored at 4ºC under N_2 atmosphere, in order to preserve the luminescence propriety of the nanocrystals.

Working solutions were prepared daily with ultrapure water.

2.4. Multi-pumping flow manifold and procedure

The developed system, shown in Figure 2, comprised three solenoid micro-pumps (P_1, P_2 and P_3) for inserting and propelling the sample, the reagent (QDs) and the carrier (H_2O). Each solenoid micro-pump was individually actuated allowing the utilisation of various sample/reagent insertion sequences and therefore the establishment of distinct strategies for reaction zone implementation. The sequential micro-pump switching on/off created a pulsed flowing stream where the pulse volume corresponded to the stroke volume. The pulse volume in combination with the pulse frequency (for each micro-pump actuation) was used to determine the flow rate of each propelled solution.

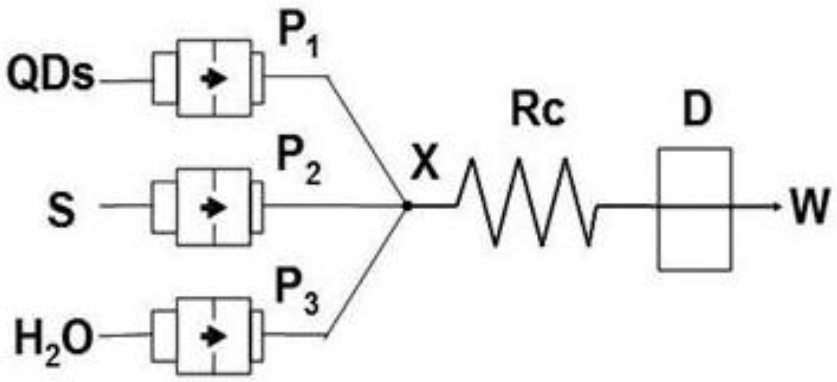

Figure 2 - Schematic diagram for the multipumping flow system: P_1, P_2 and P_3 solenoid micro-pumps; Rc - reaction coil; X – confluence point; D - fluorescence detector, λ_{exc}= 395 nm, λ_{emi} = 535-537 nm; S – sample; QDs – quantum dots solution; W – waste.

The extremely simple analytical cycle was started by establishing baseline which was accomplished with water by actuating P_3. Blank readings were obtained by measuring the fluorescence emission upon the simultaneous insertion of QDs and water. To this end P_1 and P_2 were simultaneously actuated for a pre-determined number of pulses (6 pulses each, corresponding to 60 μL of H_2O and 60 μL of QDs solution for a global volume of 120 μL) at a global flow rate of 2 mL min^{-1}(1 mL min^{-1} for each solution corresponding to a pulse frequency of 100 min^{-1}) allowing the merging of H_2O and QDs solution at the confluence point C (Fig 2). P_3 was then actuated (55 pulses of a 20 μL per stroke micro-pump) at a flow rate of 1.2 mL min^{-1} (pulse frequency of 60 min^{-1}) to transport the reaction zone through the reaction coil Rc toward the detector. A similar procedure was used for measuring the PL of samples and standards, inserted as a replacement for H_2O in P_2 (the insertion and propelling sequence was the abovementioned one). The excitation wavelength was set at 395 and the emission was an average of the signals acquired

between 535 and 537nm. Integration time was of 500 ns and each value was the average of 3 acquisitions.

2.5. Reference procedure

Aiming accuracy in evaluation of the results obtained with the developed procedure, chlorhexidine bulk drug and chlorhexidine pharmaceutical formulations were analysed according to the European Pharmacopoeia [22] by non-aqueous titration in glacial acetic acid with perchloric acid. The end-point was potentiometrically determined.

3. Results and discussion

Preliminary batch experiments aiming at evaluating the influence of several amino compounds on the photoluminescence (PL) intensity of CdTe solutions revealed that chlorhexidine, exhibiting a biguanidic structure (Fig 1), had a pronounced enhancing effect. However, the CdTe-chlorhexidine surface interaction affected quantum dots stability, which tended to aggregate, resulting in the solution precipitation. Since in a batch approach reaction equilibrium conditions are required to accomplished reproducible measurements, the precipitate formed as consequence of the increased reaction time impaired any fluorescence measurement. The implementation of the reactional scheme in a flow-based procedure relying in both a reproducible sample/reagent mixing and time-based signal measurement, under no-equilibrium conditions, appeared as an expeditious strategy to overcome this problem. Due to its versatility, mixing capacity and operational simplicity a multi-pumping flow system was selected for carrying out the assays.

In the subsequent trials, water was used as the blank and the signal obtained upon mixing with the CdTe QD solution was used as the blank fluorescence signal. The assessment of the fluorescence enhancement effect (*ΔPL (%)*) was carried out by means of the ratio between the photoluminescence intensity of the sample solution (PL_s) minus the photoluminescence intensity of the blank (PL_o) and (PL_o) according to the equation (eq. 1):

$$\Delta PL\ (\%) = ((PL_s - PL_o)/PL_o) \times 100 \qquad (1)$$

All experimental conditions were optimised in order to obtain the highest *ΔPL(%)*.

3.1. Characterization of CdTe-MPA quantum dots

The powder X-ray diffraction pattern showed the highly crystalline feature of the CdTe nanocrystals (Fig 3), and is consistent with the bulk cubic structure. Figure 4 show the normalized absorption/emission spectrum of CdTe-MPA nanocrystals. All samples showed a well resolved maximum corresponding to the first transition. The particle size of the synthesized QDs was calculated according to the expression (eq.2) [29] :

$$D = \left(9.8127 \times 10^{-7}\right)\lambda^3 - \left(1.7147 \times 10^{-3}\right)\lambda^2 + \left(1.0064\right)\lambda - \left(194.84\right) \quad (2)$$

where D is the diameter (nm) and λ (nm) the wavelength maximum corresponding to the first excitonic absorption peak of the crystal.

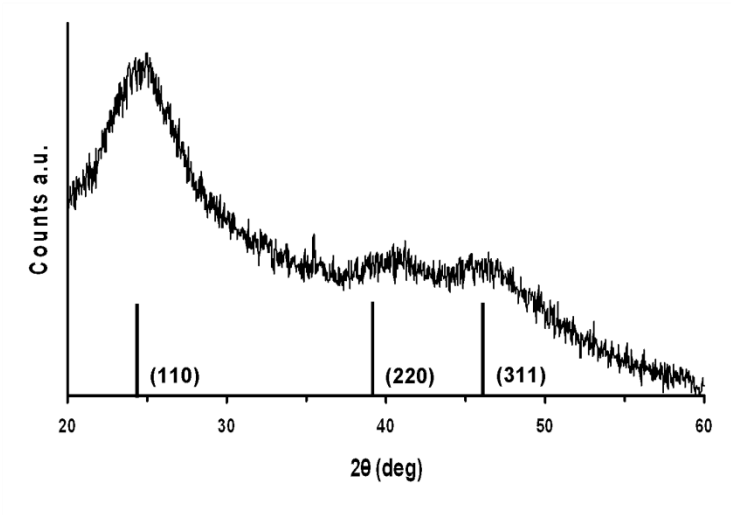

Figure 3 – XRD patterns of CdTe quantum dots.

In order to standardize the preparation of the QDs solutions it was also necessary to calculate the molar weight of the different sized nanocrystals. This was possible by establishing firstly the extinction coefficient (ε) using the expression eq.3 [29]:

$$\varepsilon = 3450\Delta E\left(D\right)^{2.4} \quad (3)$$

where ΔE is the transition energy corresponding to the first absorption peak and the unit is eV. From the ε value the molar mass can be easily estimated by measuring the absorbance of a known concentration solution and by applying the Lambert-Beer law.

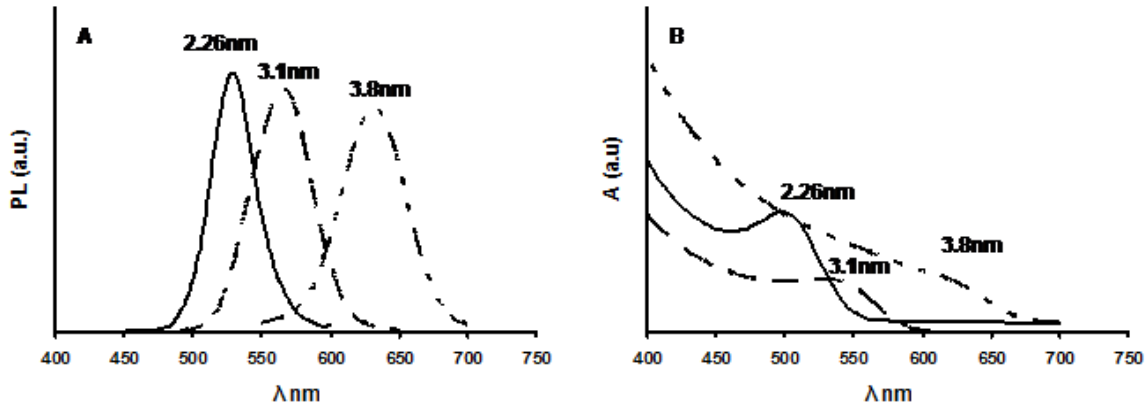

Figure 4 - Photoluminescence spectra (A) and absorption spectra (B) of CdTe QDs with different size. The excitation wavelength is 400 nm.

Fluorescence emission spectra of the three nanocrystals show maximums at 530 nm (D = 2.26 nm), 576 nm (D = 3.1 nm) and 632 nm (D = 3.8 nm). In order to evaluate the size dispersion, the PL peak width (full width at half maximum, FWHM) was assessed. For the smaller QDs the FWHM was 37 nm, being 49 nm for those with a diameter of 3.1 nm and reaching the maximum value, 53 nm for the bigger ones (D = 3.8 nm). This defocusing was expected and extensively described in literature as a consequence of the Ostwald Ripening growing mechanism.

3.2. System optimization

In order to study the reaction development and to improve its application performance in terms of sensitivity, accuracy, precision and sample rate, several parameters, both chemical and physical, were studied (Table 1).

Table 1 - Optimized parameters used in the analysis.

Parameter	Studied values	Selected values
QDs concentration (10^{-6} mol L^{-1})	1.25 - 5	2.5
Chlorhexidine concentration (10^{-3} mol L^{-1})	0.0005 - 1	0.05 – 0.5
Volume QDs (µL)	20 – 100	60
Flow rate (mL min^{-1})	1.2 – 2	1.2
Reactor length (cm)	0 – 100	60
Sampling frequency (sample hr^{-1})		63

The volume of the QDs solution was optimised aiming at assuring an easily detectable and reproducible blank PL signal at the QDs working concentrations. In order to simplify system operation, and since the pulsed flowing stream generated by micro-pumps actuation provided a good mixing, a merging zones strategy with equal volumes of sample (water for the blank) was selected as reaction zone intercalation scheme. For the four volumes assayed (20, 40, 60 and 80µL) the PL signal strongly increased with the volume increment from 20 to 60µL and then tended towards stabilization (Fig 5A). In opposition the analytical signal reproducibility increased linearly with the increment of the volume (Fig 5B), but in all instances the relative standard deviation (RDS%) was very low (<3%) confirming a good precision. As it was expected, the peak broadening showed a linear relationship with the rise in QDs volume (Fig 5C). As a consequence of these results a QDs volume of 60µL was selected for the subsequent experiments, which enabled a good compromise between sensibility and reproducibility of the analytical signal.

The influence of the flow rate used to insert the samples and to propel the reaction mixture to the detector were assessed between 1.2 and 2.0 mL min^{-1}. The obtained results revealed that this parameter had no influence on the PL signal, although the lower value provided improved reproducibility.

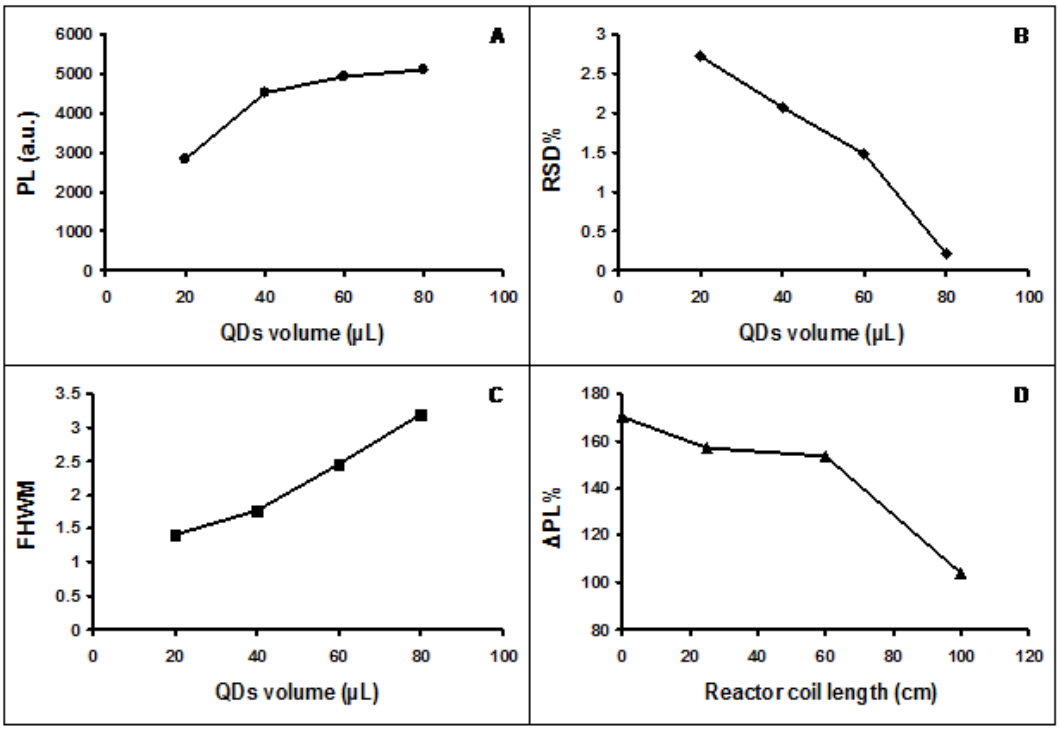

Figure 5 – Results obtained in the evaluation of several analytical parameters: 5A - photoluminescence variation versus QDs volume; 5B - relative standard deviation of the photoluminescence signal versus QDs volume; 5C - peak dispersion for the QDs volume used (FHWM, Full width at half maximum); 5D - effect of the reactor coil (Rc) length on photoluminescence enhancement (ΔPL%, fluorescence variation).

Effect of the serpentine reaction coil (Rc) length was also studied in a range from 0 to 100 cm (Fig 5D). The fluorescence enhancing effect remained almost stable for a coil length between 25 and 60 cm and diminished for longer coils. These results showed that the reaction is fast and that the formed products were unstable (as it happened in the batch method). Concerning reproducibility, this was not affected by the reactor coil length.
The influence of the pH was also evaluated. For pH values ranging from 5.7 to 10.5 it was observed that signal magnitude remained unchanged. Lower pH values weren't assayed because the QDs aren't stable in acidic media, precipitating and loosing their photoluminescence properties.

3.3. Influence of QDs size and concentration.

Fluorescence of QDs could be strongly enhanced by reaction with chlorhexidine, being the enhancing effect pronouncedly dependent of the size and concentration of nanocrystals.

Three different size QDs were assayed, A (2.26 nm) < B (3.1 nm) < C (3.8 nm) at three different concentrations 5, 2.5, and 1.25 μmol L^{-1}.

For QDs C it was only possible to test a concentration value of 2.5 μmol L^{-1}, because at 5μ mol L^{-1} an inner filter effect was observed and at 1.25 μmol L^{-1} the PL intensity was too low for the detector sensitivity. Fig 6A represents the slope of the chlorhexidine calibration curves obtained for QDs of size A and B at different concentrations. Fig 6B displays the slope value of the calibration curve for the different QDs size (A, B and C) at the same concentration (2.5 μmol L^{-1}).

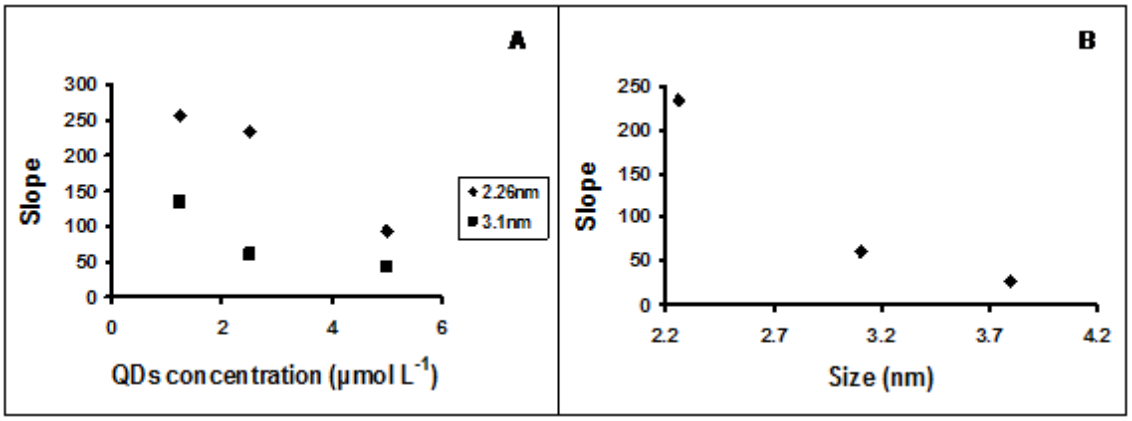

Figure 6 - Sensitivity variation for different size QDs. 6A - slope values of the chlorhexidine calibration curves obtained for QDs of different sizes (A, B) and concentrations; 6B - slope value of the chlorhexidine calibration curve for the different QDs size (A, B and C) at the same concentration (2.5 μmol L^{-1}).

By analysing the referred Figures it is evident that the QDs with the lower size (QDs A, 2.26 nm) are more sensitive to a chlorhexidine concentration variation and are therefore more efficiently enhanced. It is also perceptible that at lower QDs concentration the chlorhexidine PL enhancing effect is more pronounced. This fact can be explained by the possible interaction between chlorhexidine and the CdTe surface traps: smaller QDs are more imperfect [28] and therefore more prone to interact. The 2.26 nm QDs were therefore selected for the experiments, at a 2.5 μmol L^{-1} concentration, which assured improved reproducibility and accuracy.

3.4. Mechanism of the PL enhancing

In literature two principal mechanisms of interaction between organic ligands and QDs are reported [30-34]: the reaction with Cd^{2+} traps and the direct reaction with the capping

agents at the QDs surface. As described by Knowles *et al.* [9] an interaction between amino compounds and Cd^{2+} sites is feasible and the electron donor character of the ligand is fundamental for yielding a quenching or an enhancing effect of the nanocrystal photoluminescence. Chlorhexidine is strong electron-donor compound containing two biguanide groups, that are known to coordinate various metals ions like Co(II), Cu(II) and Ni(II) [12, 35-37]. For this reason incompletely coordinated Cd^{2+} existing on the QDs surface that act as electron-trapping surface states can establish interactions with chlorhexidine forming complexes and improving the passivation of the nanocrystal. The interaction promotes an enhancing of the QDs photoluminescence. The QDs of lower size are those with more surface traps being therefore more prone to establish interactions and to have a greater PL variation in the presence of chlorhexidine thus providing a more sensitive and selective PL response.

3.5. Analytical figures of merit

After analytical system optimisation the developed methodology was evaluated in the determination of chlorhexidine in pharmaceutical formulations. It was observed, that depending on chlorhexidine concentration, two linear working ranges were obtained: one for concentrations ranging from 0.005 $x10^{-3}$ to 0.025 $x10^{-3}$ mol L^{-1} and a second working range for chlorhexidine concentration between 0.05$x10^{-3}$ and 0.5$x10^{-3}$ mol L^{-1}. The calibration curves for the two working ranges were expressed by the following respective equations (4, 5):

$$\Delta PL = 1975.4C - 5.229 \quad (4)$$

$$\Delta PL = 196.34C + 64.632 \quad (5)$$

where ΔPL represents the relative fluorescence enhancement regarding the blank (expressed in percentage) and C is the chlorhexidine concentration expressed in 10^{-3} mol L^{-1}, with correlation coefficients of 0.9980 (n=6) and 0.994 (n=4), respectively. Due to the improved reproducibility, the second analytical working range calibration curve was used in the determinations, providing a sampling frequency of about 63 hr^{-1}.

The implemented multipumping flow system showed a good reproducibility, with a r.s.d<1.5% (n=8), and a good accuracy, with a relative deviation (RD%), regarding the reference method, lower than ±4.77 (Table 2). No interference from the compounds

commonly used as excipients was verified (up to a 100 excipient/chlorhexidine molar ratio).

Table 2 – Results obtained in the analysis of chlorhexidine in pharmaceutical formulations.

Sample	Reference method	Developed method	R.D.%[a]
Drill (tablets)	3.02 ±0.16	3.15±0.14	4.12
Diaseptyl (topic solution)	0.208±0.013	0.199±0.002	-4.77

[a]Relative deviation of the amount found by the developed method regarding the reference method.

4. Conclusion

Chlorhexidine interacts with the surface of CdTe quantum dots fostering a significant enhancing of fluorescence emission. However, it also deteriorates QDs solution stability that thus tended to aggregate and precipitate, impairing detection. This problem was overcame by implementing a pulsed multipumping flow system that enabled fast sample/reagent mixing, even under limited dispersion conditions, assuring the carrying out of reproducible measurements after short residence times yet yielding a 160% fluorescence enhancement. The obtained results confirmed the potential of combining quantum dots nanotechnology with flow-based analysis, as more drastic and sometime damaging reaction conditions could be used for assorted sensing schemes based in various surface ligand interactions, while assuring reproducible and reliable measurements. In addition, similar fluorescence enhancement effects could be exploited for improving sensitivity whenever low analyte concentration is observed, for improving nanoparticles photoluminescence or for providing high analytical signals when a fast readout should be carried out.

Acknowledgments

Authors are grateful for the financial support of the project PTDC/QUI-QUI/105514/2008 under COMPETE/QREN/FEDER. Christian Frigerio thanks FCT for the PhD grant SFRH/BD/47651/2008. The FCT support under the FCT/CAPES 2011-2012 Agreement was greatly appreciated.

References

[1] Wang C, Gao X, Su X (2010) In vitro and in vivo imaging with quantum dots. Anal Bioanal Chem 397(4):1397-1415

[2] Alivisatos AP, Gu W, Larabell C (2005) Quantum dots as cellular probes. Annu Rev Biomed Eng 7:55-76

[3] Lu ZS, Li CM (2011) Quantum dot-based nanocomposites for biomedical applications. Curr Med Chem 18(23):3516-3528

[4] Frigerio C, Ribeiro DSM, Rodrigues SSM, Abreu VLRG, Barbosa JAC, Prior JAV, Marques KL, Santos JLM (2012) Application of quantum dots as analytical tools in automated chemical analysis: A review. Anal Chim Acta 735:9-22

[5] Silvestre CIC, Frigerio C, Santos JLM, Lima JLFC (2011) Quantum dots assisted photocatalysis for the chemiluminometric determination of chemical oxygen demand using a single interface flow system. Anal Chim Acta 699(2):193-197

[6] Zhang K, Mei QS, Guan GJ, Liu BH, Wang SH, Zhang ZP (2010) Ligand replacement-induced fluorescence switch of quantum dots for ultrasensitive detection of organophosphorothioate pesticides. Anal Chem 82(22):9579-9586

[7] Ma Q, Ha E, Yang FP, Su XG (2011) Synchronous determination of mercury (II) and copper (II) based on quantum dots-multilayer film. Anal Chim Acta 701(1):60-65

[8] Azzazy HME, Mansour MMH, Kazmierczak SC (2007) From diagnostics to therapy: prospects of quantum dots. Clin Chem 40:917-927

[9] Knowles KE, Tice DB, McArthur EA, Solomon GC, Wiess EA (2010) Chemical control of the photoluminescence of CdSe quantum dot-organic complexes with a series of para-substituted aniline ligands. J Am Chem Soc 132(3):141-1050

[10] Dannhauser T, O'Neill M, Johansson K, Whitten D, Mclendon G (1986) Photophysics of quantized colloidal semiconductors dramatic luminescence enhancement by binding of simple amines. J Phys Chem 90(23):6074-6076

[11] Liang JG, Zhang SS, Ai XP, Ji XH, He ZK (2005) The interaction between some diamines and CdSe quantum dots. Spectrochim Acta A 61(13-14):2974-2978

[12] Ray P (1961) Complex compounds of biguanides and guanylureas with metallic elements. Chem Rev 61(4):313-359

[13] Fiorentino FAM, Corrêa MA, Salgado HRN (2010) Analytical methods for the determination of chlorhexidine: a review. Crit Rev Anal Chem 40(2):89-101

[14] Brougham LR, Cheng H, Pittman KA (1986) Sensitive high performance liquid chromatographic method for the determination of chlorhexidine in human serum and urine. J Chromatogr 383(2):365–373

[15] Ha Y, Cheung AP (1996) New stability-indicating high performance liquid chromatography assay and proposed hydrolytic pathways of chlorhexidine. J Pharm Biomed Anal 14(8-10):1327–1334
[16] Below H, Lehan N, Kramer A (2004) HPLC determination of the antiseptic agent chlorhexidine and its degradation products 4-chloroaniline and 1-chloro-4-nitrobenzene in serum and urine. Microchim Acta 146(2):129–135
[17] Dogan A, Nursabah EB (2011) Development and validation of RP-HPLC and ultraviolet spectrophotometric methods of analysis for the quantitative determination of chlorhexidine gluconate and benzydamine hydrochloride in pharmaceutical dosage forms. Curr Pharm Anal 7(3):167-175
[18] de Vries J, Ruben J, Arends J (1991) Determination of chlorhexidine in saliva and in aqueous solutions. Caries Res 25(6):410–414
[19] Andermann G, Buhler MO, Erhart M (1980) Rapid colorimetric analysis of chlorhexidine in pharmaceutical preparations. J Pharm Sci 69(2):215-217
[20] Abad-Villar EM, Etter SF, Thiel MA, Hauser PC (2006) Determination of chlorhexidine digluconate and polyhexamethylene biguanide in eye drops by capillary electrophoresis with contactless conductivity detection. Anal Chim Acta 561(1-2):133–137
[21] Perez-Ruiz T, Martınez-Lozano C, Sanz A, Sanchez A (1999) Flow injection extraction-spectrophotometric method for the determination of chlorhexidine in pharmaceutical preparations. J Pharm Biomed Anal 21(4):709–714
[22] European Pharmacopoeia. (2005) Council of Europe (ed.), 5th edn., Strasbourg
[23] British Pharmacopeia (2005), The Stationary Office of Behalf of the Medicines and Health Care Products Regulatory Agency (ed.), London
[24] Santos JLM, Ribeiro MFT, Dias ACB, Lima JLFC, Zagatto EAG (2007) Multi-pumping flow systems: The potential of simplicity. Anal Chim Acta 600(1-2):21-28
[25] Carneiro JMT, Dias ACB, Zagatto EAG, Santos JLM, Lima JLFC (2005) An improved sampling approach in multi-pumping flow systems applied to the spectrophotometric determination of glucose and fructose in syrups. Anal Chim Acta 531(2):279-284
[26] Prior JAV, Santos JLM, Lima JLFC (2007) Exploiting kinetic spectrophotometric determination of captopril, an angiotensin-converting enzyme inhibitor, in a multi-pumping flow system. Anal Chim Acta 600(1-2):183-187
[27] Marques KL, Santos JLM, Lima JLFC (2004), Multicommutated flow system for the chemiluminometric determination of clomipramine in pharmaceutical preparations. Anal Chim Acta 518(1-2):31-36
[28] Zou L, Gu ZY, Zhang N, Zhang YL, Fang Z, Zhu WH, Zhong XH (2008) Ultrafast synthesis of highly luminescent green- to near infrared-emitting CdTe nanocrystals in aqueous phase. J Mater Chem 18(24):2807-2815

[29] Yu WW, Qu LH, Guo WZ, Peng XG (2003) Experimental determination of the extinction coefficient of CdTe, CdSe, and CdS nanocrystals. Chem Mat 15(14):2854-2860
[30] Kuang R, Kuang X, Pan SY, Zheng XD, Duan JC, Duan YQ (2010) Synthesis of cysteamine-coated CdTe quantum dots for the detection of bisphenol A. Microchim Acta 169(1-2):109–115
[31] Uematsu T, Waki T, Torimoto T, Kuwabata S (2009) Systematic Studies on Emission Quenching of Cadmium Telluride Nanoparticles. J Phys Chem C 113(52):21621-21628
[32] Landes C, Burda C, Braun M, El-Sayed MA (2001) Photoluminescence of CdSe nanoparticles in the presence of a hole acceptor: n-butylamine. J Phys Chem B 105(15):2981-2986
[33] Cooper DR, Suffern D, Carlini L, Clarke SJ, Parbhoo R, Bradforth SE, Nadeau JL (2009) Photoenhancement of lifetimes in CdSe/ZnS and CdTe quantum dot-dopamine conjugates. Phys Chem Chem Phys 11(21):4298-4310
[34] Xia YS, Zhu CQ (2009) Interaction of CdTe nanocrystals with thiol-containing amino acids at different pH: a fluorimetric study. Microchim Acta 164(1-2):29-34
[35] Lemoine P, Chiadmi M, Bissery V, Tomas A, Viossat E (1996) Metformine compounds with the ions Co(II), Cu(II) and Ni(II). Acta Cristallogr C 52:1430-1436
[36] Călinescu M, Negreanu-Pîrjol T, Georgescu R, Călinescu O (2010) Synthesis and characterization of new copper(II) complex compounds with chlorhexidine. Part I. Cent Eur J Chem 8(3):543-549
[37] Olar R, Badea M, Grecu MN, Marinescu D, Lazar V, Balotescu C (2008) Copper(II) complexes with N,N-dimethylbiguanide. J Therm Anal Calorimetry 92(1):239-243

CHAPTER 7

A soft strategy for covalent immobilization of glutathione and cysteine capped quantum dots onto amino functionalized surfaces

ChemComm RSC Publishing

COMMUNICATION View Article Online View Journal

A soft strategy for covalent immobilization of glutathione and cysteine capped quantum dots onto amino functionalized surfaces†

Cite this: DOI: 10.1039/c3cc00145h

Received 7th January 2013,
Accepted 4th February 2013

DOI: 10.1039/c3cc00145h

www.rsc.org/chemcomm

Christian Frigerio,[a] João L. M. Santos,*[a] João A. C. Barbosa,[a] Peter Eaton,[b] M. Lucia M. F. S. Saraiva[a] and Marieta L. C. Passos[a]

Graphical Abstract

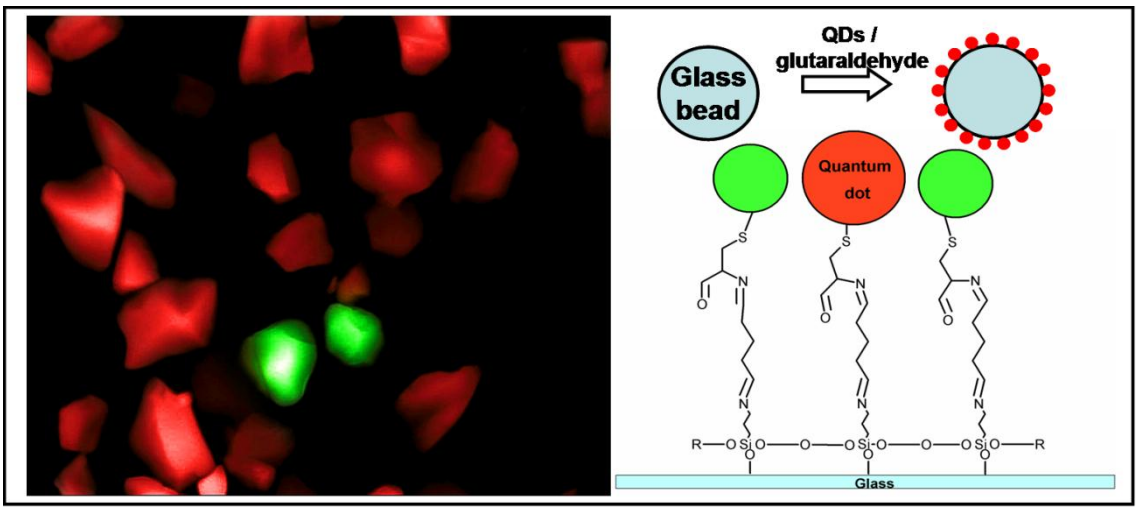

Abstract

A novel strategy for immobilization of CdTe quantum dots (QDs) onto amino functionalized solid supports was developed. QDs capped with compounds holding an amino group were covalently bonded to the substrate under mild reaction conditions, exhibiting great stability and strong luminescence.

In recent years, a considerable number of methods for the immobilization of nanoparticles onto different substrates were proposed. These developments were mainly fostered by the prospective exploitation of the unique physical and chemical properties of nanomaterials, which made them promising tools for applications in optical, electronic, chemical and biochemical devices. Like other nanoparticles, QDs were immobilized onto a great variety of supporting materials by using different approaches, such as layer-by-layer (LbL) assembly,[1] direct incorporation[2] and covalent attachment to chemically modified surfaces.[3,4] In this regard and to our knowledge, a covalent linkage is exclusively based on carbodiimide chemistry that permitted the formation of amide and ester bonds between carboxylic and amino groups under mild conditions. A significant number of papers used this technique to attach QDs to silica,[3] functionalized glass,[5] polymers,[6] biomolecules[7] and nanostructures.[8] Chemically modified materials, especially silanized surfaces, have been extensively used for the immobilization of enzymes. Due to their chemical nature enzymes demand extremely soft reaction conditions in order to retain a high catalytic activity. One of the most simple and efficient immobilization processes relies on the covalent linkage obtained upon reaction between the enzyme and solid supports previously activated with glutaraldehyde.[9] This compound can react with amine, thiol, phenol, or imidazole[10] functional groups in proteins because the most reactive amino acid side-chains are nucleophiles. These nucleophiles can attack the carbonyl group of glutaraldehyde forming an imine. In this work we have developed a glutaraldehyde-based methodology for the preparation of CdTe quantum dot-functionalized substrates. Two nucleophilic additions are used to link one of the carbonyl groups of glutaraldehyde to the aminomodified glass while the second carbonyl group binds to the a-amine of the CdTe capping agent (Fig. 1a).

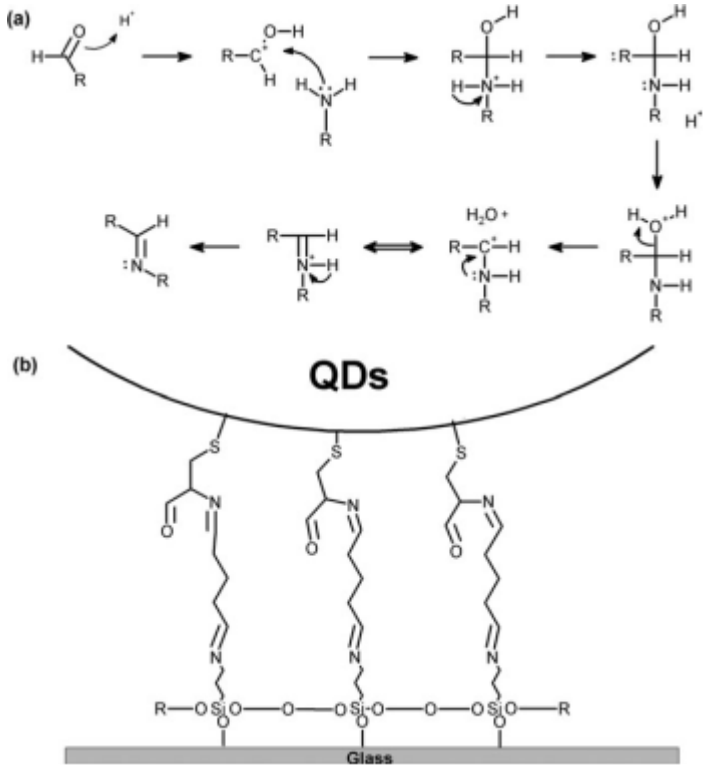

Fig. 1 (a) General scheme of a primary amine nucleophilic addition to na aldehyde. (b) Structural sketch of QD-immobilized glass.

CdTe quantum dots were prepared by wet chemistry using glutathione (GSH) and cysteine (CYS) as stabilizing agents. GSH capped QDs were synthesized in a single step by modified Quian's method.[11] Briefly, $CdCl_2$, Na_2TeO_3 and GSH (Cd : Te : GSH molar ratio 1 : 0.2 : 1.2) were added into a single reaction pot with $NaBH_4$, trisodium citrate and water. The solution pH was adjusted to 10.5 and the resulting solution was heated with vigorous stirring at 100°C under reflux for QDs growth. CYScapped nanocrystals were synthesized by using modified Zhang's method[12] upon reaction of a NaHTe solution with a mixture of $CdCl_2$ and CYS at pH 10.5, at a Cd : Te : CYS molar ratio of 1 : 0.05 : 2.4. Crude solutions of nanocrystals were precipitated with ethanol[13] to remove the excess of reactants. The precipitates were dried under vacuum. Physical and optical characterization of synthesized QDs was performed by atomic force microscopy (AFM) (Fig. S1†), powder X-ray diffraction (p-XRD) (Fig. S2†) and optical spectroscopy. The average size of the prepared QDs was 2.7 nm for GSH and 3.4 nm for CYS as observed by p-XRD and absorption spectroscopy.[14] The isolated fractions were dry stored under nitrogen and dissolved in 0.1 mol L^{-1} phosphate buffer at pH 7.5 at the desired concentration for the surface conjugation. An illustration of the linkage of QDs to the glutaraldehyde activated amino-functionalized surface by imine group formation is shown in Fig. 1b.

The immobilization process on the aminated glass beads (AGB) required no material pre-treatment. Based on the report of Peña et al.[15] the developed method consisted of: 0.060 g of aminoalkylated glass beads (aminopropyl-CPG-1400 Å, 200–400 mesh, Fluka) incubated in 1.25 mL of a 2.5% glutaraldehyde solution, for 1 h, at room temperature, with nitrogen purging every 10 min for the first 30 minutes. Glass beads were subsequently washed several times with water and 0.1 mol L^{-1} phosphate buffer at pH 7.5, to remove unreacted glutaraldehyde. Immobilization of QDs was carried out by adding 500 mL of QD solution to 0.060 g of the AGB followed by incubation at room temperature for 4 h, with nitrogen purging every 10 minutes during the first 30 minutes. After conjugation the glass beads were washed with water and 0.1 mol L^{-1} phosphate buffer at pH 7.5 until a clear supernatant to eliminate any non-immobilized QD was obtained, and then stored in water. When comparing the QD-conjugated AGB emission spectra (Fig. S3†) with that of QD solution a red shift of 14 nm for CYS-QDs and 11 nm for GSH-QDs for the emission maximum of the immobilized nanoparticles is evident. This effect can be attributed to exciton energy transfer (ET) due to dipole–dipole interactions between very close surface located QDs. ET has been described for solid QDs[16] and QD aggregates[17] and it happens when an exciton migrates from higher to lower-band gap QDs or to defect states, which act as acceptors. QD quantum yield was not affected by immobilization.

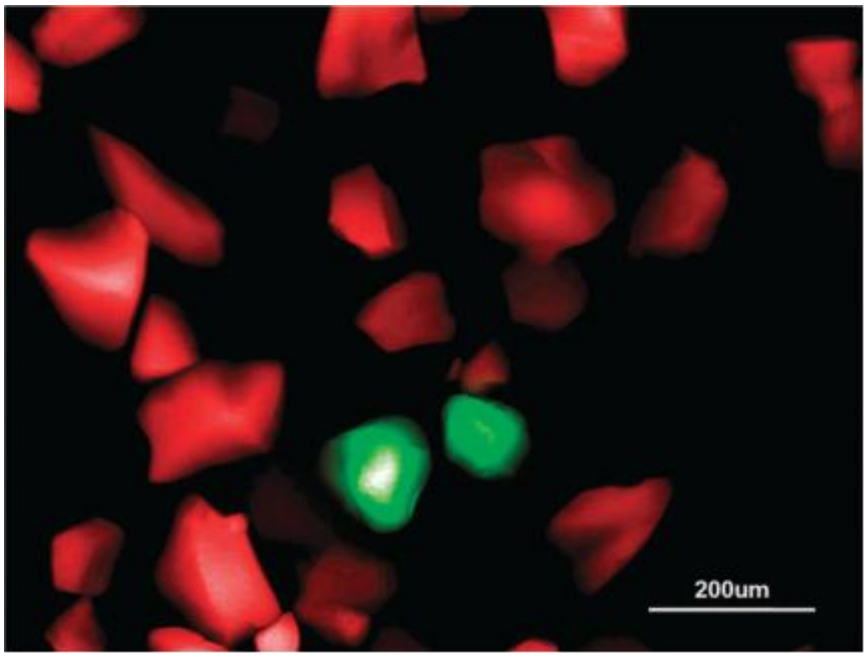

Fig. 2 Fluorescence microscopy image of AGB conjugated with CdTe–GSH (green) and CdTe–CYS (red) quantum dots.

In Fig. 2 we show the fluorescence microscopy image of the glass beads conjugated with the CdTe–GSH/CYS QDs. A strong red luminescence (λem = 621 nm) is observed for CYS-

capped QDs while a green emission (λem = 556 nm) is verified for GHScapped QDs. The image shows a very good glass bead surface coverage without visible discontinuities. Corroboration of the successful surface linkage was further provided by FTIR spectral comparison as shown in Fig. 3. In the AGB and AGB-QD–GSH spectra (Fig. 3a) the silica pattern, with bands at 470 cm^{-1} and 808 cm^{-1} (Si–O), 920 cm^{-1} (Si–OH) and 1100 cm^{-1} (Si–O), is evident. The organic layer on the glass surface was barely perceptible due to the strong contribution from glass. QD–GSH (Fig. 3a) showed one typical band ascribed to the capping, at 1580 cm^{-1} (COO^-). After the conjugation process the spectra remained almost unaltered and only very weak bands at 1654 cm^{-1} and at 2932 cm^{-1} appeared. Spectral subtraction (Fig. 3c) demonstrated that the bands at 2932 cm^{-1} and at ≈1500 cm^{-1} were QD contributions (CH aliphatic and COO^-). The presence of the 1654 cm^{-1} band was also confirmed by the second derivative spectra (Fig. 3b). This band is typical of a substituted imine ($R_2C=N–R$) and provided evidence of the formation of a covalent bond between the QDs and the AGB surface via nucleophilic addition of GSH primary amine to the aldehyde group of glutaraldehyde.

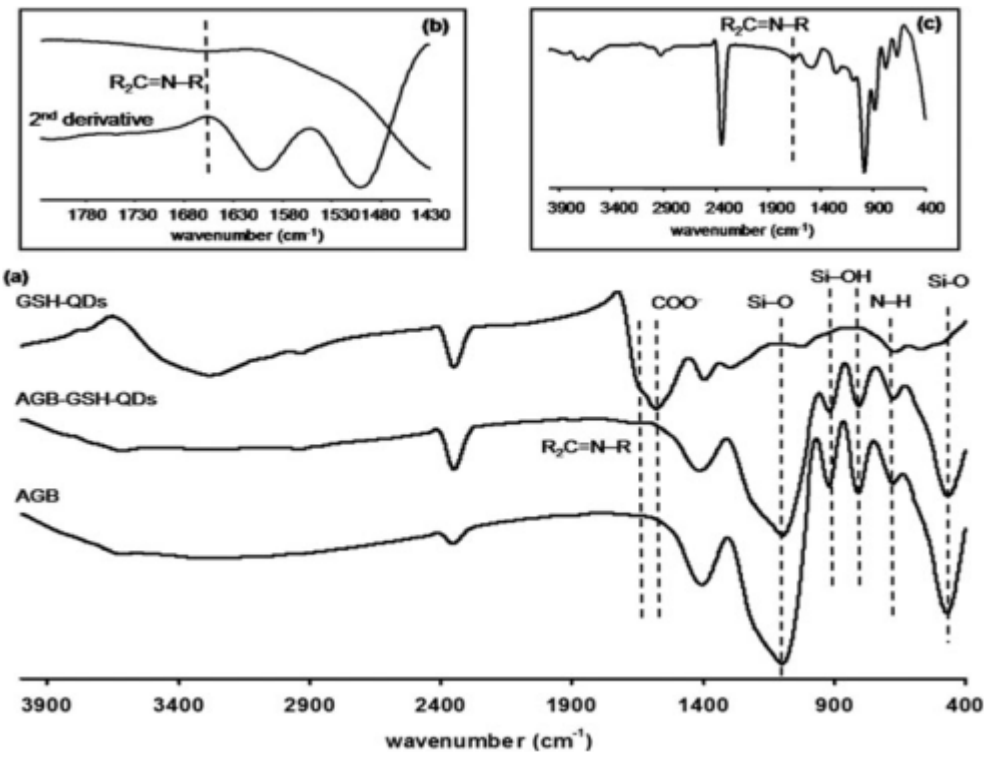

Fig. 3 (a) FTIR spectra of GSH-QDs, AGB–GSH-QDs and AGB; (b) 2nd derivative FTIR spectra in the imine region; (c) results obtained after subtraction of AGB from AGB–GSH-QDs spectra.

The luminescence of the AGB-QDs remained unaltered for at least two months in water and no trace fluorescence was found in the supernatant. A novel and efficient procedure

for the immobilization of QDs capped with compounds exhibiting an amino group has been developed. The method assures noteworthy advantages regarding similar approaches, namely in terms of simplicity of implementation and the utilization of more favorable reaction conditions that do not compromise QD optical properties. Moreover, it can provide a straightforward process for covalent immobilization of amino-capped QDs (without carboxylic groups) that could not be immobilized by using carbodiimide chemistry or even for immobilization of these QDs onto other substrates exhibiting the same amino groups as the functionalized glass. The obtained results also showed that the establishment of a covalent linkage guaranteed improved stability under aqueous conditions when compared to alternative methods based on electrostatic interactions.

This work was supported by FCT – Fundação para a Ciência e Tecnologia through grant no. PEst-C/EQB/LA0006/2011. Marieta L. C. Passos thanks FCT for the Pos-doc grant (SFRH/BPD/72378/2010) in the ambit of "POPH – QREN – Tipologia 4.1 – Formaça˜o Avançada" co-sponsored by FSE and national funds of MCTES. Christian Frigerio thanks FCT for the PhD grant SFRH/BD/47651/2008. The financial support under the project PTDC/QUI-QUI/105514/2008 under COMPETE/QREN/FEDER and under the FCT/CAPES 2011-2012 Agreement was greatly appreciated. The authors also thank J.M.A. Oliveira of Faculty of Pharmacy (FFUP) for the fluorescence microscopy images and Rute A.S. Ferreira of CICECO/University of Aveiro for quantum yield measurements.

Notes and references

1 P. T. Hammond, Adv. Mater., 2004, 16, 1271; G. Decher, Science, 1997, 277, 1232; N. A. Kotov, I. Dekany and J. H. Fendler, J. Phys. Chem., 1995, 99, 13065.
2 G. Wang, P. Zhang, H. Dou, W. Li, K. Sun, X. He, J. Han, H. Xiao and Y. Li, Langmuir, 2012, 28, 6141; P. Yang, M. Ando and N. Murase, J. Colloid Interface Sci., 2011, 354, 455; T. Nann and P. Mulvaney, Angew. Chem., Int. Ed., 2004, 43, 5393; N. Murase, P. Yang and C. Li, J. Phys. Chem. B, 2005, 109, 17855.
3 A. Shavel, N. Gaponik and A. Eychmuller, ChemPhysChem, 2005, 6, 449.
4 D. Du, W. Chen, J. Cai, J. Zhang, F. Qu and H. Li, J. Electroanal. Chem., 2008, 623, 81.
5 Y. J. Na, S. J. Park, S. W. Lee and J. S. Kim, Ultramicroscopy, 2008, 108, 1297.
6 S. Gupta, P. Uhlmann, M. Agrawal, V. Lesnyak, N. Gaponik, F. Simon, M. Stamma and A. Eychmu¨ller, J. Mater. Chem., 2008, 18, 214.
7 W. Liu, M. Howarth, A. B. Greytak, Y. Zheng, D. G. Nocera, A. Y. Ting and M. G. Bawendi, J. Am. Chem. Soc., 2008, 130, 1274; S. Wang, N. Mamedova, N. A. Kotov, W. Chen and J. Studer, Nano Lett., 2002, 2, 817; F. Song and W. C. W. Chan, Nanotechnology, 2011, 22, 494006.
8 S. Ravindran, S. Chaudhary, B. Colburn, M. Ozkan and C. S. Ozkan, Nano Lett., 2003, 3, 447.
9 O. R. Zaborsky, Immobilized enzymes, CRC Press, Cleveland, Ohio, 1973; G. R. Stark, Biochemical Aspects of Reactions on Solid Supports, Academic Press, New York, NY, 1971; H. H. Weetall, Anal. Chem., 1974, 46, 602A.
10 A. F. S. A. Habeeb and R. Hiramoto, Arch. Biochem. Biophys., 1968, 126, 16.
11 H. Qian, C. Dong, J. Weng and J. Ren, Small, 2006, 2, 747.
12 Y. Zhang, H. Zhang, M. Ma, X. Guo and H. Wang, Appl. Surf. Sci., 2009, 255, 4747.
13 N. Gaponik, D. V. Talapin, A. L. Rogach, K. Hoppe, E. V. Shevchenko, A. Kornowski, A. Eychmüller and H. Weller, J. Phys. Chem. B, 2002, 106, 7177.
14 W. W. Yu, L. Qu, W. Guo and X. Peng, Chem. Mater., 2003, 15, 2854–2860.
15 R. M. Peña, J. L. F. C. Lima and M. L. M. F. S. Saraiva, Anal. Chim. Acta, 2004, 514, 37.
16 C. R. Kagan, C. B. Murray, M. Nirmal and M. G. Bawendi, Phys. Rev. Lett., 1996, 76, 1517; S. A. Crooker, J. A. Hollingsworth, S. Tretiak and V. I. Klimov, Phys. Rev. Lett., 2002, 89, 186802; M. Achermann, M. A. Petruska, S. A. Crooker and V. I. Klimov, J. Phys. Chem. B, 2003, 107, 13782; T. Franzl, D. S. Koktysh, T. A. Klar, A. L. Rogach, J. Feldmann and N. Gaponik, Appl. Phys. Lett., 2004, 84, 2904; S. F. Wuister, R. Koole, C. de Mello Donega and A. Meijerink, J. Phys. Chem. B, 2005, 109, 5504.
17 R. Koole, P. Liljeroth, C. de Mello Donega, D. Vanmaekelbergh and A. Meijerink, J. Am. Chem. Soc., 2006, 128, 10436.

Electronic Supplementary Information

1. Experimental

1.1. Materials

Aminoalkylated glass beads (aminopropyl-CPG-1400Å, 200-400 mesh) and L-cysteine (≥99%) were purchased by Fluka (St. Louis MO, USA). Millipore water was used to prepare all solutions. Glutaraldehyde (grade II, solution 25%), cadmium chloride anhydrous (≥99%), Sodium telluride (100mesh, 99%), tellurium powder (200mesh, 99.8%), sodium borohydride ($NaBH_4$, 99%) and L-glutathione reduced (≥98%), were purchased from Sigma-Aldrich. Ethanol was purchased by Fisher Scientific (Leics, UK).

1.2. Instrumentation

1.2.1. Atomic Force Microscopy (AFM).

Samples for atomic force microscopy (AFM) were prepared by drying onto freshly cleaved mica substrates from diluted aqueous solutions. AFM measurements were made using an AFM Workshop TTAFM instrument in vibrating (intermittent contact) mode. A small (15 >µm) scanner and low gains were used to ensure high resolution. Probes from AppNano (ACT) with resonant frequency of around 300 kHz were used. Images were analysed using Gwyddion software.

1.2.2. Reflectance Fourier Transform Infrared (FTIR).

Samples in KBr pellets were freshly prepared and analysed with a Perkin-Elmer Spectrum BX FTIR.

1.2.3. Ultraviolet-Visible Spectroscopy (UV-Vis).

The UV-Vis spectra of QDs solutions were recorded on a Jasco V-660 spectrophotometer UV-Vis spectrometer between 400 and 700nm. For the size determination the QDs solutions absorbance was ≤ 0.1.

1.2.4 X-ray Diffraction (XRD).

X-ray powder diffraction (XRD) studies of the nanocrystals were carried out by using a Philips X'Pert X-ray MPD diffractometer (Cu Kα radiation). XRD data were collected at a scan rate o 40.0 s for step at step intervals of 0.04º.

1.2.5 Fluorescence spectroscopy.

Fluorescence measurements were carried out with a PerkinElmer LS-50B luminescence spectrometer. For QDs immobilized glass beads dispersion in water the PL spectra was recorded under stirring. Excitation wavelength was fixed at 400nm.

1.2.6 Fluorescence microscopy

Fluorescence microscopy was performed with a system composed by an inverted epifluorescence microscope (Eclipse TE300, Nikon, Tokyo, Japan) equipped with 10X air objectives, a monochromator (Polychrome II; TILL Photonics, Martinsried, Germany), a CCD camera (C6790; Hamamatsu Photonics, Hamamatsu, Japan), and a computer with analysis software (Aquacosmos 2.5; Hamamatsu Photonics).

2. Results

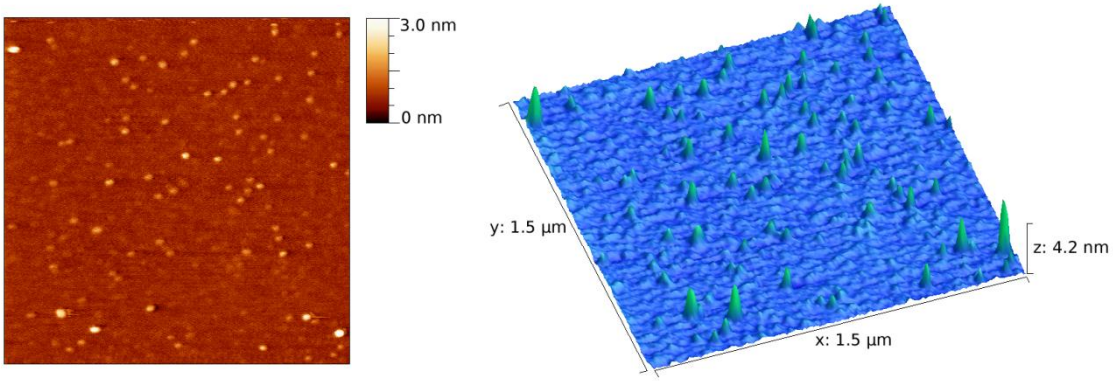

Figure S1. AFM images of 2.7nm GSH-CdTe QDs in water deposited on an atomized flat surface.

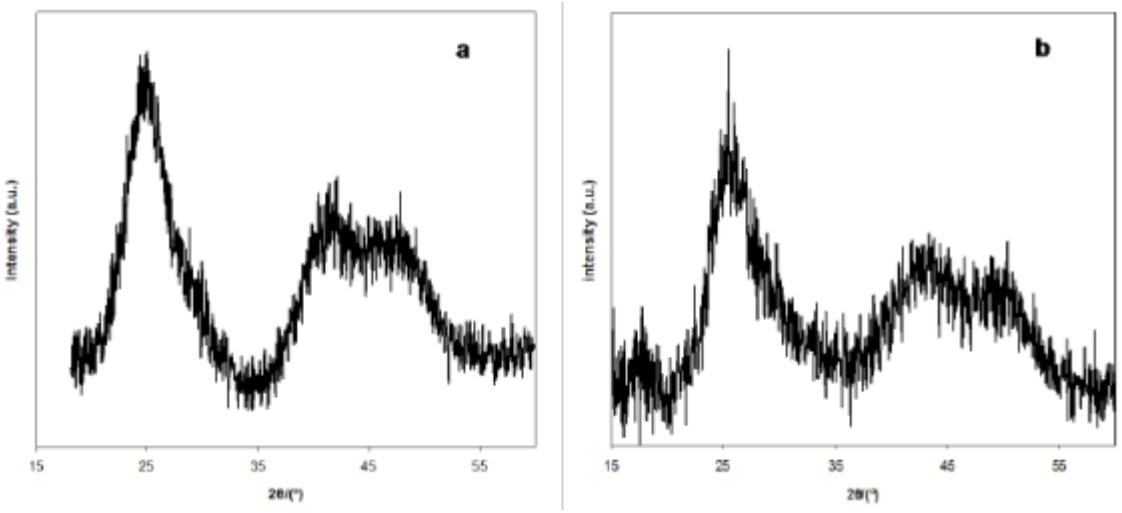

Figure S2. p-XRD of CYS (a) and GSH (b) capped QDs.

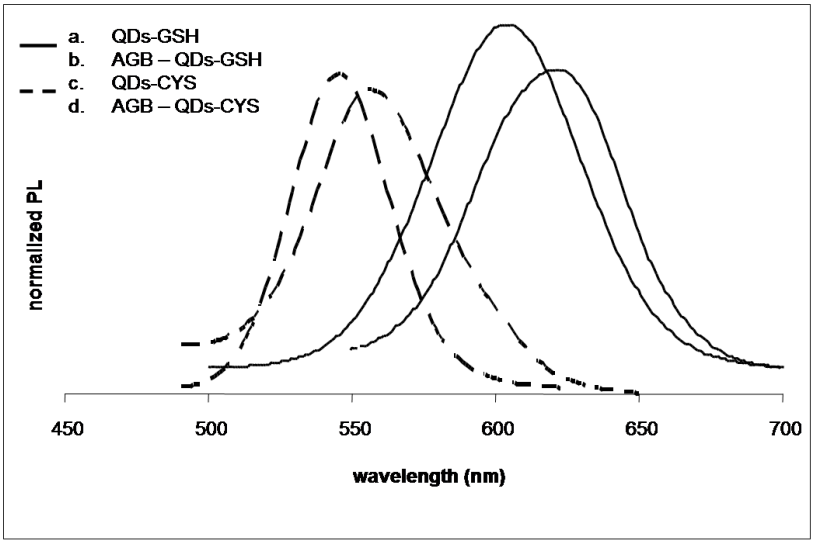

Figure S3. Comparison of QDs-conjugated AGB (AGB-QDs-GSH and AGB-QDs-CYS) emission spectra with that of QDs solution (QDs-GSH and QDs-CYS).

2.1. Quantum Yield

Quantum dots quantum yield (QY%) was not affected by immobilization and remained unaltered: 11% and 16% for CdTe-GSH and CdTe-CYS quantum dots, respectively.

CHAPTER 8

Final Conclusions

Conclusion

Although significant advances have been achieved in the past decades in the synthesis and application of QDs various aspects regarding their chemistry and their optical properties remained and still remain unclear.

In this regard, one of the main goals of this work was to study the influence of different parameters in the synthesis of quantum dots, focusing in particular on their influence on the resulting optical properties of these nanomaterials. The obtained results have demonstrated that by implementing an automated approach to carry out and to monitor the aqueous synthesis of CdTe-MPA QDs it was possible to accomplish an enhanced reproducibility of all synthesis process and, consequently, to guarantee that the prepared materials exhibited unvarying characteristics, which facilitate predicting their behaviour and their application in distinct analytical circumstances. This development, in combination with the need for utilization of higher [Te]:[Cd] precursor ratios, as a means of attaining faster synthesis with enhanced nanocrystals growth rate, likewise was referred in several papers available in literature, provided a more efficient management of the precursor concentration, especially in the case of NaHTe. The population dispersion was found to be dependent on the growth rate, but a similar pattern of focussing and defocusing regimes was established for all the rates. Differently from what reported in literature it was verified that the quantum efficiency reaches a maximum for a certain size and did not decrease for faster growing regimes.

The feasibility and robustness of implementing analytical methodologies resorting to CdTe QDs in an automated multipumping flow system (MPFS) was also demonstrated. The results attained when using quantum dots as nanosensors not only demonstrated their huge potential, confirming results already available in literature, but showed as well that their coupling to MPFS represents a noteworthy contribution for broadening the analytical scope and efficiency of such materials not only in terms of enhancing the performance of available discrete methodologies but also providing the means for implementing versatile and expeditious alternatives. Due to the extended range of variables to be optimized, the multipumping flow methodology allowed a simplification of the entire process and the gathering of the ideal conditions in a simpler and faster way. The pulsed flowing stream generated by micro-pump actuation not only permitted the attainment of very stable flow rates but also imparted a fast homogeneous mixing which contributed to improve the interactions development. Furthermore, the use of the merging zones strategy was of great benefit as it enabled the reduction of the time required for the analysis as well as of reagent consumption. Additionally, in comparison with the reference procedure, the proposed systems proved to fill many of the gaps left by those former methodologies

which always require high volume of reagents, often hazardous for the environment, expensive equipment and time-consuming sample handling operations. These results pointed out the potential use of water-soluble CdTe QDs as probes for pharmaceutical drugs by resorting to different analytical techniques.

One of the accomplishments of this work with an especial interest is related to the concept of photoluminescence enhancing. Analytical methods using fluorescent probes are generally based on the quenching of fluorescence or in the appearance, by reaction, of new emitting fluorophores. For the first time was described the possibility of measuring an enhancement of the emission after interaction of the sample with the probe. This fact is due to the nature of quantum dots emission mechanism, i.e. the presence of surface traps that can be filled or matched by the analyte with a consequent enhancing of the probability of a light emitting recombination of electron and holes. An efficient control of the reaction condition proved the feasibility of selective determinations of molecules showing great structural differences, but in all instances based on interactions with the QDs surface. In some cases this effect is only temporary, and it tends to disappear with time. For this reason multipumping flow systems are ideal to carry out rapid reactions ensuring at the same time an efficient mixture of the reagents. Results confirmed that the effect of some others parameters (especially pH) need to be studied with more detail, because they are of crucial importance for the extension of enhancing reactions.

CdTe QD were also successfully applied as chemiluminescence sensitizers enabling the chemiluminometric determination of compounds that have the potential or interacting with the nanoparticles affecting their photochemical properties and/or reactivity. Once again the mixing capacity and high automation level of MPFS provided an expeditious way of implementing reaction schemes involving nanoparticles and the generation of short-lived species that are difficult to monitor in discrete methodologies.

Despite the numerous advantages of QDs application in analytical chemistry, they also have same shortcomings being, eventually, one of the most important ones the high toxicity of the heavy metals, such as cadmium, used in their preparation. This high heavy metals content makes them quite “unfriendly” for the environment. It is also true that the generally low concentration used and the exploitation of multipumping systems can strongly reduce their impact. One of the most important advances for their application in analytical techniques is the immobilization onto solid support materials, allowing the fabrication of “continuous multiuse reactors”. This can permit an efficient exploitation of the QDs characteristic while solving or minimising the environmental concerns. Various immobilization techniques were developed in the last years, but in the most of cases they revealed some lack of stability, especially in solution. In this thesis a novel and efficient procedure for the immobilization of QDs capped with compounds exhibiting an amino

group has been developed. The method assures noteworthy advantages regarding similar approaches, namely in terms of simplicity of implementation and the utilization of more favourable reaction conditions that do not compromise QD optical properties. Moreover, it can provide a straightforward process for covalent immobilization of amino-capped QDs (without carboxylic groups) that could not be immobilized by using carbodiimide chemistry or even for immobilization of these QDs onto other substrates exhibiting the same amino groups as the functionalized glass. The obtained results also showed that the establishment of a covalent linkage guaranteed improved stability under aqueous conditions when compared to alternative methods based on electrostatic interactions.

As an overall conclusion, the work developed under the scope of this thesis confirmed the immense analytical potential of quantum dots and of their combination with flow-based techniques, allowing the implementation of distinct reaction schemes and assorted detection techniques and showed the huge field of application of such tiny, although "active", nanoparticles.